

2

REPORT DOCUMENTATION PAGE

Form Approved  
OMB No. 0704-0188

Public reporting burden for this collection of information is estimated to average 1 hour per response, including the time for reviewing instructions, searching existing data sources, gathering and maintaining the data needed, and completing and reviewing the collection of information. Send comments regarding this burden estimate or any other aspect of this collection of information, including suggestions for reducing this burden, to Washington Headquarters Services, Directorate for Information Operations and Reports, 1215 Jefferson Davis Highway, Suite 1204, Arlington, VA 22202-4302, and to the Office of Management and Budget, Paperwork Reduction Project (0704-0188), Washington, DC 20503.

AD-A231 376

1. AGENCY USE ONLY (Leave blank)	2. REPORT DATE 1990	3. REPORT TYPE AND DATES COVERED Final 15 Jul 89 - 24 Oct 90
----------------------------------	------------------------	---

4. TITLE AND SUBTITLE XIII. International Workshop on Condensed Matter Theories	5. FUNDING NUMBERS DAAL03-89-G-0036
--	--

6. AUTHOR(S) G. Bary Malik	DTIC SELECTED SERIALS B D JAN 18 1991
-------------------------------	--

7. PERFORMING ORGANIZATION NAME(S) AND ADDRESS(ES) Southern Univ Univ of Illinois at Carbondale Carbondale, Illinois 62901-3301	8. PERFORMING ORGANIZATION REPORT NUMBER
--	--

9. SPONSORING/MONITORING AGENCY NAME(S) AND ADDRESS(ES) U. S. Army Research Office P. O. Box 12211 Research Triangle Park, NC 27709-2211	10. SPONSORING/MONITORING AGENCY REPORT NUMBER ARO 27024.11-PH-CF
---	--

11. SUPPLEMENTARY NOTES  
The view, opinions and/or findings contained in this report are those of the author(s) and should not be construed as an official Department of the Army position, policy, or decision, unless so designated by other documentation.

12a. DISTRIBUTION/AVAILABILITY STATEMENT Approved for public release; distribution unlimited.	12b. DISTRIBUTION CODE
--	------------------------

13. ABSTRACT (Maximum 200 words)

The grant enabled 10 scientists from the U.S.A. to participate at the XIII. International Workshop on Condensed Matter Theories held at Campos do Jordao, Brazil in August 1989.

In keeping with the objective of the grant, emphasis was placed on theories related to high temperature superconductivity, molecular dynamics and physics of strongly correlated systems. In addition, talks on the use of maximum entropy principle to describe cooperative phenomena were presented. A large number of scientists from the host country, Brazil, participated actively.

The Workshop also helped to foster another key objective of bringing together scientists working in different areas of physics in order to facilitate interchange of ideas.

14. SUBJECT TERMS Condensed Matter Theories, Workshop, High Temperature Superconductivity, Molecular Dynamics, Superconductivity, Maximum Entropy Principle	15. NUMBER OF PAGES
	16. PRICE CODE

17. SECURITY CLASSIFICATION OF REPORT UNCLASSIFIED	18. SECURITY CLASSIFICATION OF THIS PAGE UNCLASSIFIED	19. SECURITY CLASSIFICATION OF ABSTRACT UNCLASSIFIED	20. LIMITATION OF ABSTRACT UL
---	--	---	----------------------------------

AD-A231 376

91 1 15 045

Final Report: Grant No. DAAL 03-89-G-0039  
XIII. International Workshop on Condensed Matter Theories

The grant enabled 10 scientists from the U.S.A. to participate at the XIII. International Workshop on Condensed Matter Theories held at Campos do Jordao, Brazil in August 1989. Without this grant the U.S. Participation at the Workshop would have been very minimal. The grant allowed U.S. scientists to interact effectively with their international counterparts.

The list of the scientists from the U.S.A. who have been supported by the grant is attached in Appendix 1 and the titles of their talks presented at the Workshop are listed in Appendix 2. Participants from the U.S.A. receiving the grant have acknowledged that in their respective articles.

Copies of the articles containing the subject matter presented by the participants supported by the grant are attached in Appendix 3. All presentations were invited talks. These articles have been accepted for publication in Condensed Matter Theories Vol. 5. The publisher, Plenum Publishing Corporation, expects to bring out the volume shortly.

In keeping with the objective of the grant, emphasis was placed on theories related to high temperature superconductivity, molecular dynamics and physics of strongly correlated systems. In addition, talks on the use of maximum entropy principle to describe cooperative phenomena were presented. A large number of scientists from the host country, Brazil, participated actively. Two topmost scientists from the U.S.S.R., Professor Bashkin and Pitaevski of their National Academy of Science's Institute for Physical Problems, took part.

The Workshop also helped to foster another key objective of bringing together scientists working in different areas of physics in order to facilitate interchange of ideas.

The Workshop was very effective in cross fertilization of ideas and development of new interests. For example, Dr. Proto, originally a nuclear physicist, presented the talk on the role of maximum entropy principle. Dr. Campbell, originally a solid state theorist, presented the talk on correlations in atoms. The principle investigator, originally an atomic and nuclear physicist, presented a talk on superconductivity. Another objective of the workshop, namely to serve as a forum to initiate collaborative research in the area of condensed matter theories, has also been fulfilled.

Thus, the purpose and objective of the grant have been successfully achieved.

Appendix 1

1. Dr. George A. Baker, Los Alamos National Laboratory, Los Alamos, NM.
2. Dr. Charles E. Campbell, University of Minnesota, Minneapolis, NM.
3. Dr. John W. Clark, Washington University, St. Louis, MO.
4. Dr. Manuel de Llano, North Dakota State University, Fargo, ND.
5. Dr. W. H. Dickhoff, Washington University, St. Louis, MO.
6. Dr. Rajv K. Kalia, Argonne National Laboratory, Argonne, IL.
7. Dr. E. Krotscheck, Texas A and M, College Station, TX.
8. Dr. F. B. Malik, Southern Illinois University, Carbondale, IL.
9. Dr. Roger A. Smith, Texas A and M., College Station, TX.
10. Dr. Priya Vashishta, Argonne National Laboratory, Argonne, IL.

Appendix 2

Titles and Authors of the Articles

↓ Contents: ↓

1. Thomas-Fermi Equation of State-The Hot Curve, by George A. Baker Jr. and J. D. Johnson.
2. Electron Correlation in Atoms, by Charles E. Campbell, Tao Pang and E. Krotscheck.
3. Correlated RPA Calculations for Model Nuclear Matter, by Eirene Mavromatis and John W. Clark.
4. Generalized Momentum Distributions of Quantum Fluids, by John W. Clark and Manfred L. Ristig.
5. Abnormal Occupation, Tighter Bound Cooper Pairs and High  $T_c$  Superconductivity, by M. de Llano and James P. Vary.
6. The Foundation of Nuclear Shell Model, by W. H. Dickhoff, P.P. Domitrovich, A. Polls and A. Ramos.
7. Quantum Molecular Dynamics Simulation of Electron Bubbles in a Dense Helium Gas, by Rajiv K. Kalia, Priya Vashista, S. W. de Leeuw, and John Harris.
8. Quantum Liquid Films: A Generic Many-Body Problem, by E. Krotscheck, J. L. Epstein and M. Saarela.
9. On the Role of Electron-Medium Coupling in High Temperature Superconductors, by Bary Malik.
10. Baym-Kadanoff Theory Made Even Planar, by Roger A. Smith.

Appendix 3

Copies of the Articles Containing Materials Presented at the Workshop by Participants  
Supported by the Grant.

## THOMAS-FERMI EQUATION OF STATE--THE HOT CURVE

George A. Baker, Jr. and J. D. Johnson

Theoretical Division, Los Alamos National Laboratory  
University of California, Los Alamos, N. M. 87545, USA

### ABSTRACT

We derive the high-temperature limit of the equation of state based on the Thomas-Fermi statistical theory of the atom. The resulting "hot curve" is in fact the ideal Fermi gas. We expand the thermodynamic properties of this gas in powers of the fugacity and use this expansion to construct a representation of the pressure, accurate to about 0.1 %. This representation is compared with the actual theory for aluminum and the "hot curve" is found to represent it well over a large region of interest in applications.

## 1. INTRODUCTION AND SUMMARY

The Thomas-Fermi (T-F) statistical theory of the atom<sup>1</sup> as well as the modifications due to Dirac<sup>2</sup> have long been used as a basic starting point for the computation of approximations to the equations of state.<sup>3,4</sup> In order to make use of this procedure, computer programs have been written to compute the numerical content of the theory. They consume a sufficient amount of computer time, even today, so that it is impractical to use them to compute, *ab initio*, the value of the pressure, internal energy, *etc.*, every time that a new value is required inside an application computer program. Besides, as these efforts represent only approximate equations of state, some adjustment is necessary to bring them into accord with physical reality. Consequentially, to date largely empirical fits have been used to represent the equations of state for the purposes of applications.

In this work, we are concerned with beginning an analysis of the physical structure of the equations of state of real matter. As a start, we will study the Thomas-Fermi model equation of state which represents a fair amount of the physics, at least in some regions. One method which is normally fruitful, is to consider various limits. There are currently two which are known. The first is the low-density limit. Here there is complete ionization when the system is in equilibrium and the pressure for an element of nuclear charge  $Z$  is

$$P\Omega/N = (Z + 1)kT, \quad (1.1)$$

the ideal gas equation of state. Here  $P$  is the pressure,  $\Omega$  is the volume of the system,  $N$  is the number of atoms,  $k$  is Boltzmann's constant and  $T$  is the absolute temperature. The second limit<sup>3</sup> is the low-temperature limit, or the "cold curve." Here the pressure is of the form,

$$P\Omega/N = Z^{\frac{2}{3}}\phi(Z\Omega/N), \quad (1.2)$$

where  $\phi(x)$  is a well defined function. If we think of the temperature-density, quarter-plane, these results give the limiting behavior of the T-F model along the zero-temperature and the zero-density edges. There remain the high-density and the high-temperature regions to examine for physical structure.

One might think that in the high-temperature limit it would be appropriate to describe the system in purely classical terms. Indeed if such were the case, Baker<sup>5</sup> has proven that the pressure would be of the form,

$$P\Omega/N = kT f(\Omega T^3/N, Z). \quad (1.3)$$

The Debye-Hückel correction<sup>6</sup> is of just this form. Also Baker has shown for this case that the internal energy has the particularly simple form,

$$u = 3P\Omega - \frac{3}{2}(Z + 1)NkT. \quad (1.4)$$

The statistical mechanics of Coulombic systems have been much studied.<sup>7</sup> It is now well known that there does not exist a classical (*i.e.* Planck's constant  $h = 0$ ) gas because atoms with a Coulomb interaction collapse to  $E = -\infty$ . Thus if we are to ever introduce a Coulomb attraction between the atomic nucleus and the electrons, we must necessarily include some account of the quantum effects that are needed to stabilize the system. As is also well known there are two important physical lengths to be considered. The first is the de Broglie length which is proportional to  $h/\sqrt{mkT}$ , where  $m$  is the electron mass, and which measures in a noninteracting gas the importance of quantum effects. The Coulomb interaction does not by itself provide the second length and the difficulty of its long range can not be circumvented by studying dilute systems because it contains no parameter with the dimensions of

a length. The second length is the Debye screening length which is proportional to  $e^2/kT$ . This length is however a statistical effect and should follow from the theory, but unfortunately is not there *ab initio*. Thus when we look to the high-temperature and high-density regions, if we consider the cases where  $\Omega/N \gg (e^2/kT)^3$ , then we can hope to start with a noninteracting electron gas (with a background gas of atomic nuclei) as the basic system.

In the second section, we derive the limit of Thomas-Fermi theory when the Debye screening length is negligible compared to the interparticle distance, and the de Broglie length remains arbitrary. We find that it correctly reduces to the ideal Fermi gas. We call this limit the "hot curve," because it is reached if one either fixes the density and lets the temperature go to infinity, or much less restrictively, it is also reached if one fixes the de Broglie length and then lets the temperature go to infinity. In the third section we review the theory of the ideal Fermi gas and describe how to calculate its properties in a practical manner. We derive lengthy fugacity series and find that the pressure function can be approximated to within, say 0.1%, by a low-order, two-point Padé approximant. In the final section we compare the ideal gas approximation to results for aluminum and map out its region of validity to various degrees of accuracy.

## 2. HIGH TEMPERATURE LIMIT OF THOMAS-FERMI THEORY

Thomas-Fermi theory has been applied to compute equations of state at finite temperature by Feynman *et al.*<sup>3</sup> They begin with an application of the statistical analysis of Fermi and Dirac which leads to the equation

$$\rho = \int_0^\infty \frac{2 \cdot 4\pi p^2 dp/h^3}{\exp[(p^2/2m - eV)/kT + \eta] + 1}, \quad (2.1)$$

where  $-eV$  is the potential energy. We follow them in defining for convenience the auxiliary functions

$$I_n(\eta) = \int_0^\infty \frac{y^n dy}{\exp(y - \eta) + 1}. \quad (2.2)$$

Then one uses Poisson's equation to determine  $V(r)$ . It yields

$$\frac{1}{r} \frac{d^2}{dr^2}(rV(r)) = \frac{16\pi^2}{h^3} e(2mkT)^{\frac{3}{2}} I_{\frac{1}{2}} \left( \frac{eV(r)}{kT} - \eta \right). \quad (2.3)$$

Note that in the case of no interaction that the right-hand side of (2.3) vanishes ( $e=0$ ) and so the equation implies that  $V = a + b/r$  where  $a$  and  $b$  are constants. In order to simplify the above equation, Feynman *et al.*<sup>3</sup> introduce dimensionless variables. First they define a length scale,

$$c = \left( \frac{h^3}{32\pi^2 e^2 m (2mkT)^{\frac{1}{2}}} \right)^{\frac{1}{2}} \propto T^{-\frac{1}{4}}, \quad (2.4)$$

where  $s = r/c$ . Then since  $\eta$  is independent of  $r$ , (2.3) becomes

$$\frac{d^2\beta}{ds^2} = s I_{\frac{1}{2}}(\beta/s), \quad (2.5)$$

where

$$\beta/s = (eV(r)/kT) - \eta. \quad (2.6)$$

The boundary conditions of (2.5) become, as at the origin  $V(r)$  must behave as  $Ze/r$ ,

$$\beta(0) = \alpha = Ze^2/kTc \propto T^{-3/2}. \quad (2.7)$$

The scheme employed is to suppose that each atom is confined to a sphere of volume equal to the volume per particle. This is clearly an approximation. The other boundary condition is to require that the number of electrons in the sphere is exactly equal to the nuclear charge. A little manipulation serves to show that the condition,

$$\frac{d\beta}{ds} = \beta/s \text{ at } s = b, \quad (2.8)$$

imposes this normalization in the sphere of radius  $r = cb$ . Feynman *et al.*<sup>3</sup> derive, among other things, the formula for the pressure as

$$P\Omega/N = \frac{2}{9}(ZkT) \cdot \frac{b^3}{\alpha} I_{\frac{3}{2}} \left( \frac{\beta_b}{b} \right), \quad (2.9)$$

where  $\beta_b$  is the value of  $\beta$  on the boundary  $s = b$ .

In a parallel way we may set out the corresponding formulae for the ideal Fermi gas. In this case the electron density is simply given by (2.1) with  $e = 0$ . As  $\eta$  is independent of  $r$ , one sees immediately by (2.6) that the equation for the density (2.5) is simply satisfied. Since by (2.4) and (2.7) both the length and magnitude scales depend on the electronic charge  $e = 0$ , the normalization equation (2.8), in leading order, is automatically satisfied, and so does not determine the number of electrons in this limit. Returning to (2.1), we may impose the normalization condition by integrating the density over a sphere of radius  $r$ . It gives

$$Z = \frac{16\pi^2}{3} I_{\frac{1}{2}}(-\eta) \left[ \frac{r\sqrt{2mkT}}{h} \right]^3, \quad (2.10)$$

which implies  $\eta$ . In this limit, the pressure equation (2.9), becomes,

$$P\Omega/N = \frac{2}{9}(ZkT) \left( \frac{r^3}{c^3\alpha} \right) I_{\frac{3}{2}}(-\eta), \quad (2.11)$$

a parametric expression for the pressure in terms of the  $\eta$  of (2.10). Note is made that  $c^3\alpha$  is independent of the electronic charge  $e = 0$ , so this form is valid in this noninteracting limit. Comparison with the results of Huang<sup>8</sup> for the ideal Fermi gas, reveal complete agreement, when it is remembered that for our case the spin,  $s = \frac{1}{2}$ .

Now we are ready to consider the "hot curve" limit of the Thomas-Fermi theory. In the basic equations of the theory, (2.5, 7-8), we make the following change of variables,

$$\sigma = s/\alpha^{1/3}, \quad \gamma = \beta/\alpha^{1/3}. \quad (2.12)$$

We thus obtain

$$\frac{d^2\gamma}{d\sigma^2} = \alpha^{2/3}\sigma I_{\frac{1}{2}} \left( \frac{\gamma}{\sigma} \right), \quad (2.13)$$

$$\gamma(0) = \alpha^{2/3}, \quad (2.14)$$

$$\frac{d\gamma}{d\sigma} = \frac{\gamma}{\sigma}, \text{ at the boundary.} \quad (2.15)$$

In the limit  $\alpha \rightarrow 0$  (by (2.7) this limit is equivalent to  $T \rightarrow \infty$ ), we obtain the result that  $\gamma = A\sigma$  solves (2.13-15). Again, as at (2.10) above, we have an undetermined normalization constant to be determined because in our high-temperature limit (2.15) is satisfied automatically. Again referring to (2.1) we obtain the normalization condition,

$$Z = \frac{16\pi^2}{3h^3} [r\sqrt{2mkT}]^3 I_{\frac{1}{2}} \left( \frac{\gamma}{\sigma} \right), \quad (2.16)$$

which determines  $A$  and thus the solution of (2.13-15). When we note the comparison  $A = -\eta$ , we find that this limiting solution is the same as the one we obtained for the ideal (noninteracting) Fermi gas. This result completes our demonstration of the proposition that the "hot curve" for Thomas-Fermi theory is the ideal Fermi gas!

### 3. PROPERTIES OF THE IDEAL FERMI GAS

The basic theory of the ideal Fermi gas is described by Huang.<sup>8</sup> To establish a correspondence between the results of the previous section and more standard notation, we note that in (2.16)  $\gamma/\sigma = A$ ; therefore we introduce the notation  $z = e^{-A}$ . We can then rewrite (2.16) and (2.11) as

$$\frac{ZN}{\Omega} = \frac{3Z}{4\pi r^3} = 2 \left( \frac{2\pi mkT}{h^2} \right)^{\frac{3}{2}} \frac{2}{\sqrt{\pi}} \int_0^{\infty} \frac{zy^{\frac{1}{2}} e^{-y} dy}{1 + ze^{-y}}, \quad (3.1)$$

$$\frac{P}{kT} = 2 \left( \frac{2\pi mkT}{h^2} \right)^{\frac{3}{2}} \frac{4}{3\sqrt{\pi}} \int_0^{\infty} \frac{zy^{\frac{3}{2}} e^{-y} dy}{1 + ze^{-y}}, \quad (3.2)$$

where  $P$  is the pressure due to the electrons only and does not take account of the effect of the motion of the center of mass of the atom. If we introduce the further notation,

$$\lambda = \left( \frac{h^2}{2\pi mkT} \right)^{\frac{1}{2}}, \quad (3.3)$$

$$f_{\frac{3}{2}}(z) = \frac{2}{\sqrt{\pi}} \int_0^{\infty} \frac{zy^{\frac{1}{2}} e^{-y} dy}{1 + ze^{-y}} = \sum_{l=1}^{\infty} \frac{(-1)^{l+1} z^l}{l^{\frac{3}{2}}}, \quad (3.4)$$

$$f_{\frac{5}{2}}(z) = \frac{4}{3\sqrt{\pi}} \int_0^{\infty} \frac{zy^{\frac{3}{2}} e^{-y} dy}{1 + ze^{-y}} = \sum_{l=1}^{\infty} \frac{(-1)^{l+1} z^l}{l^{\frac{5}{2}}}, \quad (3.5)$$

where the series expansions are convergent for  $|z| \leq 1$ . We may now rewrite (3.1-2) as

$$\zeta = \frac{ZN\lambda^3}{2\Omega} = f_{\frac{3}{2}}(z), \quad (3.6)$$

and

$$\frac{P\Omega}{ZNkT} = \frac{f_{\frac{5}{2}}(z)}{f_{\frac{3}{2}}(z)}, \quad (3.7)$$

where  $\zeta$  is the de Broglie density. The procedure to calculate the pressure of the ideal Fermi gas is now, in principle, quite straightforward. Eq. (3.6) is solved for  $z$  and then that value is substituted into (3.7).

To evaluate these expressions numerically we choose the following method. First we revert the series expansion (3.6) to give  $z(\zeta)$  as a series in  $\zeta$ . Then we substitute it into (3.7) to obtain

$$\frac{P\Omega}{ZNkT} = g(\zeta). \quad (3.8)$$

We have calculated the leading 36 terms of the series expansion. The method used is the classical Lagrange formula for the reversion of series.<sup>9</sup> The only point of difficulty is that a large number of decimal places are lost in the computation in this case. We have therefore taken the precaution of using at least 58 decimal places to carry out these computations. The results are listed in Table 1.

TABLE 1.  $(P\Omega/ZNkT)$  as a series in the de Broglie density

0	1.0000000000	0000000000	0000000000	0000000000	000000000000000000E+000
1	1.7677669529	6636881100	2110905262	1225982120	8984422118509147E-001
2	-3.3000598199	1683655758	8617889323	8790328003	89171139305782E-003
3	1.1128932846	6542504524	9253533917	1305775999	1375768224181E-004
4	-3.5405040951	9736538278	3050093233	4626176046	46439677965E-006
5	8.3863470395	6925729619	7125848681	6212474298	427436245E-008
6	-3.6620617873	4852703663	1688233937	9045807824	8643167E-010
7	-1.0280607154	3957929799	3273512206	9735581999	5254513E-010
8	7.0550978435	7253454626	0275709452	8261969773	09158E-012
9	-2.6859639507	9285424406	0526716388	7926863588	4377E-013
10	4.0571834908	0612166197	1056127182	3091151601	35E-015
11	2.7970439770	9162019148	3071234746	1358106846	6E-016
12	-2.8379673439	5952590529	6631787032	9726025304	E-017
13	1.3992940717	5922219970	7552151122	203412696E	-018
14	-3.6303052861	0821033013	0082398676	2418074E-0	20
15	-6.0257400821	7251347692	8112664253	67093E-022	
16	1.2989538153	2549763684	7035089386	73544E-022	
17	-8.1719971340	6344259697	7319803759	795E-024	
18	2.9413082494	4946667164	3606073469	73E-025	
19	-2.0285711098	2088612486	4658243931	E-027	
20	-5.7410636166	7615749309	984730023E	-028	
21	4.8461575378	3763503589	33968480E-	029	
22	-2.2369786852	5871386652	1846940E-0	30	
23	4.7888680538	7474310454	78772E-032		
24	2.0304880286	8391265410	8553E-033		
25	-2.7811009124	7360566430	414E-034		
26	1.6149810555	1163427972	12E-035		
27	-5.2554355032	5730228297	E-037		
28	-1.3309033541	33284697E-	039		
29	1.4721238409	86015824E-	039		
30	-1.1062516681	9956070E-0	40		
31	4.7267873838	86169E-042			
32	-7.6386716803	536E-044			
33	-6.5324794996	62E-045			
34	7.1193401844	5E-046			
35	-3.8268661579	E-047			
36	1.097950074E	-048			

The above series expansion was derived for  $|z| \leq 1$ , but the above series plainly corresponds to a larger range. In the limit as  $z \rightarrow \infty$  Huang shows that

$$f_{\frac{3}{2}}(z) \asymp \frac{4}{3\sqrt{\pi}}(\log z)^{\frac{3}{2}} \left[ 1 + \frac{\pi^2}{8(\log z)^2} + \dots \right] + O(z^{-1}). \quad (3.9)$$

From the identity,<sup>8</sup>  $z \frac{d}{dz} f_{\frac{3}{2}}(z) = f_{\frac{3}{2}}(z)$  one can easily also derive the asymptotic behavior of  $f_{\frac{3}{2}}(z)$ , and thus from (3.7) the asymptotic behavior of  $g(\zeta)$ . We obtain,

$$g(\zeta) \asymp \frac{2}{5} \left( \frac{3\sqrt{\pi}}{4} \right)^{\frac{3}{2}} \zeta^{\frac{2}{3}} \text{ as } \zeta \rightarrow \infty. \quad (3.10)$$

With this information and the series of Table 1, we may construct a two point Padé approximant<sup>10</sup> to  $[g(\zeta)]^3$  of the form  $[N + 2/N]$  which is exact through order  $\zeta^{2N+1}$  at the origin, and is also asymptotically correct as  $\zeta \rightarrow \infty$ . We find excellent convergence for this method and that for  $0 \leq \zeta < \infty$  we get an accuracy of about 0.1 per cent for  $g(\zeta)$  from the approximation,

$$g(\zeta) \approx \left[ \frac{1 + 0.61094880\zeta + 0.12660436\zeta^2 + 0.0091177644\zeta^3}{1 + 0.080618739\zeta} \right]^{\frac{1}{3}}. \quad (3.11)$$

Thus the total pressure would be (including the center of mass motion)

$$P = \frac{NkT}{\Omega} \{1 + Zg(\zeta)\}. \quad (3.12)$$

In the case where the temperature is fixed and  $\Omega \rightarrow \infty$ , the low-density limit, not only does the Debye density go to zero, as required to obtain the ideal Fermi gas limit of Thomas-Fermi theory, but also  $\zeta \rightarrow 0$ . In this case, as  $g(0) = 1$ , (3.12) reduces to (1.1) and thereby supplies an alternate derivation of the low-density limit of Thomas-Fermi theory.

As Huang<sup>8</sup> points out, the internal energy,  $U$ , for this case follows simply from (3.12) as,

$$U = \frac{3}{2}P\Omega. \quad (3.13)$$

Epstein<sup>11</sup> shows from the thermodynamic relation  $dS = (dU + PdV)/T$ , the above results, and Nernst's heat postulate that the entropy of the ideal Fermi gas is simply given by

$$S_e = ZNk \left( \frac{5}{2}g(\zeta) - \log z(\zeta) \right), \quad (3.14)$$

where the limit as  $T \rightarrow 0$  is the limit  $\zeta \rightarrow \infty$  by (3.6) and as Epstein further points out  $S_e \rightarrow 0$  in this limit. If we add the contribution of the motion of the center of mass to the entropy, we get

$$S = Nk \left[ -(Z+1) \log \zeta + \frac{5}{2} + Z \left( \frac{5}{2}g(\zeta) - \log[z(\zeta)/\zeta] \right) \right] + \text{constant}, \quad (3.15)$$

The Helmholtz free energy is now given directly by  $A = U - TS$ . The Gibbs thermodynamic potential is also directly given and is  $G = U - TS + P\Omega$ .

It now remains to give a representation of  $\log z(\zeta) = \log \zeta + \log[z(\zeta)/\zeta]$  to complete the representation of the thermodynamic quantities for the ideal Fermi gas. Since  $\log z \propto \zeta^{\frac{2}{3}}$ , the problem of deriving a representation for  $\log[z(\zeta)/\zeta]$  should be similar to that of the representation (3.11). We give in Table 2 the necessary series coefficients in  $\zeta$  for  $z(\zeta)$  to work on this representation, but we will leave it for the future. Thermodynamic consistency depends on the equation between the two representations

$$g(\zeta) + \zeta g'(\zeta) = \zeta \frac{d \log z(\zeta)}{d\zeta}. \quad (3.16)$$

TABLE 2. The fugacity  $z$  as a series in the de Broglie density

1	1.0000000000	0000000000	0000000000	0000000000	000000000000000000E+000
2	3.5355339059	3273762200	4221810524	2451964241	7968844237018294E-001
3	5.7549910270	1247451636	1707316601	4181450799	416243291041327E-002
4	5.7639604009	1025440341	8852781947	0758923518	58214221729707E-003
5	4.0194941515	2300959555	6172119656	7773364832	0998466829345E-004
6	2.0981898872	2604799054	4860297423	5099614729	957102872728E-005
7	8.6021310842	6030566004	3913343164	3181688359	0277772573E-007
8	2.8647148623	7664872936	8242210245	0573640824	266032220E-008
9	7.9528314678	5241689019	4817612245	1032872937	5035650E-010
10	1.8774425910	0567756220	4988130993	7541387605	437996E-011
11	3.8247968264	1809029592	4653344686	7070280382	2264E-013
12	6.8432943010	1907998578	8027623030	3596055059	29E-015
13	1.0762104093	0537917245	5417733813	6774703889	3E-016
14	1.5124110216	1988369105	9052478125	978137640E	-018
15	2.0715738792	9770436279	3713783632	7032961E-0	20
16	1.3846671521	9900108771	8574969994	14568E-022	
17	5.3288541784	7605238410	1301497951	755E-024	
18	3.5079551301	2368023505	6432045696	E-027	
19	-5.9656175104	9257472195	3065263300	E-027	
20	5.2969138512	2627670501	874181389E	-028	
21	-2.5226985875	2718441504	10473445E-	029	
22	6.0209616883	8744484633	512535E-03	1	
23	1.8543035351	4383646428	76522E-032		
24	-3.0176817670	7158240262	6353E-033		
25	1.8757233170	6238133052	809E-034		
26	-6.7714760730	2256395698	9E-036		
27	3.7182598930	255841378E	-038		
28	1.4954203444	742341364E	-038		
29	-1.2728642729	99667053E-	039		
30	6.0377265821	589225E-04	1		
31	-1.3644496192	99721E-042			
32	-5.3539191733	757E-044			
33	7.8650740191	78E-045			
34	-4.7690907071	0E-046			
35	1.6535692458	E-047			
36	-2.3890246E-0	50			
37	-4.2646358E-0	50			

An alternate procedure would be to determine  $z(\zeta)$  directly from this equation subject to the boundary condition  $\lim_{\zeta \rightarrow 0} z(\zeta)/\zeta = 1$ . This equation is an identity in the exact theory and not an extra condition.

From the theoretical point of view the most satisfactory procedure would be to construct a sufficiently accurate representation of, say, the Helmholtz free energy  $A$  that would provide adequately accurate derivatives  $(\frac{\partial A}{\partial V})_T = -P$ , and  $(\frac{\partial A}{\partial T})_V = -S$ . Using (3.13), (3.15) (ignoring the constant), and integrating (3.16) we have for the Helmholtz free energy,

$$\begin{aligned}
 A &= -P\Omega + (Z+1)NkT \log \zeta + ZNkT \log [z(\zeta)/\zeta] \\
 &= NkT \left[ (Z+1)(\log \zeta - 1) + Z \int_0^\zeta [g(\eta) - 1] \frac{d\eta}{\eta} \right], \quad (3.17)
 \end{aligned}$$

for which the series expansion in  $\zeta$  can be easily derived from Table 1. The inability to assign an absolute entropy for the ordinary ideal gas, leaves  $A$  uncertain by a

linear term in  $T$ . It remains to be seen which of the procedures outlined above are computationally most efficient.

#### 4. COMPARISON OF IDEAL FERMI GAS TO THOMAS-FERMI THEORY

We now show the extent of agreement for aluminum between the ideal Fermi gas and the Thomas-Fermi theory. We use the computer program of D. A. Liberman<sup>12</sup> to compute the T-F numbers. We present the results in the figures as contours of percentage differences (electron properties only).

For the pressure, Figure 1 shows in temperature-density parameter space the 1%, 10%, and 30% contours, as one goes from the top curve of the figure to the bottom, respectively. The expected feature is that for high-temperature and/or low density the ideal gas is accurate. The 10% contour, for example, will serve as our "hot envelope," that is to say, the limit of the validity of the "hot curve" approximation. For low-temperature and high-density the ideal Fermi gas is again a good representation of the T-F theory because the electrons are being forced to the pressure-ionized, degenerate, free electron gas. Since as the density increases the kinetic energy per atom is forced by the Pauli principle to increase proportional to the density to the two-thirds power (relativistic corrections are ignored here) and the potential energy is expected to increase only as the one-third power of density, the free-electron-gas energy becomes dominate. This effect is beginning to be evident in the behavior of the 30% contour. The ranges of temperature and density shown are those of interest for a great many applications. Thus the ideal Fermi gas well reproduces the T-F pressure over a substantial region.

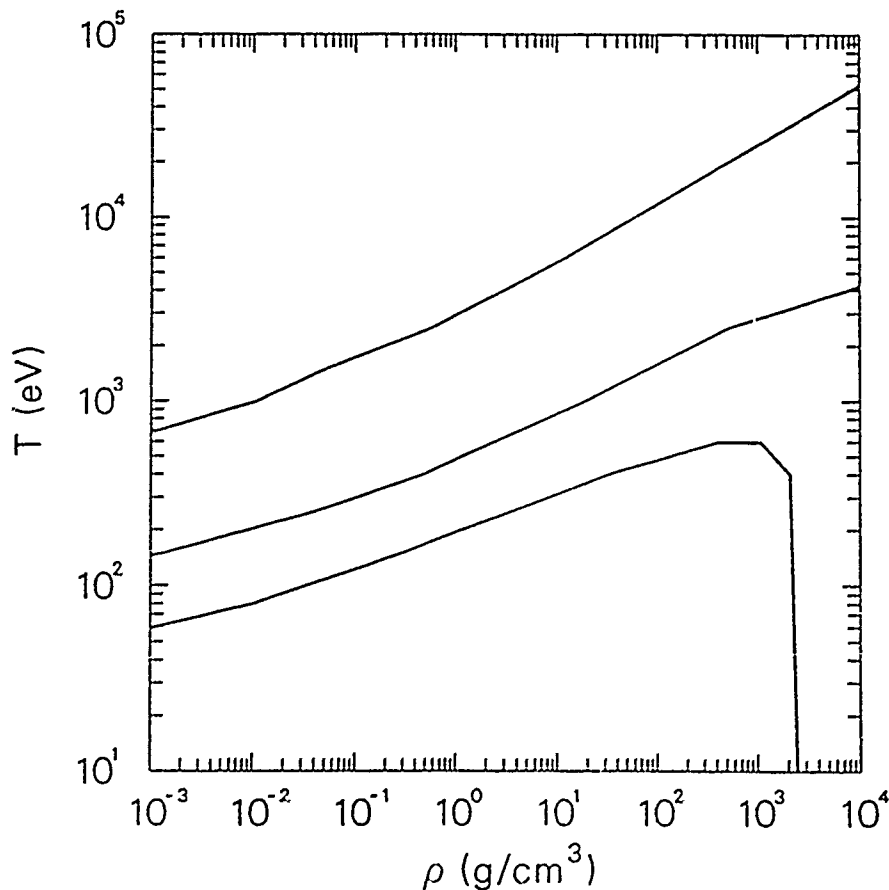


Figure 1. Pressure contours.

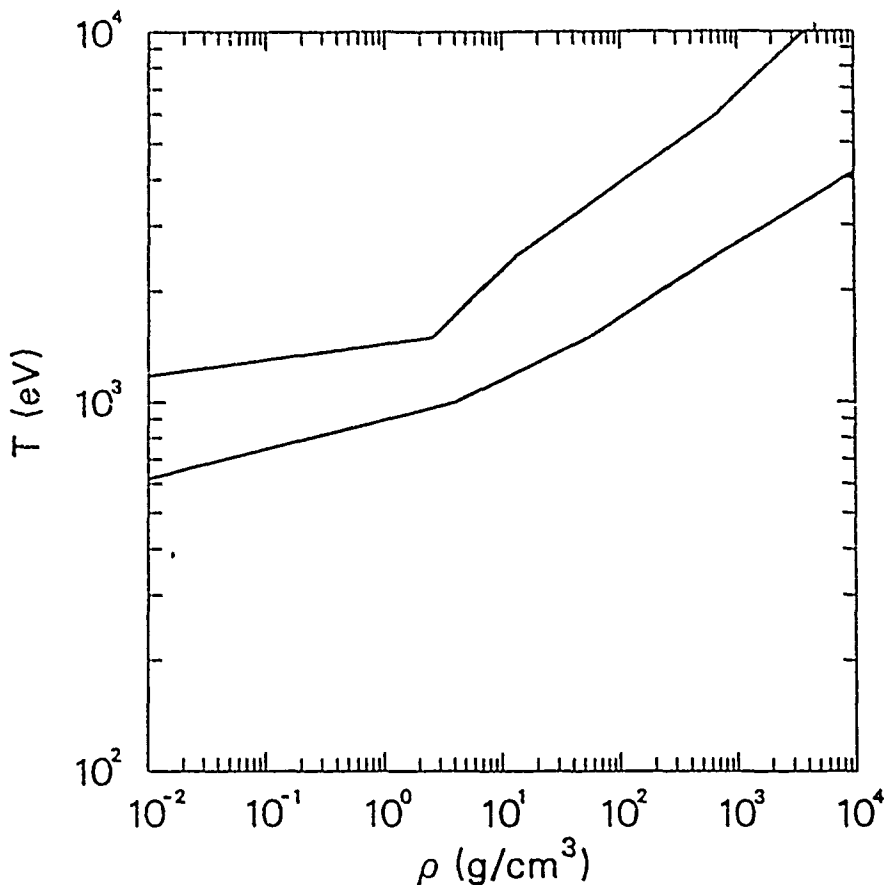


Figure 2. Energy contours.

Figure 2 shows the results for the internal energy. Here we see only the 10% and 30% contours because the ideal Fermi gas does not represent the T-F energy as well as it does the pressure. This result is at least partly due to what, in effect, is an extra term present in the T-F energy and not in the T-F pressure. The bound electrons do not contribute to the pressure but do have a large effect on the energy, for the temperature and density both small. Since the free gas has no bound electrons, there is more difficulty in matching the T-F energy. However, there is again a "hot envelope."

We did one other study that was beyond our original intent. Our goal is really not to find an analytic representation of the T-F theory, but to obtain a fit to the T-F with the zero-temperature isotherm subtracted. Thus it is of interest to compare just such a result to the ideal gas with its zero-temperature isotherm subtracted. We expect an even better correspondence between these pressures, with exact agreement both at low-density/high-temperature and zero temperature. Figure 3 shows again the 1%, 10%, and 30% contours for pressure and indeed there is improvement over Figure 1 with the "hot envelope" now at lower temperatures. We do not show the contours that appear at low temperature as they are not of interest to us in this study. The odd vertical steps arise because really the two contours at that point loop back under themselves and come back to the lower curves due to the forced agreement at zero temperature. We did not put in these loops because we felt that was a misrepresentation of the high-temperature behavior.

The energy contours with zero-temperature isotherm subtracted are not presented because the results did not turn out as well as for the pressure. This result is again caused by the absence of the bound state energy in the free Fermi gas.

In general we see the "hot envelope" and reasonable agreement between the free

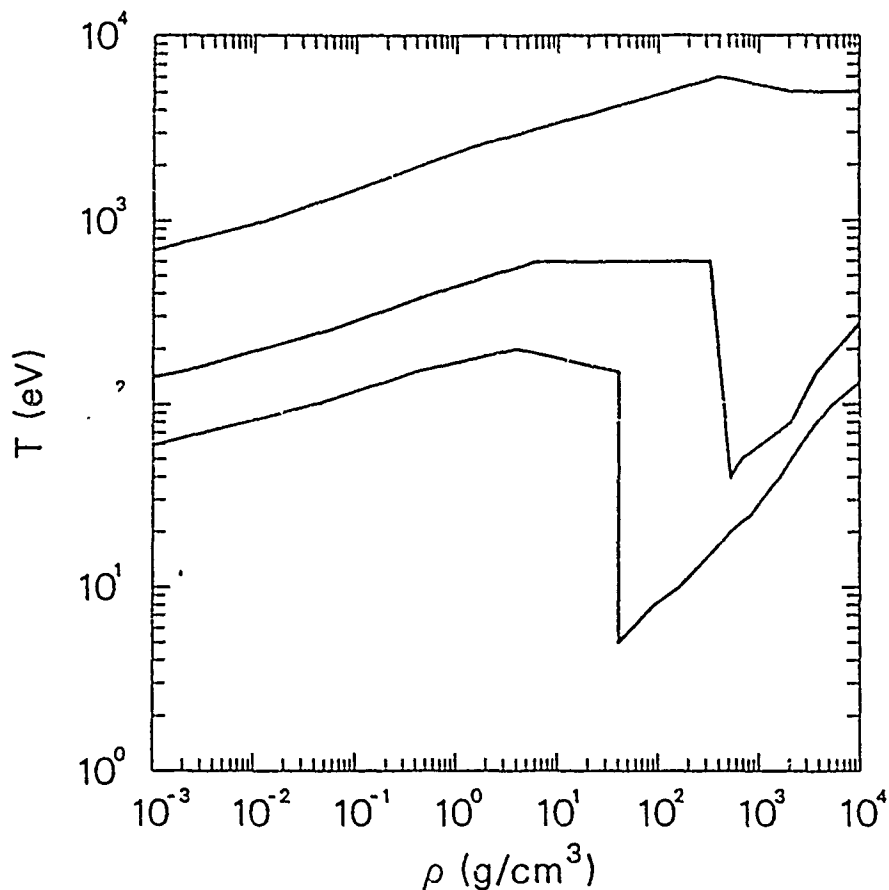


Figure 3. Pressure contours for the zero temperature isotherm subtracted.

Fermi gas and T-F theory for a large region of pressure. We understand the difference between the pressure and internal energy.

This work was performed under the auspices of the U. S. Department of Energy. In addition, one of the authors (G.B.) is happy to acknowledge partial travel support from the U.S. Army Research Office and from Fundunesp to permit his attendance at the *XIII International Workshop on Condensed Matter Theories*.

## REFERENCES

1. L. H. Thomas, Proc. Cambridge Phil. Soc. **23**, 542 (1927); E. Fermi, Z. Physik **48**, 73 (1928).
2. P. A. M. Dirac, Proc. Cambridge Phil. Soc. **26**, 376 (1930).
3. R. P. Feynman, N. Metropolis, and E. Teller Phys. Rev. **73**, 1561 (1949).
4. R. D. Cowan and J. Ashkin, Phys. Rev. **105**, 144 (1957).
5. G. A. Baker, Jr., Am. J. Phys. **27**, 29 (1959).
6. A. S. Eddington, "The Internal Constitution of Stars" (Dover, 1959, New York).
7. N. G. Van Kampen, in "Fundamental Problems in Statistical Mechanics" edited by E. G. D. Cohen (Wiley, 1968, New York) pg. 306.
8. K. Huang, "Statistical Mechanics" (Wiley, 1963, New York).
9. E. T. Copson, "An Introduction to the Theory of Functions of a Complex Variable" (Oxford Univ. Press, 1948, London).
10. G.A. Baker, Jr, "Essentials of Padé Approximants" (Academic, 1975, New York); G. A. Baker, Jr. and P. R. Graves-Morris, "Padé Approximants, Part I: Basic Theory and Part II: Extensions and Applications" part of the "Encyclopedia of Mathematics and its Applications, Vols. 13 & 14" (Cambridge Univ. Press, 1981, London).

11. P. S. Epstein, "Textbook of Thermodynamics" (Wiley, 1937, New York).
12. D. A. Liberman, private communication. This computer code is a straightforward programming of the T-F theory as presented in reference 3.

## ELECTRON CORRELATIONS IN ATOMS

C.E. Campbell<sup>†</sup>, Tao Pang<sup>†</sup>, and E. Krotscheck<sup>‡</sup>

<sup>†</sup> School of Physics and Astronomy

University of Minnesota

Minneapolis, Minnesota 55455, U.S.A.

<sup>‡</sup> Theoretical Physics Institute,

School of Physics and Astronomy, University of Minnesota

Minneapolis, Minnesota 55455

and

Center for Theoretical Physics, Department of Physics

Texas A & M University College Station, Texas 77843, U.S.A.

## INTRODUCTION

Theories of electron correlations in condensed matter systems with a high degree of density variation and/or electron localization may be tested in many-electron atoms and ions, where nearly exact correlation energies are known. We have adapted the inhomogeneous, non-local Feenberg-Jastrow Euler-Lagrange theory developed by Krotscheck and his collaborators<sup>1,2</sup> to apply to atomic systems. Correlation energies for four electron and ten electron closed shell atoms (*Be* and *Ne*, respectively) are in good agreement with the known results. We also calculate the pair correlation functions, which are found to exhibit an extreme sensitivity to the location of the pair of electrons within the atom.

In the next section we define the theory and the approximations which are necessary within the theory. A more complete discussion of this theory in the context of other inhomogeneous quantum fluids is given by Krotscheck *et al.* elsewhere in this volume.

The third section contains the results of this work for *Be* and *Ne*. We conclude with a brief discussion.

The Hamiltonian for an inhomogeneous system is

$$H = -\frac{1}{2} \sum_i^N \nabla_i^2 + \sum_i^N v_1(r_i) + \sum_{i<j} v_2(r_{ij}), \quad (1)$$

where  $v_1(r)$  is the external potential,  $v_2(r_{ij})$  is the two-body potential, and  $N$  is the number of electrons in the system. In the present case,  $v_1(r) = -Z/r$  where  $r$  is the distance to the nucleus, and  $v_2(r) = 1/r$ , where we use atomic units ( $\hbar = c = m = 1$ ), and the nucleus is taken to have an infinite mass.

The Jastrow-Feenberg wave function space is defined by:

$$|\Psi\rangle = \exp \left\{ \frac{1}{2} \left[ \sum_i u_1(r_i) + \sum_{i<j} u_2(r_i, r_j) \right] \right\} |\Phi\rangle \quad (2)$$

where  $|\Phi\rangle$  is a Slater determinant of one body orbitals which are mutually orthonormal, and  $u_1(r)$  and  $u_2(r_i, r_j)$  are the one- and two-body Jastrow pseudopotentials. Each of these functions is determined by functional variation to minimize the energy expectation value,  $E$ :

$$\frac{\delta E}{\delta u_n} = \frac{\delta}{\delta u_n} \frac{\langle \Psi | H | \Psi \rangle}{\langle \Psi | \Psi \rangle} = 0, \quad (n = 1, 2) \quad (3)$$

The optimal  $u_1(r)$  depends solely on the choice of the single-particle orbitals  $\psi_i$  which are solutions of the correlated Hartree-Fock equation:

$$\left[ -\frac{1}{2} \nabla^2 + U_{\text{ext}}(r) + V_H(r) \right] \psi_i(r) + \int d^3r' V_g(r, r') \rho_1(r, r') \psi_i(r') = \epsilon_i \psi_i(r), \quad (4)$$

where  $V_H(r)$  is the generalized Hartree potential,  $V_g(r, r')$  is the exchange/correlation interaction, and  $\rho_1(r, r')$  is the one body density matrix of the wave function.

The two-body Euler-Lagrange equation involves the two-body Jastrow pseudopotential  $u_2(r_i, r_j)$  and the pair distribution function  $g(r, r')$ , defined by

$$g(r_1, r_2) \rho_1(r_1) \rho_1(r_2) = N(N-1) \frac{\int d^3r_3 \dots d^3r_N |\Psi(r_1, \dots, r_N)|^2}{\int d^3r_1 \dots d^3r_N |\Psi(r_1, \dots, r_N)|^2}, \quad (5)$$

where  $\rho_1(r)$  is the one-body density of the system, as well as other diagrammatically defined two-body and three-body functions.

The chief remaining task in the formal theory is to find a tractable relationship between the ingredients of the wave function ( $\Phi$ ,  $u_1(r)$ , and  $u_2(r, r_j)$ ) and the derived quantities such as the density, pair distribution function, exchange/correlation energy, etc. For highly correlated systems, this is achieved using the fermion version of the hypernetted chain resummation (FHNC), which then requires an approximation for manageable calculations. In this work we use the minimal acceptable approximation, FHNC//0, whose chief ingredient is the "direct" two-point distribution function  $g_{dd}(r, r')$ , which is one plus the sum of all direct two-point Born-Mayer type diagrams where there is no exchange between the two external points ( $r, r'$ ) with any internal points. Thus  $g_{dd}(r, r')$  is a renormalized version of  $\exp(u_2(r, r'))$ , and  $\Gamma_{dd}(r, r') = g_{dd}(r, r') - 1$  can be viewed as the dimensionless correlation hole around

a particle at  $\mathbf{r}'$  as a function of  $\mathbf{r}$ . In the FHNC//0 approximation, the pair distribution function is given by

$$g(\mathbf{r}, \mathbf{r}') = [1 + \Gamma_{dd}(\mathbf{r}, \mathbf{r}')] \left\{ g_F(\mathbf{r}, \mathbf{r}') + \frac{1}{\sqrt{\rho_1(\mathbf{r})\rho_1(\mathbf{r}')}} [S_F * \tilde{\Gamma}_{dd} * S_F - \tilde{\Gamma}_{dd}] (\mathbf{r}, \mathbf{r}') \right\}, \quad (6)$$

where  $S_F(\mathbf{r}, \mathbf{r}')$  and  $g_F(\mathbf{r}, \mathbf{r}')$  are the structure factor and pair distribution function of the uncorrelated state  $|\Phi\rangle$ .  $[A * B](\mathbf{r}, \mathbf{r}')$  means the convolution integral of the two two-body functions, and the tilda above a function is defined by  $\tilde{A}(\mathbf{r}, \mathbf{r}') = \sqrt{\rho_1(\mathbf{r})}A(\mathbf{r}, \mathbf{r}')\sqrt{\rho_1(\mathbf{r}'')}$ .

## RESULTS FOR Be AND Ne

The energy of atomic systems is almost entirely accounted for by Hartree Fock. Correlations in electronic systems are significant only for low density regimes, which means the outer part of the atomic systems. The correlation energy  $E_c$  is defined as the difference between the total energy  $E_{TOT}$  and the Hartree Fock energy  $E_{HF}$ :

$$E_c = E_{TOT} - E_{HF} \quad (7)$$

This correlation energy consists of two parts. a positive contribution which comes from the fact that the single particle orbitals  $\psi_i$  are solutions of the *correlated* Hartree-Fock equation, and thus are not the best *uncorrelated* Hartree-Fock orbitals, and the remaining contributions which arise primarily from the difference between the particle-hole interaction and the bare Coulomb interaction, as well as the differences between the fully correlated  $g(\mathbf{r}, \mathbf{r}')$  and the uncorrelated  $g_F(\mathbf{r}, \mathbf{r}')$ . This latter negative quantity exceeds the positive Hartree Fock shift, giving a total negative value for the correlation energy.

This correlation energy is of the order of 1% or less of the total energy. Nevertheless, Clementi and Veillard<sup>3</sup> have obtained this energy from experiments on four and ten electron atomic systems. Their results, shown in the Table, have been corrected for center of mass energy and relativistic effects, and thus can be compared directly to our results for non-relativistic atoms with an infinite mass nucleus. It is seen from the table that our results are in good agreement with these experiments; some differences should be expected from the FHNC//0 approximation, which produces approximately 10% errors in the case of jellium.

*Table:* Correlation energies for Neon and Beryllium atoms in atomic units. a: experimental data<sup>3</sup>; b: present work; c: LSD results<sup>4</sup>; d: generalized gradient expansion of LM<sup>5</sup>; and e: generalized gradient expansion of Perdew<sup>6</sup>.

	a	b	c	d	e
Be	-0.0944	-0.096	-0.224	-0.099	-0.094
Ne	-0.39	-0.33	-0.74	-0.41	-0.39

The density profile of these atoms is very close to the Hartree Fock densities, although the small differences which appear in the low density tail of the atoms is a significant effect in the correlation energies.

Fig. 1a.  $g(r, r')$  in Neon for an electron located at the origin, i.e.  $r' = 0$  a.u.  $x = r\hat{r} \cdot \hat{r}'$  is the projection of  $r$  on  $r'$  and  $y = r \left[ 1 - (\hat{r} \cdot \hat{r}')^2 \right]^{\frac{1}{2}}$ . The atomic center is at the origin. Atomic units are used.

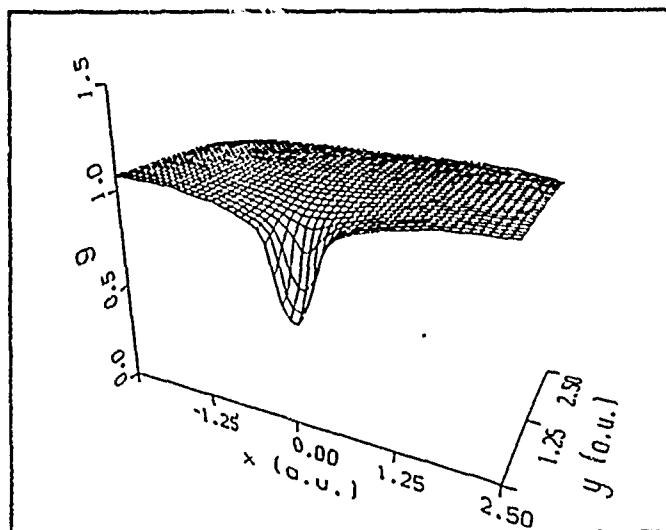


Fig. 1b. Same as Fig. 1a for a particle located a distance 1 a.u. from the nucleus

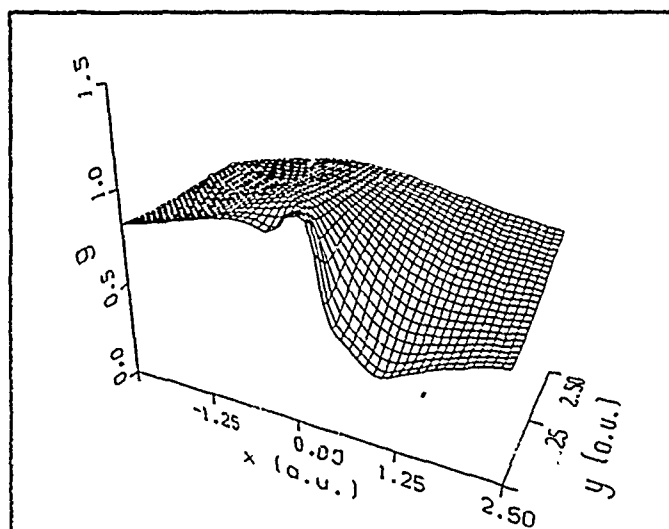


Fig. 1c. Same as Fig. 1a for a particle located at a distance 2 a.u. from the nucleus.

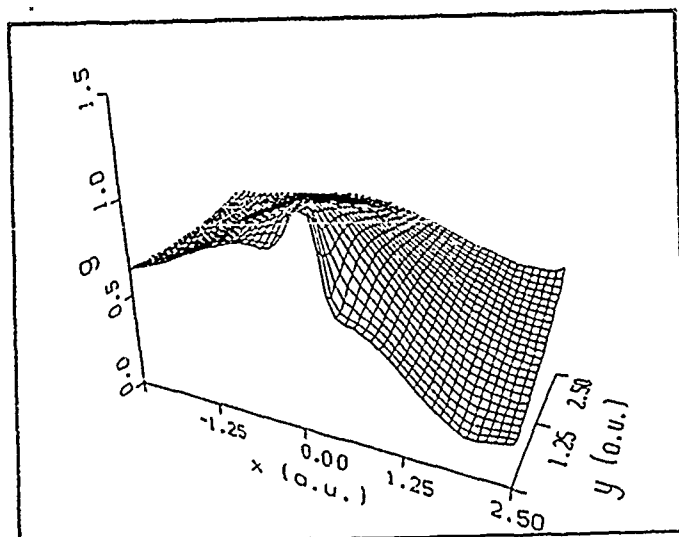


Fig. 2a. Same as Fig. 1b for the Hartree-Fock approximation  $g_F(r, r')$ .

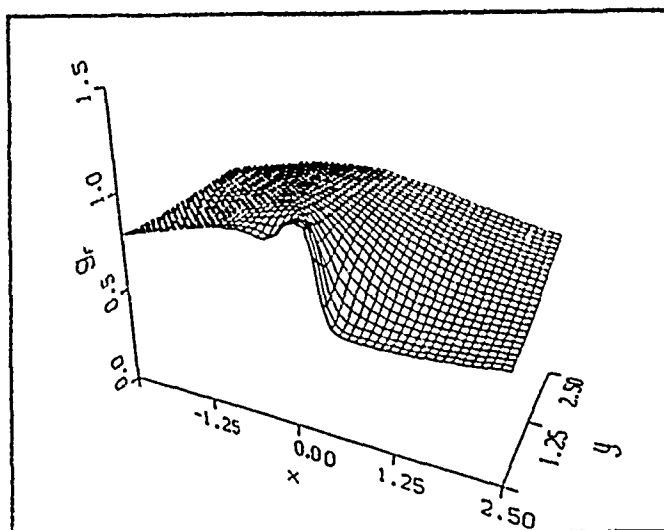
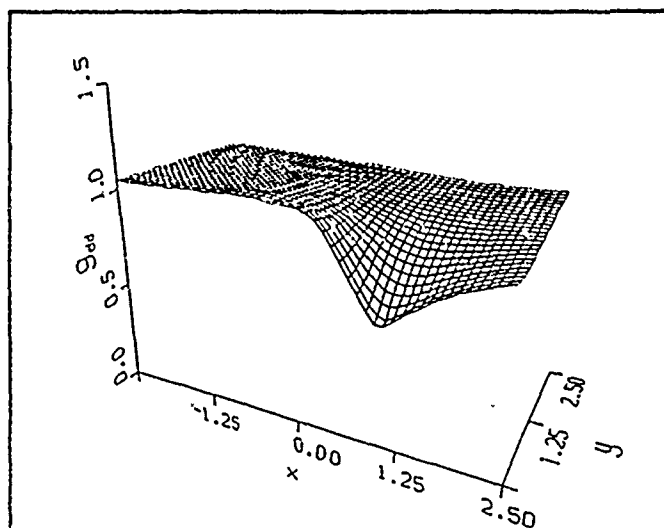


Fig. 2b. Same as Fig. 1b for the correlation contribution  $g_{dd}(r, r') = 1 + \Gamma_{dd}(r, r')$ .



The pair distribution function is a familiar tool for examining two-body correlations in classical and quantum fluid systems, and gives a similar but more complex view of these correlations in inhomogeneous systems. The spherical symmetry of closed shell atomic systems simplifies the exhibition of this structure somewhat. Thus  $g(r, r')$  depends only on the distances  $r$  and  $r'$  from the origin and the angle between the two vectors. In Figure 1 we present this function as a function of  $r$  for fixed  $r'$ , where the origin (the nucleus) and  $r'$  define the  $x$  axis, and  $g(r, r')$  is plotted above the plane defined by  $r$  and  $r'$ . (For the spherical atom, all such planes are equivalent). It can be seen in Figure 1 that the exchange-correlation hole (the depression of the value of  $g(r, r')$  as  $r$  approaches  $r'$ ) becomes increasingly important as  $r'$  increases into the low density tail of the atom. Of course even the Hartree Fock result must contain an exchange hole by the Pauli principle, so the question of how much of the exchange-correlation hole can be attributed to exchange (i. e., statistical correlations) and how much to correlation (i.e., dynamical correlations) requires further examination. Fortunately, as Eq. 6 shows, these effects factor to a very good approximation. Thus  $g(r, r')$  is approximately the product of  $g_{dd}(r, r')$  and  $g_F(r, r')$ , where the former is dominated by dynamic correlations and is 1 if the two-body interaction vanishes, and the latter

is the free particle pair distribution function, therefore containing only statistical correlations. These two quantities and  $g$  are each shown in a particular case in Figure 2, where it is seen that these two factors each make their own distinct contribution to the exchange-correlation hole as well as the rest of the two-body structure.

One version of the local density approximation is obtained by approximating  $g(\mathbf{r}, \mathbf{r}')$  by  $g_J(|\mathbf{r} - \mathbf{r}'|, \langle \rho \rangle_{\mathbf{r}, \mathbf{r}'})$ , where  $g_J(r, \rho)$  is the pair distribution function for jellium at density  $\langle \rho \rangle_{\mathbf{r}, \mathbf{r}'}$ , which is some representative density in the vicinity of the two points  $\mathbf{r}, \mathbf{r}'$ , e.g., the geometric or arithmetic average of  $\rho(\mathbf{r})$  and  $\rho(\mathbf{r}')$ . It is clear from the figures that these approximations are not appropriate for  $g(\mathbf{r}, \mathbf{r}')$ ; indeed, it also fails for  $g_F(\mathbf{r}, \mathbf{r}')$ .

## DISCUSSION

Small atoms provide one of the most stringent tests of a theory of electron correlations, since the density falls very rapidly to zero away from the nucleus. Consequently our results for neon and beryllium are very encouraging. Preliminary results for other closed shell four and ten electron systems ( $Ne^{+6}$ ,  $Mg^{+2}$ , and  $Ca^{+10}$ ) are similarly encouraging. In principle, the theory can also be applied to open shell systems; however the lack of spherical symmetry will require additional effort.

It is abundantly clear in these simple systems that the local density approximation is inadequate for the correlation energies. This was expected by those who introduced this approximation<sup>7</sup> and was demonstrated by comparisons between LDA theories<sup>4</sup> and experiments for the four and ten electron closed shell atoms as is seen in the Table. It is also seen there that adjusted gradient expansions<sup>5,6</sup> give agreement with experiment which is comparable to our theory. However it was necessary in each of these gradient expansions to fit the data either at one atom (Perdew<sup>6</sup> adjusts his theory to fit  $Ne$ ) or to several systems (Langreth and Mehl<sup>5</sup>, who fit  $Be$ ,  $Ne^{+6}$ , and  $Ne$ ); an unadjusted gradient expansion actually gives worse agreement with experiment than the LDA. Thus we conclude that the Jastrow Euler-Lagrange theory is a very promising method for including non-local density effects in atomic and molecular systems.

Since this theory is also a theory of the pair distribution function, it provides much information about the two-body structure of the system, and permits a fairly clean separation between dynamic correlations and statistical correlations.

## ACKNOWLEDGEMENTS

We would like to thank Professor V. Aguilera-Navarro for organizing this stimulating workshop, and the Army Research Office for travel support in conjunction with this workshop. This research was supported in part by the National Science Foundation, the Robert A. Welch Foundation, the Theoretical Physics Institute of the University of Minnesota, the Graduate School of the University of Minnesota and the Minnesota Supercomputer Institute. One of us (EK) would like to thank the Theoretical Physics Institute of the University of Minnesota for warm hospitality.

## REFERENCES

1. E. Krotscheck, Phys. Rev. B31, 4258 (1985).
2. E. Krotscheck and W. Kohn, Phys. Rev. Lett. 57 (1986) 862; E. Krotscheck, G.-X. Qian, and W. Kohn, Phys. Rev. B32 (1985) 5693.
3. E. Clementi, J. Chem. Phys. 38 (1963) 2248; A. Veillard and E. Clementi, J. Chem. Phys. 45 (1968) 2415.
4. Y. Tong and L. J. Sham, Phys. Rev. 144 (1966) 1.
5. D. C. Langreth and M. J. Mehl, Phys. Rev. B28 (1983) 1809.
6. J. Perdew, Phys. Rev. B33 (1986) 8822.
7. W. Kohn and P. Vashishta, in *Theory of the inhomogeneous electron gas*, p. 79 ff, edited by S. Lundqvist and N. H. March (Plenum, N.Y. 1983).

## CORRELATED RPA CALCULATIONS FOR MODEL NUCLEAR MATTER

Eirene Mavrommatis

Physics Department, University of Athens  
Panepistimioupoli, 15771 Athens, Greece

John W. Clark

McDonnell Center for the Space Sciences  
and Department of Physics  
Washington University, St. Louis, Missouri 63130

### INTRODUCTION

One of the most exciting prospects on the current nuclear scene is the promise that precision high-energy electron scattering experiments will reveal new (and perhaps unforetold) aspects of nuclear structure and dynamics. The search is on for distinctive signatures of subnucleonic degrees of freedom, and especially for manifestations of the underlying quarkic substructure of nuclei. However, to reach any definite conclusions regarding such effects, it is necessary that we know, with precision, the values which are predicted for the measured quantities by the conventional picture of nuclei. In the conventional picture, a nucleus is composed of nucleons alone, moving nonrelativistically. The nucleonic constituents are considered to interact via bare potentials which reproduce the few-nucleon data while obeying certain constraints imposed by fundamental symmetries and by meson-exchange theory. Even at this rather superficial level, one is confronted with a very difficult many-body problem, essentially nonperturbative because of the strong short-range interactions among the nucleons. It should therefore be no surprise that mean-field theory (in old language, the shell model) fails in experimental settings where large momentum transfers take place and the high-momentum components of the nuclear wave function are being probed. A proper understanding of the quantitative implications of the conventional nuclear picture requires a careful and coherent treatment of the fine-scale spatial correlation structure and the collective properties which emerge from solution – or approximate solution – of the many-nucleon Schrödinger equation of the nucleus. Only when this refined microscopic description is achieved, and the conventional picture still found wanting, can a legitimate claim be made that the relevant experiments have penetrated to a more fundamental level of nuclear hadronic dynamics.

One focal point of the ongoing refinement of conventional nuclear theory is the longitudinal response function  $R_L(q, \omega)$  of heavy nuclei in the quasielastic regime. In treating this property, mean-field theory has proven inadequate and it is necessary (but perhaps not sufficient) to incorporate the dynamical correlations among nucleons in a consistent and accurate manner. A microscopic understanding of the dynamic structure function  $S(q, \omega)$  of the hypothetical problem of infinite, symmetrical nuclear matter should yield valuable

insights into the effects of correlations in the observed longitudinal response. In particular, Fantoni and Pandharipande<sup>1</sup> have argued for an approximate proportionality of  $R_L(q, \omega)$  and  $S(q, \omega)$  at large  $q$ , the proportionality factor being given by the absolute square of the proton form factor (see also Ref. 2).

The work of Fantoni and Pandharipande<sup>1</sup> and Fabrocini and Fantoni,<sup>2</sup> based on the method of correlated basis functions (CBF),<sup>3,4</sup> represents a substantial advance over all previous efforts on this problem, providing state-of-the-art evaluation of the longitudinal response function of nuclear matter (and more directly, its dynamic structure function  $S(q, \omega)$ ), with a realistic two-nucleon interaction and simulated three-body potential as input. Within the CBF scheme, the calculation was performed, roughly speaking, at the Tamm-Dancoff level. The correlated random-phase approximation<sup>5,6,4</sup> (CRPA), which performs the ring sums within CBF perturbation theory, opens the way for considerable improvement of some aspects of this calculation, particularly at the lower momentum transfers where the effects of the particle-hole force are most evident. In this paper we present an initial application of CRPA theory to infinite nuclear matter. The goals of the calculation are modest: Preliminary to a full calculation with a realistic nucleon-nucleon interaction with elaborate state-dependence, we shall explore the predictions of CRPA for a simplified model of the nucleon-nucleon interaction which has frequently been used as a test case, namely the  $v_2$  potential.<sup>7</sup> Moreover, we shall apply a simplified, local version of CRPA which has proven successful in applications to spin-polarized liquid  ${}^3\text{He}$  and the electron gas. It is found that this approach already leads to results of qualitative or semi-quantitative value, which may be systematically improved as the techniques of CRPA, and more generally the CBF theory of dynamical response, are further developed.

In a broader context, microscopic evaluation of the density-density response function  $\Pi(\sigma, \omega)$  of nuclear matter (whose imaginary part gives  $S(q, \omega)$ ), together with consistent evaluation of the self-energy  $\Sigma(k, E)$ , yield fundamental information about the elementary excitations of this hypothetical hadronic system. The properties of collective modes, typified by the zero-sound dispersion relation, may be extracted from  $\Pi(q, \omega)$ , while the nature of single-particle excitations is revealed by  $\Sigma(k, E)$ , from which one may derive an energy-dependent effective mass. These properties have obvious importance for a deeper understanding of nuclei. They are likewise basic to a description of the structure, dynamics, and thermal history of neutron stars – being essential to the evaluation of such quantities as the specific heat, viscosity, superfluid gap, etc. Since empirical constraints on the properties of neutron-star material are limited in the extreme, such astrophysical applications make it doubly important to hone and test our many-body calculational methods.

#### LOCAL CORRELATED RANDOM-PHASE APPROXIMATION

The correlated random-phase approximation (CRPA) extends ordinary RPA to strongly-interacting systems like liquid  ${}^3\text{He}$ , nuclear matter, and nuclei. Since this approach has been developed in detail in other places,<sup>5,6,4,8,9</sup> we shall only describe its main features and display the working formulas of a local approximation proposed by Krötschek.<sup>6</sup> Here, “local” implies that the particle-hole force is taken to depend only on the momentum transfer  $\hbar q = |\mathbf{p} - \mathbf{h}|$  in the direct particle-hole channel (apart from momentum-conserving delta functions). We confine our attention to the uniform, infinite Fermi medium, for which the appropriate model states are Slater determinants of plane waves, and complete the specification of the underlying correlated basis by the adoption of a Jastrow correlating factor  $F = \prod_{i < j} f(r_{ij})$ .

In terms of an irreducible particle-hole ( $ph$ ) interaction  $U$  which CBF theory generates for a given bare (and possibly singular) two-body potential, correlated RPA for our problem looks exactly like the familiar RPA for a weak potential, aside from a minimal energy dependence of  $U$  which can usually be ignored. Implementation of the full CRPA

approach including exchange nonlocalities is in principle straightforward, but in practice requires considerable numerical effort, entailing (for example) discretization of the matrix eigenvalue equations on a grid in momentum space.<sup>8</sup> To provide a simpler alternative, Krotscheck<sup>6</sup> has constructed a *local, energy-independent* approximation to  $U$  which is designed to preserve certain fundamental relations of the ingredients of  $U$  to the static structure function  $S(q)$  of the Jastrow ground-state trial function and to its graphical derivative  $S'(q)$ . One of these relations is the optimization condition on the Jastrow pair correlation function  $f(r)$ , which reads

$$\frac{\delta \langle H \rangle_o}{\delta \ln f^2(r)} \equiv \Delta(r) = 0 \quad . \quad (1)$$

In this expression,  $\langle H \rangle_o$  is the energy expectation value in the Jastrow trial ground state  $\Pi f(r_{ij})\Phi_o$ , where  $\Phi_o$  represents the noninteracting Fermi sea. The proposed local approximation to the particle-hole interaction is simply

$$U(q) = \Delta(q)S^{-2}(q) + \frac{\hbar^2 q^2}{4m} [S^{-2}(q) - S_F^{-2}(q)] \quad , \quad (2)$$

where  $S_F(q)$  is the static structure function of the noninteracting Fermi gas and

$$\Delta(q) = \rho \int d^3 r \exp(i\mathbf{q}\cdot\mathbf{r}) \Delta(r) = \frac{\hbar^2 q^2}{4m} [S(q) - 1] + S'(q) \quad . \quad (3)$$

The Jastrow  $S(q)$  entering (2)-(3) may be evaluated with good accuracy by solving the (nonlinear) FHNC/C equations, while its graphical derivative  $S'(q)$ , appearing in (3), may be obtained by solving the (linear) FHNC/C' equations.<sup>10</sup> The vanishing of  $\Delta$  is equivalent to the optimization condition. Hence for *optimal* Jastrow correlations the particle-hole force  $U(q)$  depends only on  $S(q)$  and properties of the noninteracting system. For optimal correlations, the choice (2) for  $U(q)$  is just what is needed to regain  $S(q)$  from the density-density response function through the fluctuation-dissipation theorem, if the collective approximation  $\Pi_o^c = (\hbar^2 q^2 / m) [\hbar^2 \omega^2 - (\hbar^2 q^2 / 2m S_F(q))^2]^{-1}$  is used for the particle-hole propagator.<sup>6,11</sup>

Having adopted a local particle-hole force, one has quite standard algebraic RPA formulas which lead to the familiar RPA expressions for the density-density response function and self-energy<sup>12,13</sup>:

$$\Pi(q, \omega) = \frac{\Pi_o(q, \omega)}{1 - U(q)\Pi_o(q, \omega)} \quad , \quad (4)$$

$$\Sigma(k, \Omega) = U(0) + U_{\text{Fock}}(k) + \frac{i\hbar}{(2\pi)^4 \rho} \int d^3 q d\Omega' G_o(\mathbf{k}-\mathbf{q}, \Omega-\Omega') U^2(q) \Pi(q, \Omega) \quad . \quad (5)$$

In (4), the response function  $\Pi_o(q, \omega)$  is the particle-hole propagator of the free Fermi gas, i.e., the Lindhard function. In (5),  $G_o$  is the free single-particle Green's function,  $U_o$  is a constant (related to the chemical potential), and  $U_{\text{Fock}}(k)$  is the Fock term of the particle-hole force  $U(q)$ .

The dynamic structure function and the properties of zero sound (if present) are derived from the relation (4) in the usual manner. Trivially,

$$S(q, \omega) = -\frac{1}{\pi} \text{Im} \Pi(q, \omega) \quad . \quad (6)$$

The zero-sound dispersion relation  $\omega = \omega_{zs}(q)$  is determined by the roots of the denominator of (4), i.e. the roots of

$$1 - U(q) \text{Re} \Pi_o(q, \omega) = 0 \quad (7)$$

in the region where  $\text{Im } \Pi_o(q, \omega) = 0$ . The strength  $Z_{zs}$  of the zero-sound mode is given by

$$Z_{zs}^{-1}(q) = U^2(q) \left[ \frac{d}{d\omega} \text{Re } \Pi_o(q, \omega) \right]_{\omega=\omega_{zs}} \quad (8)$$

Note that we are considering only the density channel; more generally a spin-isospin decomposition can be made, and collective modes other than zero sound can be studied.

A version of the single-particle energy spectrum can be obtained from the self-energy (5) using the on-shell prescription

$$\epsilon_k = t_k + \Sigma(k, \Omega), \quad \Omega = t_k = \hbar^2 k^2 / 2m. \quad (9)$$

The on-shell effective mass  $m^*$  is then given by

$$(m^*)^{-1} = k^{-1} d\epsilon_k / dk \quad (10)$$

A qualitative shortcoming of the local correlated RPA (LCRPA), seen in the form (4) of the polarization propagator, is that the effects of dynamical correlations on the *continuous* portion of  $S(q, \omega)$ , in regions of the  $(q, \omega)$  plane where  $\Pi_o(q, \omega)$  vanishes, are not accessible. It is in fact just such effects which were examined many years ago by Czyz and Gottfried.<sup>14</sup> Thus any useful comparison with their work is precluded. Although the  $(q, \omega)$  domain corresponding to individual  $1p\ 1h$  excitations is the same in LCRPA as in the free system, the RPA denominator in expression (4) introduces nontrivial correlation effects in that region; moreover, outside that region, for  $\text{Im } \Pi_o(q, \omega) = 0$ , zero sound may emerge as a distinct collective mode, corresponding to vanishing of the denominator.

Local CRPA will also suffer, at a quantitative level, from the static nature of the effective interaction  $U(q)$  appearing in (4). By contrast, dynamic screening is known to be important in the electron gas at metallic densities.<sup>15</sup> Moreover, one does not expect the momentum dependence of the self-energy to be faithfully predicted within the LCRPA scheme, especially in the very delicate example of unpolarized liquid  $^3\text{He}$  (Ref. 11). In spite of its shortcomings, LCRPA offers a simple and straightforward microscopic touchstone for phenomenological theories of comparable structure, such as the polarization-potential model.

In the polarization-potential approach of Aldrich and Pines,<sup>16</sup> which has been adapted to nuclear problems by Pines, Quader, and Wambach,<sup>17</sup> the density-density response function  $\Pi(q, \omega)$  is expressed in a form similar to (4). However, the Lindhard function appearing in (4) is replaced by a more complicated propagator accounting both for a single-pair effective mass different from the bare value and for the presence of multipair excitations. Secondly, the static, local particle-hole interaction  $f_s^i(q)$  of this approach is supplemented by a wave-vector and frequency-dependent contribution  $(\omega^2/q^2)f_v^i(q)$  corresponding to backflow. Beyond these structural differences there is the important conceptual distinction that our particle-hole interaction is determined microscopically, whereas the polarization potentials of the Aldrich-Pines theory are determined by a combination of sum rules and phenomenology.

## RESULTS FOR $\nu_2$ HOMEWORK MODEL

Based on the local correlated RPA scheme, we have carried out a numerical study of the dynamical response of a model of nuclear matter which is extremely simple, yet may capture important aspects of its correlation structure. The bare interaction between the nucleons is taken as the  $\nu_2$  "homework-model" potential.<sup>7</sup> This two-nucleon potential consists of the central part of the  $^3S_1 - ^3D_1$  component of the Reid soft-core interaction, assumed to act in *all* partial waves. It has seen wide use in tests of many-body methods (see, for example, Refs. 18,19). Specifically,

$$v_2(r) = [9924.3\exp(-4.2r) - 3187.8\exp(-2.8r) + 105.468\exp(-1.4r) - 10.463\exp(-0.7r)]/(0.7r) \quad (11)$$

Our calculations are based, primarily, on the parameterized Jastrow correlation factor

$$f(r) = \exp[-Ae^{-Br}(1 - e^{-r/D})/r] \quad (12)$$

with parameters which minimize the Jastrow ground-state energy expectation value  $E_J$  at single-particle level degeneracy  $\nu = 4$  and given density,  $E_J$  being computed by the Metropolis Monte Carlo algorithm.<sup>20</sup> Additionally, we have examined the particle-hole force generated by two versions of the correlation function

$$f(r) = (1 - e^{-r^2/b^2})^n + gr^m e^{-r^2/\gamma^2} \quad (13)$$

studied by Benhar *et al.*<sup>21</sup> In the simpler version (B1), the parameter  $g$ , which measures the overshoot of  $f(r)$  above unity, is set zero and the remaining parameters  $b$  and  $n$  fixed by minimization of the energy expectation value truncated at three-body cluster order. In the other version (B2), the three-body cluster approximation to the energy is minimized (approximately) with respect to the five parameters  $b$ ,  $g$ ,  $\gamma$ ,  $m$  and  $n$ , subject to the sequential (or normalization) condition<sup>22</sup> as constraint.

The three correlation functions are labeled (in order) C, B1, and B2. None of these choices is optimal in the sense of being a solution of the Euler equation (1). The sequential condition imposed in the case of B2 is probably too stringent, while B1 is presumably too crude a choice, although both alternatives have the virtue of promoting good convergence of the cluster expansion of the Jastrow energy expectation value. The function C, being determined through a Monte Carlo evaluation, may provide a decent representation of the true optimal function, except in the large- $r$  region which contributes little to the ground-state energy. The deviation at large  $r$  will, however, be reflected in the behavior of  $U(q)$  at small  $q$ . In particular, it will produce a significant departure of  $\Delta(q)$  from zero at low  $q$  values. In the present work, as in Ref. 9, we have chosen to set  $\Delta(q)$  equal to zero, since the behavior of the  $U(q)$  at small  $q$  is already suspect due to the local approximation itself. This conforms with a strategy suggested by Krotscheck,<sup>6</sup> who, in considering the Bijl-Feynman dispersion relation, found that it is a better approximation to assume that the correlation function has been optimized – even if the actual optimization has not been carried through – than to include the  $\Delta(q)$  correction.

Numerical results with the C correlations have been obtained for symmetrical nuclear matter, i.e., level degeneracy  $\nu = 4$ , at  $k_F = 1.39 \text{ fm}^{-1}$ , corresponding to a density  $\rho = 0.182 \text{ fm}^{-3}$  near nuclear saturation; and for pure neutron matter, i.e.,  $\nu = 2$ , at  $k_F = 1.75, 2.25, 2.90 \text{ fm}^{-1}$ , corresponding to three densities  $\rho = 0.182, 0.386, 0.822 \text{ fm}^{-3}$  of relevance to the study of neutron stars. For both level degeneracies we have examined a range of wave-number transfers  $q$  from 0 to about  $4 \text{ fm}^{-1}$ . Results with B1 and B2 correlations are available only for symmetrical nuclear matter, at Fermi wave number  $k_F = 1.4 \text{ fm}^{-1}$ .

For reference, we have also generated nuclear-matter ( $\nu = 4$ ) results for the case that the two nucleon interaction is replaced by a pure hard-core potential of core radius  $c = 0.5 \text{ fm}$ . As in an earlier calculation,<sup>9</sup> where  $c = 0.4 \text{ fm}$  was studied, the simple form

$$f(r) = 0 \quad , \quad r \leq 0 \quad , \\ = 1 - \exp[-\mu(r - c)] \quad , \quad r > c \quad (14)$$

is assumed for the Jastrow pair correlation function. An optimal determination of the parameter  $\mu$  has been carried out by Flynn<sup>23</sup> within the FHNC/C approximation, for both core sizes ( $c = 0.4$  and  $0.5 \text{ fm}$ ).

We confine our discussion to a selection of results for symmetrical nuclear matter. (A more detailed report will be published elsewhere.) The CBF particle-hole interaction appropriate to the  $v_2$  potential at  $k_F = 1.39 \text{ fm}^{-1}$ , for the C choice of  $f(r)$ , is shown in Fig. 1, along with the  $c = 0.5 \text{ fm}$  hard-sphere result at the same density. Due to the difference between the respective correlation functions (the  $v_2$  correlations being slightly stronger beyond 1 fm), the particle-hole force for  $v_2$  is actually somewhat more repulsive at low-to-medium  $q$ 's than that for the hard-core potential. Both potentials support a collective mode corresponding to zero sound. In both cases, this mode is found to emerge from the particle-hole continuum around  $0.3\text{-}0.4 \text{ fm}^{-1}$  and sink back into it at about  $1.53 \text{ fm}^{-1}$ . The zero-sound dispersion relation  $\omega_{zs}(q)$  and the strength  $Z_{zs}(q)$  of the zero-sound mode are plotted in Fig. 2, for the  $v_2$  potential. The corresponding curves for the hard-core potential are nearly coincident with those for  $v_2$ .

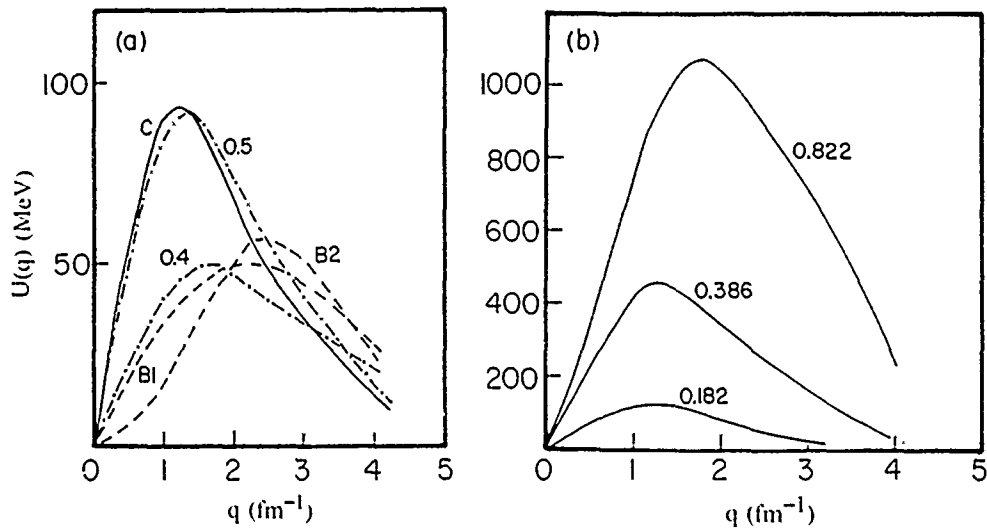
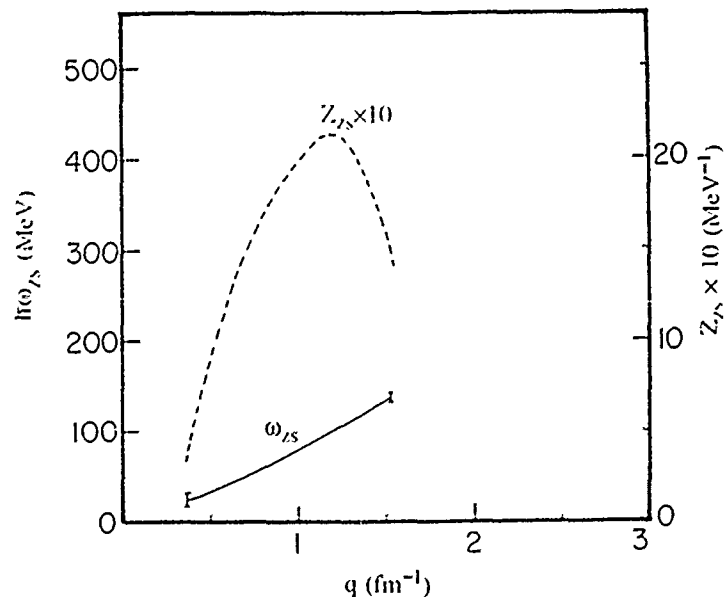


Fig. 1. Wave-number dependence of local particle-hole interaction  $U(q)$  for  $v_2$  model of nuclear matter, based on correlation functions C, B1, and B2 (as labeled); and for hard-sphere nucleons with  $c = 0.4$  and  $0.5 \text{ fm}$  (as labeled), based on optimized correlation function (14). Density near  $0.18 \text{ nucleons/fm}^3$ .

Fig. 2. Zero sound dispersion relation  $\omega_{zs}(q)$  (solid curve) and wave number dependence of zero sound strength  $Z_{zs}(q)$  (dashed), for  $v_2$  model of nuclear matter at  $k_F = 1.39 \text{ fm}^{-1}$ , based on C correlation function.



It may seem surprising that the effective interaction derived from the soft-core  $v_2$  potential is so close to that for the hard-core potential. The concurrence implies that the two potentials are similarly effective in lifting particles from below to above the Fermi surface, at least when the momentum transferred to the particle-hole pair is not excessive and the density is near the saturation value for nuclear matter. In turn this observation suggests that a useful measure of the strength of the particle-hole force may be furnished by the wound parameter of Brueckner theory, which may be interpreted as the average depletion of the Fermi sea produced by the given bare interaction. Indeed, the wound parameters for the two potentials ( $v_2$  and  $c = 0.5$  fm hard core) are quite similar. As is well known,<sup>18</sup> the Jastrow variational analog of the Brueckner wound parameter is  $\kappa = \rho \int d^3r [f(r) - 1]^2 [1 - v^{-1} l^2(k_F r)]$ , where  $l(x) = 3x^{-3}(\sin x - x \cos x)$ . For the C choice of the correlation function, we have  $\kappa = 0.232$ , which is to be compared with the value  $\kappa = 0.263$  for correlation function (14) with  $\mu = \mu_{\text{opt}} = 2.5 \text{ fm}^{-1}$ .

We may carry these considerations somewhat further by examining the curves in Fig. 1 labeled B1 and B2. The particle-hole force  $U(q)$  for B1 or B2 is seen to differ substantially from that corresponding to correlation function C, being much weaker at smaller  $q$  values (below  $2 \text{ fm}^{-1}$ ) and somewhat stronger at large  $q$ . The large differences cannot be due to the slight discrepancy in densities ( $0.185 \text{ fm}^{-3}$  (B1 and B2) compared to  $0.182 \text{ fm}^{-3}$  (C)). Instead, it must be a reflection of the reduction in the flexibility of  $f(r)$  entailed by a procedure employing a truncated cluster expansion, the range of variation being restricted to functions for which the cluster expansion of the energy is rapidly convergent. The substantial difference in predictions for  $U(q)$  is (as expected) accompanied by substantial differences in the wound parameters for B1 and B2, from those for the correlation function C. The specific values are  $\kappa = 0.146$  (B1) and  $\kappa = 0.143$  (B2). Our thesis that the wound parameter is a major determinant of the overall behavior of  $U(q)$ , gains additional support from the observation that correlation functions B1 and B2, with approximately the same wound parameters, yield  $U(q)$  results which are quantitatively as well as qualitatively similar. To complete the comparison, we have included in Fig. 1 a  $U(q)$  curve for a  $c = 0.4$  fm hard-sphere interaction at  $k_F = 1.39 \text{ fm}^{-1}$ , described by means of the correlation function (14) with  $\mu = \mu_{\text{opt}} = 3 \text{ fm}^{-1}$ . The corresponding wound parameter is  $\kappa = 0.139$ . Once again it is seen that correlation functions with similar wound parameters yield similar results for the particle-hole force  $U(q)$ .

The discussion now focuses on the results obtained for the C choice of correlations. The dynamic structure function  $S(q, \omega)$  of the  $v_2$  model of nuclear matter, derived from the LCRPA treatment, is plotted as a function of energy transfer  $\hbar\omega$  in Figs. 3-6, at fixed  $q$  values of  $1.47, 2.03, 2.76,$  and  $3.87 \text{ fm}^{-1}$ , respectively. These choices for  $q$  are close to values at which experimental data on the longitudinal response function  $R_L(q, \omega)$  of medium- and large- $A$  nuclei are available<sup>24-26</sup> and/or are (reasonably) close to  $q$  values examined in the microscopic calculation of Fantoni and Pandharipande.<sup>1</sup> In the figures we trace, for comparison, the Fermi-gas structure function  $S_F(q, \omega)$  as well as the LCRPA result for the  $c = 0.5$  hard-core. It has been argued by Fantoni and Pandharipande that the longitudinal dynamic structure function  $S_L(q, \omega)$  of nuclear matter should not be very different from  $S(q, \omega)$  over the range  $q = 1.5-2.8 \text{ fm}^{-1}$ , and, accordingly, that the theoretical nuclear-matter  $S(q, \omega)$  multiplied by the square of a suitably chosen proton form factor, may be sensibly compared with the experimental response function  $R_L(q, \omega)$  of heavy nuclei (cf. also Refs. 2,27). At a deeper level, such comparisons exploit the generally accepted view that meson-exchange currents, pion production, delta excitation, etc., should not be very important in the *longitudinal* response function, for the  $q$  values considered here.<sup>28</sup> In this view one must look elsewhere for a dramatic breakdown of the conventional picture of the nucleus as a nonrelativistic many-body problem with only nucleonic degrees of freedom.

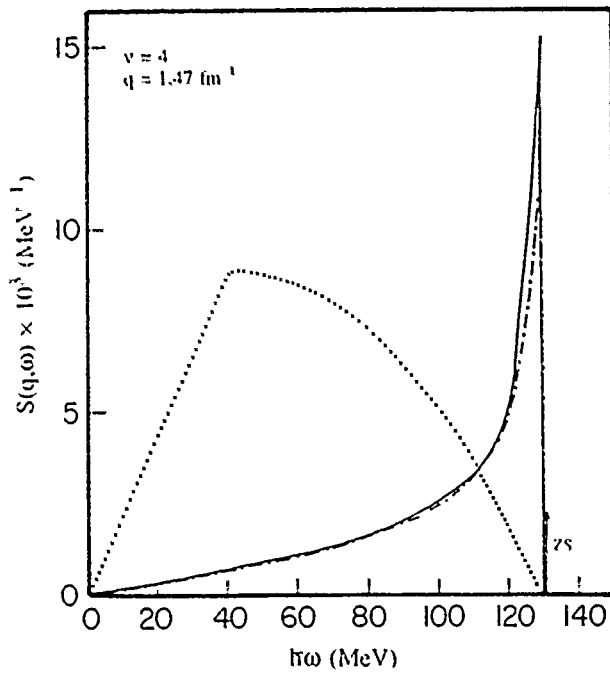


Fig. 3. Dynamic structure function  $S(q, \omega)$  versus energy transfer  $\hbar\omega$  at fixed wave number transfer  $q = 1.47 \text{ fm}^{-1}$  and  $k_F = 1.39 \text{ fm}^{-1}$ . Solid curve: for  $v_2$  model of nuclear matter based on C correlation function. Dot-dashed: for hard sphere nucleons with  $c = 0.5 \text{ fm}$ . Dotted: for free nucleons. Zero sound contribution in  $v_2$  case is indicated by vertical spike.

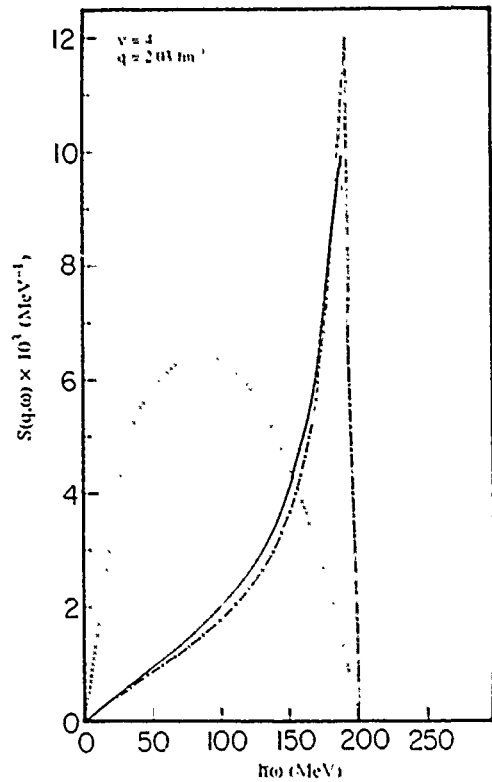


Fig. 4. Same as Fig. 3, except  $q = 2.03 \text{ fm}^{-1}$  and there is no zero sound.

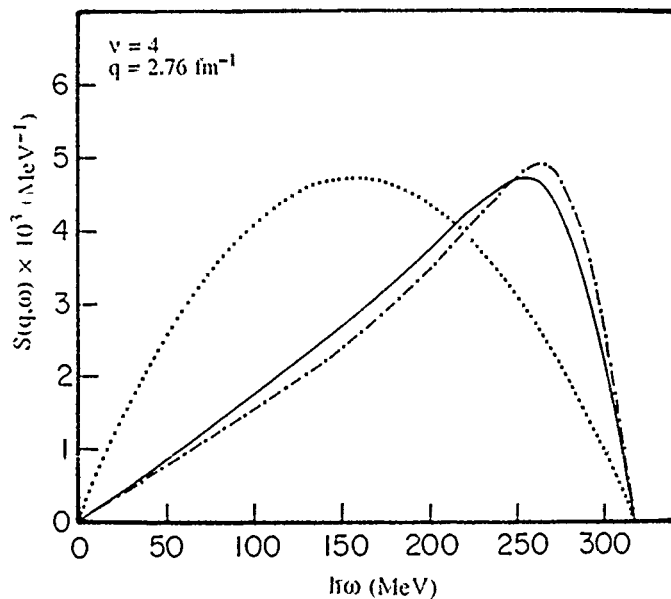


Fig. 5. Same as Fig. 3, except  $q = 2.76 \text{ fm}^{-1}$  and there is no zero sound.

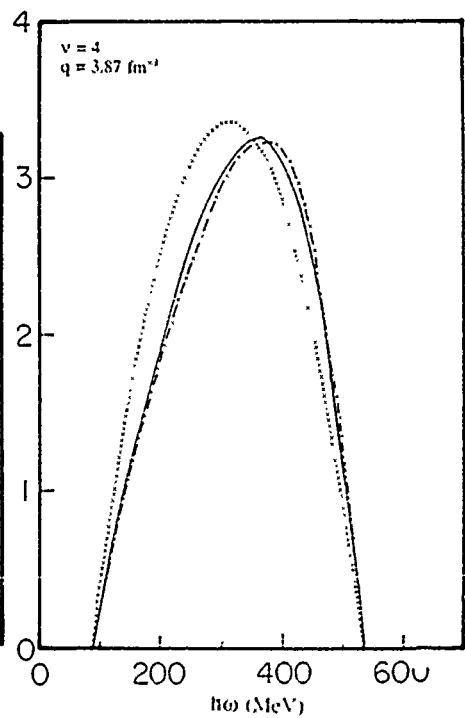


Fig. 6. Same as Fig. 3, except  $q = 3.87 \text{ fm}^{-1}$  and there is no zero sound. Vertical scale as in Fig. 5.

As seen in Figs. 3-6, the LCRPA calculation shows the well-known quenching of the response at low energies, compared to the independent-particle-model result.<sup>28-30</sup> This effect is perhaps too severe in our results at the lower  $q$  values. The predictions for  $S(q, \omega)$  are very similar for  $\nu_2$  and hard-core potentials, suggesting that the response in the relevant  $q$  regime is insensitive to the choice of bare, state-independent central potential, provided the wound parameter is kept roughly the same. For a given  $q$ , the strength is shifted to values of  $\hbar\omega$  higher than the experimental peak energy. This effect, as well as the excessive quenching at low  $\omega$ , is presumably due to the overly repulsive character of the  $\nu_2$  and hard-core potentials, which act equally in all partial waves, in contrast to the strong partial-wave dependence of realistic nucleon-nucleon interactions. Indeed, in the cases  $q = 1.47 \text{ fm}^{-1}$  and  $q = 2.03 \text{ fm}^{-1}$  (corresponding respectively to 290 MeV/c and 400 MeV/c), there is a very pronounced peak at the upper end of the allowed range of energy transfer, which is rather unphysical. As mentioned earlier, aside from zero sound, the LCRPA gives no response outside the  $(q, \omega)$  region relevant for the noninteracting system, so the strength which would otherwise be distributed to higher energies seems to be "piling up" at the high- $\omega$  boundary. The similar trends seen in the results of Fantoni and Pandharipande and of Pines, Quader and Wambach are much milder. As we go to high  $q$ , the departures of the LCRPA result for  $S(q, \omega)$  from the Fermi gas curve, and from the microscopic prediction of Fantoni and Pandharipande, become less noticeable. This is an obvious consequence of the decreasing importance of  $U(q)$  at larger momentum transfers. Since, quite generally, we may expect the particle-hole force to become negligible in the large- $q$  regime, predictions for  $S(q, \omega)$  should be relatively insensitive to the choice of the bare interaction, or to the treatment within conventional nuclear many-body theory, at large enough  $q$ . Of course, excitation of subnucleonic degrees of freedom may become a significant factor in this domain.

For symmetrical nuclear matter at  $k_F = 1.39 \text{ fm}^{-1}$ , a preliminary evaluation<sup>31</sup> of the LCRPA self-energy (5) using the techniques of Ref. 32 yields  $m^* = 1.1m$  for the on-shell effective mass at the Fermi momentum and shows no significant enhancement of  $m^*(k)$  in the vicinity of the Fermi surface (cf. Ref. 33). If the  $\nu_2$  interaction is allowed to act only in S waves (more appropriate in the nuclear context), a value of  $m^*(k_F)$  near  $0.8m$  should be obtained.<sup>34,19</sup>

## CONCLUSIONS

The density-density response function of symmetrical nuclear matter and pure neutron matter has been studied under simplifying conditions, leading to a microscopic theory – the local correlated random-phase approximation – requiring as input only the static structure function corresponding to a Jastrow description of the ground state. This theory has the virtues of easy application and straightforward interpretation of its predictions. Relative to an ordinary local RPA treatment, it takes account, approximately, of important dispersive, polarization, and geometrical effects arising from the strong interactions. In spite of its limitations, the theory has considerable value in establishing qualitative trends. For example, it is found that predictions for the dynamic structure factor do not depend very strongly on the choice of central, state-independent potential, so long as the wound parameter remains essentially unchanged.

One serious limitation of the theory as implemented here lies in the choice of the  $\nu_2$  model interaction as the bare force. It is well known that state dependence of the nuclear interaction and especially the presence of a tensor component have important consequences for most nuclear properties. The dynamic response is no exception, particularly at low momentum transfer.<sup>35</sup> Nevertheless, before proceeding to a realistic interaction like Urbana or Argonne  $\nu_{14}$ , and to the introduction of three-nucleon interactions, the intrinsic limitations of the local correlated RPA approach should be quantified. As implemented

here for parameterized correlation functions which do not strictly obey the Euler optimality condition, one such limitation is the neglect of the  $\Delta(q)$  term in the formula (2) for the particle-hole force. We have argued that this is not likely to produce significant additional errors in the description of the particle-hole interaction, since the correlation function assumed in our primary calculations (of form (12)) is believed to be nearly optimal. Deviations from optimality will mainly affect  $U(q)$  at small  $q$  – but in this region the local approximation must itself be considered questionable. These arguments notwithstanding, the importance of the  $\Delta(q)$  term, for the correlations used here, is currently under numerical investigation, and optimal correlations will be implemented in future calculations.

The next step is to assess the effects of nonlocalities in the particle-hole force. Within the CBF description of elementary excitations, this will involve numerical solution of the full CRPA equations, with explicit inclusion of exchange.<sup>8</sup> Such a treatment is needed to remove the unphysical feature of local CRPA that (apart from possible collective modes) the response is confined to the  $(q, \omega)$  domain in which the dynamic structure function of the noninteracting system is nonzero.

A truly quantitative description of the response and elementary excitations in nuclear systems will require a theory which goes beyond correlated RPA to the explicit inclusion of correlated multipair effects. Work in this direction has begun.

This research was supported in part by the Condensed Matter Theory Program of the Division of Materials Research, and by the Nuclear Theory Program of the Physics Division of the National Science Foundation, under Grant No. DMR-8519077. Support during the initial stages of the project was provided by the U. S. National Aeronautics and Space Administration under NASA Innovative Grant NAGW-122 to Washington University. J. W. C. thanks the Army Research Office for a travel grant.

#### REFERENCES

1. S. Fantoni and V. R. Pandharipande, Nucl. Phys. **A473**, 234 (1987).
2. A. Fabrocini and S. Fantoni, Nucl. Phys. A, in press.
3. E. Feenberg, *Theory of Quantum Fluids* (Academic, New York, 1969).
4. J. W. Clark and E. Krotscheck, Springer Lecture Notes in Physics **198**, 127 (1984).
5. J. M. C. Chen, J. W. Clark, and D. G. Sandler, Zeits. Physik **A305**, 223 (1982).
6. E. Krotscheck, Phys. Rev. A **26**, 3536 (1962).
7. V. R. Pandharipande, R. B. Wiringa, and B. D. Day, Phys. Lett. **57B**, 205 (1975).
8. N.-H. Kwong, Ph.D. thesis, California Institute of Technology (1982), unpublished.
9. E. Mavrommatis, R. Dave, and J. W. Clark, in *Condensed Matter Theories*, Vol. 2, ed. P. Vashishta, R. K. Kalia and R. F. Bishop (Plenum, New York, 1987), p. 249.
10. E. Krotscheck, R. A. Smith, J. W. Clark, and R. M. Panoff, Phys. Rev. B **24**, 6383 (1981).
11. E. Krotscheck, in *Quantum Fluids and Solids, Sanibel, Florida, 1983*, ed. E. D. Adams and G. G. Ihas (AIP, New York, 1983), p. 132.
12. G. E. Brown, *Many Body Problems* (North-Holland, Amsterdam, 1972).
13. W. M. Alberico, R. Cenni, and A. Molinari, Riv. del Nuovo Cim. **1**, 1 (1978).
14. W. Czyż and K. Gottfried, Ann. of Phys. **21**, 47 (1963).
15. F. Green, D. N. Lowy, and J. Szymanski, Phys. Rev. Lett. **48**, 638 (1982).
16. C. H. Aldrich III and D. Pines, J. Low Temp. Phys. **25**, 677 (1976); **32**, 689 (1978).
17. D. Pines, K. F. Quader, and J. Wambach, Nucl. Phys. **A477**, 365 (1988).
18. J. W. Clark, Prog. Part. Nucl. Phys. **2**, 89 (1979); and references cited therein.

19. A. Ramos, A. Polls, and W. H. Dickhoff, Nucl. Phys. A, in press.
20. D. Ceperley, G. V. Chester, and M. H. Kalos, Phys. Rev. B **16**, 3081 (1977).
21. O. Benhar, C. Ciofi degli Atti, A. Kallio, L. Lantto, and P. Toropainen, Phys. Lett. **60B**, 129 (1976); O. Benhar, C. Ciofi degli Atti, S. Fantoni, S. Rosati, A. Kallio, L. Lantto, and P. Toropainen, Phys. Lett. **64B**, 395 (1976).
22. J. W. Clark and M. L. Ristig, Phys. Rev. C **5**, 1553 (1972).
23. M. F. Flynn, private communication.
24. Z. E. Meziani *et al.*, Phys. Rev. Lett. **52**, 2130 (1984).
25. M. Dedy *et al.*, Phys. Rev. C **33**, 1897 (1986).
26. C. C. Blatchley *et al.*, Phys. Rev. C **34**, 1243 (1986).
27. D. B. Day *et al.*, Phys. Rev. C **40**, 1011 (1989).
28. J. M. Laget, Springer Lecture Notes in Physics **137**, 148 (1981); Physics Reports **69**, 1 (1981).
29. J. W. van Orden, Ph.D. thesis, Stanford University (1978), unpublished.
30. R. Rosenfelder, Ann. of Phys. **128**, 188 (1980).
31. R. D. Dave, private communication.
32. J. P. Blaizot and B. L. Friman, Nucl. Phys. **A372**, 69 (1981).
33. E. Krotscheck, J. W. Clark, and A. D. Jackson, Phys. Rev. B **28**, 5088 (1983).
34. W. H. Dickhoff, private communication.
35. A. Dellafiore and F. Matera, Phys. Rev. C **40**, 960 (1989).

# GENERALIZED MOMENTUM DISTRIBUTIONS OF QUANTUM FLUIDS

John W. Clark

McDonnell Center for the Space Sciences  
and Department of Physics  
Washington University, St. Louis, MO 63130 USA

Manfred L. Ristig

Institut für theoretische Physik  
Universität zu Köln, D-5000 Köln 41 BRD

## INTRODUCTION

The two-body density matrix  $\rho_2(\mathbf{r}_1, \mathbf{r}_2, \mathbf{r}'_1, \mathbf{r}'_2)$  of the ground state of a quantum fluid is a rich repository of information about its correlation structure. For example, the restricted version  $\rho_1(\mathbf{r}_1, \mathbf{r}_2, \mathbf{r}'_1) = \rho_2(\mathbf{r}_1, \mathbf{r}_2, \mathbf{r}'_1, \mathbf{r}_2)$  plays a crucial role in the description of final-state interactions in a novel theory of the deep-inelastic neutron scattering from the helium liquids,<sup>1</sup> capturing the correlation effects which give rise to deviations from the impulse approximation out to very high momentum and energy transfers. This contribution will focus on the microscopic evaluation of  $\rho_2(\mathbf{r}_1, \mathbf{r}_2, \mathbf{r}'_1)$  for uniform Fermi and Bose fluids. For simplicity, we assume that the ground state of either system is adequately described by a Jastrow trial function of the appropriate symmetry.

The formal structural analysis of the two-body density-matrix elements is most efficiently carried out in the configuration-space representation, and will be pursued using well-established cluster-expansion procedures,<sup>2,3</sup> followed by hypernetted-chain resummation of cluster diagrams.<sup>4,5</sup> On the other hand, the physical interpretation of the results is more vividly expressed in the momentum representation, i.e. in terms of the *generalized momentum distribution*

$$n(\mathbf{p}, \mathbf{q}) = \sum_{\hat{k}} \langle \Psi | a_{\hat{k}+\mathbf{q}}^\dagger a_{\hat{p}-\mathbf{q}}^\dagger a_{\hat{p}} a_{\hat{k}} | \Psi \rangle, \quad (1)$$

which is related to  $\rho_2(\mathbf{r}_1, \mathbf{r}_2, \mathbf{r}'_1)$  by Fourier transformation. (Here,  $\hat{k}$  denotes the single-particle orbital with quantum numbers  $k, \sigma$ , where  $\sigma$  is the spin projection, while  $\hat{k} - \mathbf{q} = (k - q, \sigma)$ .) Using the formal results obtained for the structure of  $\rho_2(\mathbf{r}_1, \mathbf{r}_2, \mathbf{r}'_1)$  - involving its closed expression in certain sums of irreducible cluster diagrams - we have been able to achieve a clean decomposition of  $n(\mathbf{p}, \mathbf{q})$  into contributions from various scattering processes occurring in the medium. In comparing Bose and Fermi cases, certain features arising from exchange (Pauli kinematic effects)

will also be evident. Quantitatively, the contributions from these assorted physical effects are determined by a set of form factors, which are susceptible to evaluation by hypernetted-chain techniques. We shall present numerical results for the form factors depending on a single momentum variable, and test the quality of an estimate for  $n(\mathbf{p}, \mathbf{q})$  used by Silver<sup>1</sup> as input for his theory of final-state effects in deep-inelastic neutron scattering.

The microscopic treatment of  $n(\mathbf{p}, \mathbf{q})$  will be developed for a Fermi system of arbitrary single-particle level degeneracy  $\nu$ . The corresponding results for the Bose case may then be obtained by taking the limits  $\nu \rightarrow \infty$  and  $k_F \rightarrow 0^+$  while keeping the density  $\rho = \nu k_F^3 / 6\pi^2$  constant.

The role of  $n(\mathbf{p}, \mathbf{q})$  in deep-inelastic neutron scattering becomes more tangible when we write this quantity as

$$n(\mathbf{p}, \mathbf{q}) = \langle \Psi | \rho_{\mathbf{q}} a_{\hat{\mathbf{p}}-\mathbf{q}}^\dagger a_{\hat{\mathbf{p}}} | \Psi \rangle - n(p) \quad , \quad (2)$$

where  $\rho_{\mathbf{q}}$  is the density fluctuation operator (with  $\mathbf{q} \neq 0$ ) and  $n(p)$  is the single-particle momentum distribution function. The expectation value (2) may be interpreted as a transition matrix element for scattering of a particle out of orbital  $\hat{\mathbf{p}} = (\mathbf{p}, \sigma')$  into another orbital  $\hat{\mathbf{p}} - \mathbf{q} = (\mathbf{p} - \mathbf{q}, \sigma')$ , the process being mediated by a density fluctuation of wave vector  $\mathbf{q}$ . Thus, an evaluation of  $n(\mathbf{p} - \mathbf{q})$  amounts to a calculation of the rightmost single-atom vertex in the Fig. 1.

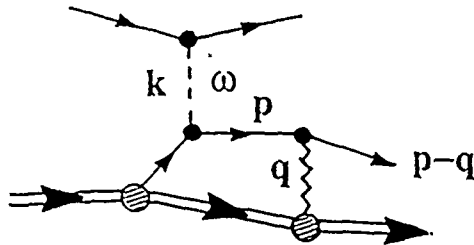


Fig. 1. Deep-inelastic scattering of neutrons from a (normal) helium liquid, involving final-state interactions mediated by a density fluctuation of the target system (a phonon of wave vector  $\mathbf{q}$ ).

### STRUCTURAL RESULTS FOR $\rho_2(\mathbf{r}_1, \mathbf{r}_2, \mathbf{r}'_1)$

The ground-state wave function of the  $N$ -particle Fermi system, supposed to constitute a uniform fluid, is taken in the Jastrow-Slater form  $\Psi = C^{-1} \Pi_{i<j} f(r_{ij}) \Phi$ , where  $\Phi$  is the usual Slater determinant of plane-wave orbitals, filling a Fermi sea characterized by Fermi wave number  $k_F$  and level degeneracy  $\nu$ , while  $f(r_{ij})$  is a Jastrow pair correlation function to be determined by minimization of the energy expectation value. The constant  $C$  is introduced to normalize  $\Psi$  to unity. The results to be described below can be generalized in a straightforward manner to the case that the Jastrow correlating factor is replaced by a Feenberg function.<sup>6</sup>

The first step of the formal development is to recognize that the generalized momentum distribution function (1) may be expressed as follows

$$n(\mathbf{p}, \mathbf{q}) = \delta_{\mathbf{q}0} (N-1) n(p) + (1 - \delta_{\mathbf{q}0}) \langle \Psi | N(\hat{\mathbf{p}}, \mathbf{q}) | \Psi \rangle \quad (3)$$

in terms of the one-body momentum distribution  $n(p)$  and the expectation value of a symmetric sum of two-body operators,

$$N(\hat{\mathbf{p}}, \mathbf{q}) = \sum_{i<j}^N [e^{i\mathbf{q}\cdot\mathbf{r}_i} o_{\hat{\mathbf{p}}-\mathbf{q}, \hat{\mathbf{p}}}(j) + e^{i\mathbf{q}\cdot\mathbf{r}_j} o_{\hat{\mathbf{p}}-\mathbf{q}, \hat{\mathbf{p}}}(i)] \quad . \quad (4)$$

The action of the one-body operator  $o_{\hat{p}-\mathbf{q},\hat{p}}(i)$  is specified by

$$o_{\hat{p}-\mathbf{q},\hat{p}}|\hat{k}\rangle = \delta_{\hat{p}\hat{k}}|\hat{p}-\mathbf{q}\rangle, \quad \langle \hat{k}|o_{\hat{p}-\mathbf{q},\hat{p}} = \delta_{\hat{k},\hat{p}-\mathbf{q}}\langle \hat{p}|. \quad (5)$$

Standard procedures are available for cluster-expanding the expectation value of a sum of two-body operators, the most familiar case being the potential energy corresponding to a sum of pair potentials.<sup>7</sup> These procedures have been applied to yield explicit results for the cluster contributions to  $n(\mathbf{p}, \mathbf{q})$  through three-body order, plus selected four-body contributions. The generalized Ursell-Mayer diagrammatic representation introduced in Ref. 2 facilitates the bookkeeping. At two-body order there are 7 cluster diagrams, at three-body there are 138, etc., the number growing very rapidly. The analysis becomes more transparent when we go over to the position representation, inverting the Fourier relation

$$n(\mathbf{p}, \mathbf{q}) = \frac{1}{\nu} \frac{\rho}{N} \int \rho_2(\mathbf{r}_1 \mathbf{r}_2 \mathbf{r}'_1) e^{-i\mathbf{p}\cdot(\mathbf{r}_1 - \mathbf{r}'_1)} e^{-i\mathbf{q}\cdot(\mathbf{r}_1 - \mathbf{r}_2)} d\mathbf{r}_1 d\mathbf{r}_2 d\mathbf{r}'_1 \quad (6)$$

to obtain the corresponding cluster expansion for the two-body density-matrix elements  $\rho_2(\mathbf{r}_1 \mathbf{r}_2 \mathbf{r}'_1)$ . There is a very simple recipe for accomplishing this diagrammatically. One simply removes the arrows representing specific plane-wave orbitals and changes the field points which they originally intersected into root points. It then becomes evident that most of the diagrams are reducible (factorizable), i.e., they consist of products of simpler graphs.

In the context of extensive technical experience with cluster expansions, the diagrams which have been explicitly generated are sufficient to reveal the structure of  $\rho_2(\mathbf{r}_1 \mathbf{r}_2 \mathbf{r}'_1)$  out to infinite cluster order. An exact representation of this quantity is provided by the expression

$$\rho_2(\mathbf{r}_1 \mathbf{r}_2 \mathbf{r}'_1) = \rho_{2D}(\mathbf{r}_1 \mathbf{r}_2 \mathbf{r}'_1) [L(\mathbf{r}_1 \mathbf{r}'_1) + L(\mathbf{r}_1 \mathbf{r}_2 \mathbf{r}'_1)] \quad (7)$$

The first factor collects the direct-direct portions of the full set of diagrams contributing to  $\rho_2(\mathbf{r}_1 \mathbf{r}_2 \mathbf{r}'_1)$ . By definition,<sup>7</sup> direct-direct diagrams do not have exchange lines attached to any of the root (or reference) points  $\mathbf{r}_1$ ,  $\mathbf{r}_2$ , and  $\mathbf{r}'_1$ . The complementary set of graphs contains only diagrams with exchange lines beginning and/or ending at two or three reference points. Of these graphs, the ones with exchange lines at two reference points combine to form the two-point exchange factor  $L(\mathbf{r}_1 \mathbf{r}'_1)$ , while the graphs with exchange lines at all three reference points compose the three-point function  $L(\mathbf{r}_1 \mathbf{r}_2 \mathbf{r}'_1)$ . Either of these exchange functions vanishes if any one of the coordinates in its argument recedes to an infinite distance from the others. In the Bose limit ( $\nu \rightarrow \infty$ ,  $k_F \rightarrow 0^+$ ,  $\rho$  constant), the function  $L(\mathbf{r}_1 \mathbf{r}'_1)$  approaches unity and the three-point function  $L(\mathbf{r}_1 \mathbf{r}_2 \mathbf{r}'_1)$  goes to zero. As expected, only the direct-direct contribution  $\rho_{2D}$  survives. Returning to (7) at finite  $\nu$ , this component may be compared, at a diagrammatic level, with the structural result which was derived for the Bose-fluid  $\rho_2(\mathbf{r}_1 \mathbf{r}_2 \mathbf{r}'_1)$  in Ref. 8. We arrive thereby at the representation

$$\rho_{2D}(\mathbf{r}_1 \mathbf{r}_2 \mathbf{r}'_1) = \rho \rho_{1D}(\mathbf{r}_1 \mathbf{r}'_1) f(|\mathbf{r}_1 - \mathbf{r}_2|) f(|\mathbf{r}'_1 - \mathbf{r}_2|) \exp[-P(\mathbf{r}_1 \mathbf{r}_2) - P(\mathbf{r}'_1 \mathbf{r}_2) - P(\mathbf{r}_1 \mathbf{r}_2 \mathbf{r}'_1)] \quad (8)$$

The generating functions  $P(\mathbf{r}_1 \mathbf{r}_2) = P(|\mathbf{r}_1 - \mathbf{r}_2|) \equiv P(r)$  and  $P(\mathbf{r}_1 \mathbf{r}_2 \mathbf{r}'_1)$  are irreducible quantities - sums of irreducible diagrams - just as in the Bose case. To give at least a hint of their character, Fig. 2 shows the leading cluster contributions to these functions. We may remind the reader of the relevant diagrammatic conventions.<sup>2,8</sup> Open circles represent root points (lower left circle:  $\mathbf{r}_1$ , lower right circle:  $\mathbf{r}'_1$ , upper

circle:  $r_2$ ). Solid circles denote field points and imply an integration  $\rho \int$ . A wavy [dashed] line stands for the correlation bond  $f(r_{ab}) - 1$  [respectively,  $f^2(r_{ab}) - 1$ ], where  $r_{ab} = |\mathbf{r}_a - \mathbf{r}_b|$ , and  $\mathbf{r}_a$  and  $\mathbf{r}_b$  are the coordinate points (solid or open circles) connected by the bond. The diagrams shown explicitly in Fig. 2 are in fact the same as the leading diagrams which occur for the Bose fluid. However, as in the familiar examples of the momentum distribution function  $n(p)$  and the one-body density matrix  $\rho_1(\mathbf{r}_1, \mathbf{r}'_1)$ , additional, non-Bose diagrams will arise from the systematic introduction of exchange insertions at the field points of the Bose diagrams of higher orders.<sup>7,2</sup> These insertions are characterized by the presence of exchange lines at one or both end points. An exchange line, drawn solid with an arrow attached, represents the Slater statistical bond  $l(k_F r_{ab})$ ,  $l(x) = 3x^{-3} \sin x - x \cos x$ .

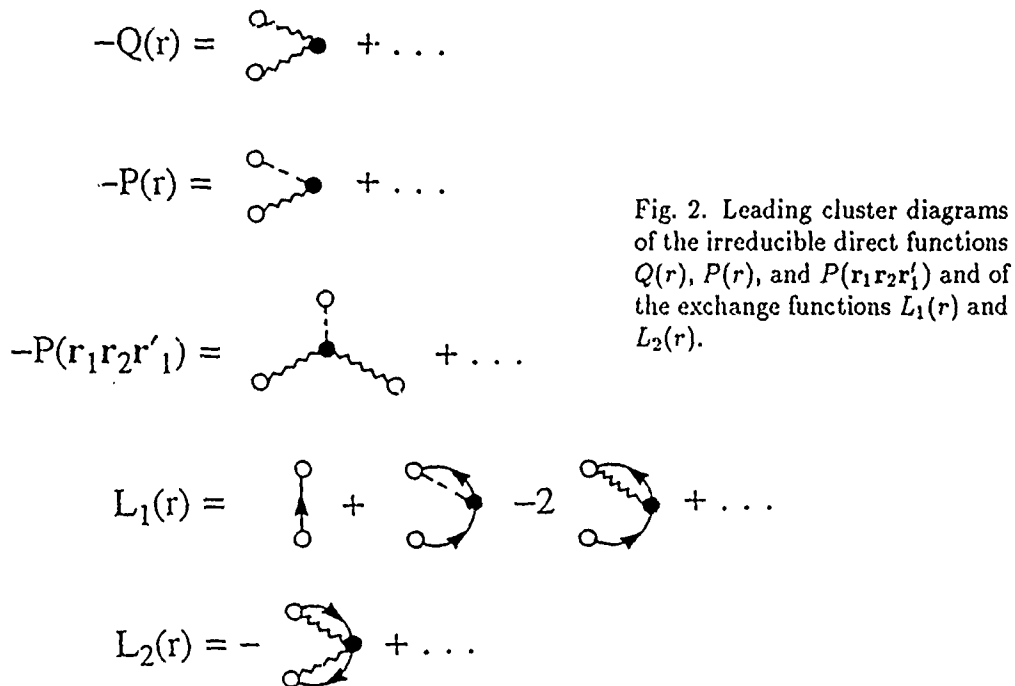


Fig. 2. Leading cluster diagrams of the irreducible direct functions  $Q(r)$ ,  $P(r)$ , and  $P(\mathbf{r}_1, \mathbf{r}_2, \mathbf{r}'_1)$  and of the exchange functions  $L_1(r)$  and  $L_2(r)$ .

The function  $\rho_{1D}(\mathbf{r}_1, \mathbf{r}'_1)$  appearing as a factor in (8) is just the direct-direct component of the full Fermi one-body density matrix  $\rho_1(\mathbf{r}_1, \mathbf{r}'_1)$ . The structure of  $\rho_{1D}$  is well known from previous work.<sup>2-4</sup> This quantity is generated by the irreducible phase-phase correlation function  $Q(\mathbf{r}_1, \mathbf{r}'_1)$  (see Fig. 2, and Figs. 8 and 10 of Ref. 2), according to

$$\rho_{1D}(\mathbf{r}_1, \mathbf{r}'_1) = \rho n_o \exp[-Q(\mathbf{r}_1, \mathbf{r}'_1)] \quad (9)$$

where  $n_o = \exp Q(\mathbf{r}_1, \mathbf{r}_1)$  is an overall strength factor.

At this point we have identified three sums of irreducible diagrams, namely  $Q(r)$ ,  $P(r)$ , and  $P(\mathbf{r}_1, \mathbf{r}_2, \mathbf{r}'_1)$  (where, and throughout,  $r \equiv |\mathbf{r}_1 - \mathbf{r}_2|$ ). As in the Bose case analyzed earlier<sup>8</sup> (and in the more familiar example of the generating function  $U(r)$  of the hypernetted-chain representation  $g(r) = f^2(r)e^{-U(r)}$  of the Bose radial distribution function<sup>7</sup>), these functions may be decomposed into nodal and elementary components. Fig. 2 shows in fact the leading diagrams of nodal type; elementary diagrams first appear in the next cluster order. In practice, the diagram sums  $Q(r)$ ,  $P(r)$ , and  $P(\mathbf{r}_1, \mathbf{r}_2, \mathbf{r}'_1)$  may be evaluated approximately, to all orders, by solving sets of Fermi-hypernetted-chain (FHNC) equations,<sup>7,4,5</sup> incorporating, stepwise, larger and larger classes of elementary diagrams. The simplest approximation, denoted FHNC/0, involves the neglect of all elementary components.

Fermi exchange effects arise implicitly from insertions at the field points of the

Bose diagrams contributing to  $Q(r)$ ,  $P(r)$ , and  $P(\mathbf{r}_1\mathbf{r}_2\mathbf{r}'_1)$ . Exchange manifests itself more explicitly in the second factor of the structural relation (7). We now examine the functions  $L(\mathbf{r}_1\mathbf{r}'_1)$  and  $L(\mathbf{r}_1\mathbf{r}_2\mathbf{r}'_1)$  in more detail.

Consider that, due to the disappearance of correlations at large distances, the quantity  $\rho_2(\mathbf{r}_1\mathbf{r}_2\mathbf{r}'_1)$  must reduce simply to  $\rho\rho_1(\mathbf{r}_1\mathbf{r}'_1)$  when  $r_2 \rightarrow \infty$ . On the other hand, consider that the one-body density matrix  $\rho_1(\mathbf{r}_1, \mathbf{r}'_1)$  is known to have the structure<sup>2,4,5</sup>

$$\rho_1(\mathbf{r}_1\mathbf{r}'_1) = \rho_{1D}(\mathbf{r}_1\mathbf{r}'_1)[L_1(\mathbf{r}_1\mathbf{r}'_1) + L_2(\mathbf{r}_1\mathbf{r}'_1)] \quad (10)$$

in terms of the direct-direct component  $\rho_{1D}$  of (9) and the exchange functions  $L_1$  and  $L_2$  (denoted  $N_1$  and  $N_2$  in Refs. 2,4). The exchange functions  $L_1$  and  $L_2$  are in turn known, both formally and numerically, within FHNC theory.<sup>4,5</sup> The diagrams contributing to these functions through three-body cluster order are indicated in Fig. 2. The foregoing considerations, together with the vanishing of the function  $L(\mathbf{r}_1\mathbf{r}_2\mathbf{r}'_1)$  as  $r_2 \rightarrow \infty$ , lead to the identification

$$L(\mathbf{r}_1\mathbf{r}'_1) = L_1(\mathbf{r}_1\mathbf{r}'_1) + L_2(\mathbf{r}_1\mathbf{r}'_1) \quad (11)$$

The structure of the three-point exchange function  $L(\mathbf{r}_1\mathbf{r}_2\mathbf{r}'_1)$  cannot be determined from asymptotic properties; it is instead inferred from the raw results for the cluster expansion of  $\rho_2(\mathbf{r}_1\mathbf{r}_2\mathbf{r}'_1)$ , along with the resolution (7). Many diagrams are seen to factorize, consistent with the following expression in terms of irreducible diagram sums  $P_{\alpha\beta}$ ,  $P_{\alpha\beta\gamma}$ :

$$\begin{aligned} L(\mathbf{r}_1\mathbf{r}_2\mathbf{r}'_1) = & -\nu^{-1}l(r)l(r') \\ & + l(r)[P_{cc}(r') + P_{dcc}(\mathbf{r}'_1\mathbf{r}_2\mathbf{r}_1)] + l(r')[P_{cc}(r) + P_{dcc}(\mathbf{r}_1\mathbf{r}_2\mathbf{r}'_1)] \\ & + l(\mathbf{r}_1\mathbf{r}'_1)[P_{de}(r) + P_{de}(r') + P_{ded}(\mathbf{r}_1\mathbf{r}_2\mathbf{r}'_1)] \\ & + P_{cdc}(\mathbf{r}_1\mathbf{r}_2\mathbf{r}'_1) + P_{cdc}^2(\mathbf{r}_1\mathbf{r}_2\mathbf{r}'_1) + P_{cec}(\mathbf{r}_1\mathbf{r}_2\mathbf{r}'_1) \\ & - \nu[P_{cc}(r) + P_{dcc}(\mathbf{r}_1\mathbf{r}_2\mathbf{r}'_1)][P_{cc}(r') + P_{dcc}(\mathbf{r}'_1\mathbf{r}_2\mathbf{r}_1)] \quad (12) \end{aligned}$$

The two- and three-point irreducible exchange functions  $P_{\alpha\beta}$  and  $P_{\alpha\beta\gamma}$  are classified according to the presence or absence of exchange lines at the root points. The category to which a given function belongs is indicated by its subscripts  $\alpha\beta$  or  $\alpha\beta\gamma$ , according to the conventional scheme<sup>7</sup>: *cc* (circular), *de* (direct-exchange), *dcc* (direct-circular), *ded* (direct-exchange-direct), *cdc* (circular-direct-circular), and *cec* (circular-exchange-circular). The direct-direct functions  $P(r)$  and  $P(\mathbf{r}_1\mathbf{r}_2\mathbf{r}'_1)$  fit in the same scheme, with *dd* subscripts (omitted for simplicity). All of these functions may be separated into their nodal and elementary parts, and the techniques of Fermi-hypernetted-chain theory invoked for their numerical evaluation. It is to be noted that the two-point functions  $P_{\alpha\beta}$  arise already in the theory of the Fermi one-body density matrix and have been thoroughly studied within the FHNC framework.<sup>4,5</sup>

The requirement that the fully-diagonal portion  $\rho_2(\mathbf{r}_1\mathbf{r}_2\mathbf{r}_1)$  coincide with  $\rho^2 g(r_{12})$ , where  $g(r_{12})$  is the radial distribution function for the assumed wave function, imposes certain relations on the quantities  $P(r)$ ,  $P(\mathbf{r}_1\mathbf{r}_2\mathbf{r}'_1)$ ,  $P_{\alpha\beta}$ , and  $P_{\alpha\beta\gamma}$ , namely

$$\begin{aligned} -2P(r) - P(\mathbf{r}_1\mathbf{r}_2\mathbf{r}_1) &= N_{dd}(r) + E_{dd}(r) \quad , \\ P_{cc}(r) + P_{dcc}(\mathbf{r}_1\mathbf{r}_2\mathbf{r}_1) &= N_{cc}(r) + E_{cc}(r) \quad , \\ 2P_{de}(r) + P_{ded}(\mathbf{r}_1\mathbf{r}_2\mathbf{r}_1) &= N_{de}(r) + E_{de}(r) \quad , \\ P_{cdc}(\mathbf{r}_1\mathbf{r}_2\mathbf{r}_1) &= N_{dc}(r) + E_{de}(r) \quad , \\ P_{cec}(\mathbf{r}_1\mathbf{r}_2\mathbf{r}_1) &= N_{ee}(r) + E_{ce}(r) \quad . \end{aligned} \quad (13)$$

The nodal ( $N$ ) and elementary ( $E$ ) diagram sums on the right-hand side are just those (with the corresponding subscripts) which arise in the FHNC analysis of  $g(r)$  (cf. Ref. 7).

## FORM FACTORS

We now determine the structure of the generalized momentum distribution function  $n(\mathbf{p}, \mathbf{q})$  of (1) by exploiting the structural results (7) (8), (9), (11), and (12) for the two-body density-matrix elements  $\rho_2(\mathbf{r}_1 \mathbf{r}_2 \mathbf{r}'_1)$  appearing in Fourier integral (6). To arrive at a decomposition of  $n(\mathbf{p}, \mathbf{q})$  which accomplishes a clean separation of contributions from differing physical processes, the function  $\rho_2(\mathbf{r}_1 \mathbf{r}_2 \mathbf{r}'_1)$  is first decomposed into a part containing all terms generated purely by two-point functions, and a remainder in which the terms also depend on the irreducible three point functions,

$$\rho_2(\mathbf{r}_1 \mathbf{r}_2 \mathbf{r}'_1) = \rho_2^{(2)}(\mathbf{r}_1 \mathbf{r}_2 \mathbf{r}'_1) + \rho_2^{(3)}(\mathbf{r}_1 \mathbf{r}_2 \mathbf{r}'_1) \quad , \quad (14)$$

the notation being transparent. The last term vanishes if the various three-point functions  $P(\mathbf{r}_1 \mathbf{r}_2 \mathbf{r}'_1)$  and  $P_{\alpha\beta\gamma}(\mathbf{r}_1 \mathbf{r}_2 \mathbf{r}'_1)$  are set equal to zero.

Next, we appeal to the Fermi-hypernet equations resulting from the FHNC analysis of the one-body density matrix.<sup>4,5</sup> These equations relate the bare correlation function  $f(r)$  to the spatial distribution functions defined by the direct and nodal diagram sums  $X_{Q\alpha\beta}(r)$  and  $N_{Q\alpha\beta}(r)$  introduced in Refs. 4,5,  $N_{Qdd}(r)$ , in particular, being identified with the nodal part of  $P(r)$ :

$$\begin{aligned} g_{Qdd}(r) &= 1 + F_{dd}(r) = 1 + X_{Qdd}(r) + N_{Qdd}(r) \quad , \\ g_{Qcc}(r) &= 1 + F_{cc}(r) = 1 + X_{Qcc}(r) + N_{Qcc}(r) \quad , \\ g_{Qde}(r) &= 1 + F_{de}(r) = 1 + X_{Qde}(r) + N_{Qde}(r) \quad . \end{aligned} \quad (15)$$

The hypernet equations read

$$\begin{aligned} f(r)e^{-P(r)} &= g_{Qdd}(r) \quad , \\ f(r)e^{-P(r)}P_{cc}(r) &= \nu^{-1}l(r)F_{dd}(r) + F_{cc}(r) \quad , \\ f(r)e^{-P(r)}P_{de}(r) &= F_{de}(r) \quad . \end{aligned} \quad (16)$$

Eqs. (16) permit us to eliminate the bare correlation factor  $f(r)$  from each term of the explicit expression for the decomposition (14), with the results

$$\begin{aligned} \rho_2^{(2)}(\mathbf{r}_1 \mathbf{r}_2 \mathbf{r}'_1) &= \rho\rho_1(\mathbf{r}_1 \mathbf{r}'_1)g_{Qdd}(r)g_{Qdd}(r') \\ &\quad + \rho\rho_1 D(\mathbf{r}_1 \mathbf{r}'_1)l(\mathbf{r}_1 \mathbf{r}'_1)[g_{Qdd}(r)F_{de}(r') + g_{Qdd}(r')F_{de}(r)] \\ &\quad - \nu\rho\rho_1 D(\mathbf{r}_1 \mathbf{r}'_1)[\nu^{-1}l(r) - F_{cc}(r)][\nu^{-1}l(r') - F_{cc}(r')] \end{aligned} \quad (17)$$

and

$$\begin{aligned} \rho_2^{(3)}(\mathbf{r}_1 \mathbf{r}_2 \mathbf{r}'_1) &= \rho_2^{(2)}(\mathbf{r}_1 \mathbf{r}_2 \mathbf{r}'_1)\{\exp[-P(\mathbf{r}_1 \mathbf{r}_2 \mathbf{r}'_1)] - 1\} \\ &\quad + \rho\rho_1 D(\mathbf{r}_1 \mathbf{r}'_1)g_{Qdd}(r)g_{Qdd}(r')\exp[-P(\mathbf{r}_1 \mathbf{r}_2 \mathbf{r}'_1)] \\ &\quad \times [l(r)P_{dcc}(\mathbf{r}'_1 \mathbf{r}_2 \mathbf{r}_1) + l(r')P_{dcc}(\mathbf{r}_1 \mathbf{r}_2 \mathbf{r}'_1) \\ &\quad \quad + l(\mathbf{r}_1 \mathbf{r}'_1)P_{ded}(\mathbf{r}_1 \mathbf{r}_2 \mathbf{r}'_1) + P_{cdc}(\mathbf{r}_1 \mathbf{r}_2 \mathbf{r}'_1) + P_{cdc}^2(\mathbf{r}_1 \mathbf{r}_2 \mathbf{r}'_1) \\ &\quad \quad + P_{cec}(\mathbf{r}_1 \mathbf{r}_2 \mathbf{r}'_1) - \nu P_{dcc}(\mathbf{r}_1 \mathbf{r}_2 \mathbf{r}'_1)P_{dcc}(\mathbf{r}'_1 \mathbf{r}_2 \mathbf{r}_1) \\ &\quad \quad - \nu P_{cc}(r)P_{dcc}(\mathbf{r}'_1 \mathbf{r}_2 \mathbf{r}_1) - \nu P_{cc}(r')P_{dcc}(\mathbf{r}_1 \mathbf{r}_2 \mathbf{r}'_1)] \quad . \end{aligned} \quad (18)$$

(Here  $r = |\mathbf{r}_1 - \mathbf{r}_2|$  (as usual) and  $r' = |\mathbf{r}'_1 - \mathbf{r}_2|$ .)

Inserting (14) into the integral (6), and using the results (17) and (18), we obtain the decomposition

$$\begin{aligned}
n(\mathbf{p}, \mathbf{q}) = & N\delta_{\mathbf{q}0}n(p) \\
& + F_{dd}(q)[n(p) + n(|\mathbf{p} - \mathbf{q}|)] \\
& + F_{de}(q)[n_{DI}(p) + n_{DI}(|\mathbf{p} - \mathbf{q}|)] \\
& - n_o[\theta(k_F - p) - F_{cc}(p)][\theta(k_F - |\mathbf{p} - \mathbf{q}|) - F_{cc}(|\mathbf{p} - \mathbf{q}|)] \\
& + n^{(2)'}(\mathbf{p}, \mathbf{q}) + n^{(3)'}(\mathbf{p}, \mathbf{q}) \quad . \quad (19)
\end{aligned}$$

Thus, the component  $n(\mathbf{p}, \mathbf{q}) - N\delta_{\mathbf{q}0}n(p)$  of the generalized momentum distribution depending nontrivially on two momenta is written as a sum of (i) separable contributions involving form factors

$$F_{\alpha\beta}(q) = \rho \int F_{\alpha\beta}(r)e^{i\mathbf{q}\cdot\mathbf{r}} dr \quad (20)$$

and either the one-body momentum distribution

$$n(p) = \nu^{-1} \int \rho_1(r)e^{i\mathbf{p}\cdot\mathbf{r}} dr \quad , \quad (21)$$

a modified momentum distribution

$$n_{DI}(p) = \nu^{-1} \int \rho_{1D}(r)l(r)e^{i\mathbf{p}\cdot\mathbf{r}} dr \quad , \quad (22)$$

or the the strength factor  $n_o$  [second, third, and fourth terms of (19), respectively], (ii) a non-separable integral  $n^{(2)'}(\mathbf{p}, \mathbf{q})$  involving only two-point quantities, and (iii) another three-point integral  $n^{(3)'}(\mathbf{p}, \mathbf{q})$  generated from the component (18) of  $\rho_2(\mathbf{r}_1, \mathbf{r}_2, \mathbf{r}'_1)$ . Explicitly, the fifth term is

$$n^{(2)'}(\mathbf{p}, \mathbf{q}) = \frac{1}{\nu} \frac{\rho}{N} \int K(\mathbf{r}_1, \mathbf{r}_2, \mathbf{r}'_1)e^{-i\mathbf{p}\cdot(\mathbf{r}_1 - \mathbf{r}'_1)} e^{-i\mathbf{q}\cdot(\mathbf{r}_1 - \mathbf{r}_2)} d\mathbf{r}_1 d\mathbf{r}_2 d\mathbf{r}'_1 \quad , \quad (23)$$

where

$$\begin{aligned}
K(\mathbf{r}_1, \mathbf{r}_2, \mathbf{r}'_1) = & \rho\rho_1(\mathbf{r}_1, \mathbf{r}'_1)F_{Qdd}(r)F_{Qdd}(r') \\
& + \rho\rho_{1D}(\mathbf{r}_1, \mathbf{r}'_1)l(\mathbf{r}_1, \mathbf{r}'_1)[F_{Qdd}(r)F_{de}(r') + F_{Qdd}(r')F_{de}(r)] \\
& - \nu\rho[\rho_{1D}(\mathbf{r}_1, \mathbf{r}'_1) - \rho n_o][\nu^{-1}l(r) - F_{cc}(r)][\nu^{-1}l(r') - F_{cc}(r')] \quad . \quad (24)
\end{aligned}$$

The contribution (23) may be reduced to a three-dimensional integral in momentum variables.

In momentum space, the sequential relation

$$\int \rho_2(\mathbf{r}_1, \mathbf{r}_2, \mathbf{r}'_1) d\mathbf{r}_2 = (N - 1)\rho_1(\mathbf{r}_1, \mathbf{r}'_1) \quad (25)$$

becomes

$$n(\mathbf{p}, \mathbf{q} = 0) = (N - 1)n(p) \quad . \quad (26)$$

Specializing (19) to  $q = 0$ , and substituting into (26), there results a condition on the form factors. If we employ this condition in (19) itself, we may recast the decomposition of  $n(\mathbf{p}, \mathbf{q})$  in the form

$$\begin{aligned}
n(\mathbf{p}, \mathbf{q}) = & (N - 1)\delta_{q0}n(p) \\
& + (1 - \delta_{q0})F_{dd}(q)[n(p) + n(|\mathbf{p} - \mathbf{q}|)] \\
& + (1 - \delta_{q0})F_{de}(q)[n_{DI}(p) + n_{DI}(|\mathbf{p} - \mathbf{q}|)] \\
& - n_o(1 - \delta_{q0})[\theta(k_F - p) - F_{cc}(p)][\theta(k_F - |\mathbf{p} - \mathbf{q}|) - F_{cc}(|\mathbf{p} - \mathbf{q}|)] \\
& + (1 - \delta_{q0})n^{(2)'}(\mathbf{p}, \mathbf{q}) + (1 - \delta_{q0})n^{(3)'}(\mathbf{p}, \mathbf{q}) \quad . \quad (27)
\end{aligned}$$

This expression achieves the desired separation of contributions from the various scattering processes underlying the generalized momentum distribution function (cf. Ref. 8). The first term reproduces the trivial result for dynamically and statistically uncorrelated particles (except that the momentum distribution function  $n(p)$  appearing in (27) is that for the fully correlated Fermi system). The correlations prevailing in the interacting fluid permit the scattering of a fermion from orbital  $\hat{p}$  to another orbital  $\hat{p} - \mathbf{q}$ , with the intervention of a phonon to conserve momentum. The effect of this process and the corresponding time-reversed mechanism are described by the second term in (27). The associated exchange scattering effects are embodied in the third term, which is proportional to the exchange form factor  $F_{de}(q)$ . To interpret the fourth line of (27), we note that if the particles are noninteracting, but the statistical correlations are turned on, the totally uncorrelated result  $(N - 1)\delta_{q0}n(p)$  must be corrected by a Pauli kinematic term  $-(1 - \delta_{q0})\theta(k_F - p)\theta(k_F - |\mathbf{p} - \mathbf{q}|)$ . For the present case of interacting fermions, the dynamical correlations, manifested in virtual single-particle excitations out of the Fermi sea, lead to tails on the step distributions (the  $F_{cc}$  terms). The dynamical correlations also produce an overall quenching of the effect, through the strength factor  $n_o$  ( $0 \leq n_o \leq 1$ ). The last line of (27) contains terms of "higher order" which act to correct the various processes just considered.

Upon taking the Bose limit of (27), we recover the corresponding decomposition of the generalized momentum distribution of a Bose fluid as derived in Ref. 8, namely

$$\begin{aligned}
n(\mathbf{p}, \mathbf{q}) = & \delta_{q0}(N - 1)n(p) \\
& + (1 - \delta_{q0})(\delta_{p0} + \delta_{p\mathbf{q}})Nn_oF_1(q) \\
& + (1 - \delta_{q0})(1 - \delta_{p0})(1 - \delta_{p\mathbf{q}})n'(\mathbf{p}, \mathbf{q}) \quad , \quad (28)
\end{aligned}$$

the non-condensate portion being given by

$$\begin{aligned}
n'(\mathbf{p}, \mathbf{q}) = & F_1(q)[n'(p) + n'(|\mathbf{p} - \mathbf{q}|)] \\
& + \frac{\rho^2}{N} \int \rho_1(\mathbf{r}_1\mathbf{r}'_1)F_1(\mathbf{r}_1\mathbf{r}_2\mathbf{r}'_1)e^{-i\mathbf{p}\cdot(\mathbf{r}_1 - \mathbf{r}'_1)}e^{-i\mathbf{q}\cdot(\mathbf{r}_1 - \mathbf{r}_2)}d\mathbf{r}_1d\mathbf{r}_2d\mathbf{r}'_1 \quad . \quad (29)
\end{aligned}$$

Only the direct contributions to (27) survive. Thus the third and fourth lines are to be omitted, and the form factor  $F_{dd}(q)$  is to be identified with the function  $F_1(q)$  studied in the earlier paper. The function  $F_1(\mathbf{r}_1\mathbf{r}_2\mathbf{r}'_1)$  entering (29) is specifically

$$F_1(\mathbf{r}_1\mathbf{r}_2\mathbf{r}'_1) = F_1(r)F_1(r') + [1 + F_1(r)][1 + F_1(r')]\{\exp[-P(\mathbf{r}_1\mathbf{r}_2\mathbf{r}'_1)] - 1\}. \quad (30)$$

The three addends of (28) have the following interpretations as contributions from distinct scattering processes taking place in the many-body medium (see Fig. 3): The trivial first term corresponds to the null scattering process 3(a). The third term

accounts for 3(b), in which a boson is scattered from orbital  $\mathbf{p}$  outside the condensate to another non-condensate orbital  $\mathbf{p} - \mathbf{q}$  by transferring momentum  $\hbar\mathbf{q}$  to a density fluctuation. The other two processes shown, 3(c) and 3(d), are described by the second line of (28) and involve the zero-momentum condensate. They correspond, respectively, to creation of a particle of momentum  $-\hbar\mathbf{q}$  by the condensate and to absorption of a particle of momentum  $\hbar\mathbf{p}$  into it, a phonon being created in each case to conserve momentum.

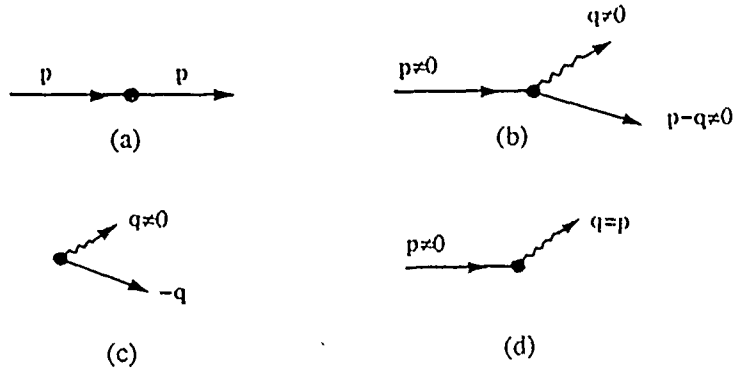


Fig 3 Scattering processes contributing to the generalized momentum distribution function  $n(\mathbf{p}, \mathbf{q})$  of a Bose fluid with a macroscopic zero-momentum condensate (cf. Eq. (28) and following text).

Finally, we should address the issue of the practical validity of the sequential relation (25) or (26). In the Bose limit, we may split this relation into two conditions, one applying at  $p = 0$  (the condensate condition) and the other applying at finite  $p$  (and involving terms smaller by a factor  $1/N$ ). These conditions read  $1 + 2F_1(q = 0) = 0$  and  $n^{(2)'}(\mathbf{p}, 0) + n^{(3)'}(\mathbf{p}, 0) = 0$ , respectively. As discussed in Ref. 8, they constrain the choice of correlation factor in the Bose case. In particular, it may be shown that the condensate condition is satisfied for *optimal* Jastrow correlations, even at the HNC/0 level of approximation (i.e., neglecting elementary contributions), but fails for a generic  $f(r)$ . In the Fermi case, the situation is rather different: the sequential relation (26) is fulfilled identically for *any* Jastrow trial function, and indeed, even if this choice is extended to include multi-body correlations of Feenberg type. The universal satisfaction of (26) is a consequence of the presence of Pauli exchange correlations, implied by the Slater determinant  $\Phi$ . Technically, this property may be attributed to a Fermi cancellation phenomenon of the type encountered in the FHNC analysis of the static structure function  $S(q)$  (cf. Ref. 7). While formally exact, the required cancellation, and hence the sequential relation, is violated to some degree in any finite-order approximation within the HNC/n sequence.

## NUMERICAL RESULTS FOR SINGLE-MOMENTUM FORM FACTORS

In correcting the impulse approximation to deep-inelastic scattering from the helium liquids for final-state interactions, Silver<sup>1</sup> has used the simple approximation

$$\rho_2(\mathbf{r}_1 \mathbf{r}_2 \mathbf{r}'_1) \simeq \rho \rho_1(\mathbf{r}_1 \mathbf{r}'_1) g(|\mathbf{r}_1 - \mathbf{r}_2|) \quad (31)$$

for the required two-body density-matrix elements. This approximation may be tested microscopically within variational theory, by hypernetted-chain evaluation of the functions  $\rho_2(\mathbf{r}_1 \mathbf{r}_2 \mathbf{r}'_1)$ ,  $\rho_1(\mathbf{r}_1 \mathbf{r}'_1)$ , and  $g(r)$ .

In the framework of the Jastrow variational theory developed here for Fermi systems of arbitrary level degeneracy, Silver's approximation (31) corresponds to certain rough first estimates of various quantities appearing in the contributions (17) and (18) to (14), en route to the construction of  $n(\mathbf{p}, \mathbf{q})$  via (27). In more detail, it is equivalent to the replacements

$$\rho_1(\mathbf{r}_1 \mathbf{r}'_1) \simeq \rho_{1D}(\mathbf{r}_1 \mathbf{r}'_1) l(\mathbf{r}_1 \mathbf{r}'_1) \quad , \quad (32)$$

$$F_{dd}(r) + F_{de}(r) \simeq g(r) - 1 \quad , \quad F_{dd}(r') \simeq 0 \quad , \quad F_{de}(r') \simeq 0 \quad (33)$$

$$\nu^{-1} l(r) - F_{cc}(r) \simeq 0 \quad , \quad (34)$$

and to neglect of the "pure-three-point" contribution  $\rho_2^{(3)}(\mathbf{r}_1 \mathbf{r}_2 \mathbf{r}'_1)$  of Eq. (18). In momentum space, relation (32), the first member of (33), and relation (34) become, respectively,

$$n(p) \simeq n_{DI}(p) \quad , \quad (35)$$

$$F_{dd}(q) + F_{de}(q) \simeq S(q) - 1 \quad , \quad (36)$$

$$\nu^{-1} \theta(k_F - p) - F_{cc}(p) \simeq 0 \quad , \quad (37)$$

where  $S(q)$  is the static structure function corresponding to the radial distribution function  $g(r)$ . As may be seen by taking the Bose limit, the corresponding replacements implied in the Bose case are

$$F_1(r) \simeq g(r) - 1 \quad , \quad F_1(r') \simeq 0 \quad , \quad (33')$$

$$F_1(q) \simeq S(q) - 1 \quad , \quad (36')$$

and neglect of the three-point function  $F_1(\mathbf{r}_1 \mathbf{r}_2 \mathbf{r}'_1)$ .

The most striking feature of Silver's approximation is, of course, its violation of time-reversal invariance, evident in the asymmetric treatment of at least one of the pairs  $F_{dd}(r)$ ,  $F_{dd}(r')$  and  $F_{de}(r)$ ,  $F_{de}(r')$  by (33), and of the pair  $F_1(r)$ ,  $F_1(r')$  by (33').

To make a quantitative judgment of the efficacy of approximations (32)-(37), (33'), and (36'), we have calculated the distribution functions and form factors entering these relations, for liquid  $^4\text{He}$  and liquid  $^3\text{He}$  at their respective equilibrium densities ( $\rho = 0.0218 \text{ \AA}^{-3}$  and  $\rho = 0.01658 \text{ \AA}^{-3}$ ). For the Bose liquid we have used a Jastrow correlation factor  $f(r)$  optimized by a paired-phonon analysis<sup>9</sup>; a Schiff-Verlet form<sup>10</sup>  $f(r) = \exp[-(b/r)^5/2]$  was chosen in the Fermi case, with  $b = 2.9547 \text{ \AA}$  (cf. Ref. 11). The numerical evaluations were carried out in the Bose or Fermi hypernetted-chain approximation (HNC/0 or FHNC/0) in which the elementary-diagram contributions to the various quantities are set zero. This approximation should be adequate for the immediate task of testing the ansatz (31).

Our results are summarized in Figs. 4-6.

Figure 4 compares the form factor  $F_1(q)$  (solid curve) with the overshoot  $S(q) - 1$  of the static structure function (dashed curve), testing (36') [or the first member of (33')] in liquid  $^4\text{He}$ . The two functions have roughly similar shapes, but depart substantially at small  $q$ . At  $q = 0$ , the numerical result for  $F_1(q)$  goes to the correct asymptotic result  $-1/2$  (as it should, since the 'condensate' condition derived from the sequential relation must be met in HNC/0 when  $f(r)$  is optimized). On the other hand, the estimate (36') deviates from the correct limit by a wide margin, since  $S(0)$  must vanish for the optimized  $f(r)$ .

Figures 5 and 6 address the situation in liquid  ${}^3\text{He}$ . The shortcomings of the estimate (36) [or, equivalently, the first member of (33)] are revealed in Fig. 5, which shows  $S(q) - 1$  and the sum of form factors  $F_{dd}(q) + F_{dc}(q)$ . Within the FHNC/0 approximation, the departure from assumption (36) is clearly exposed and again is particularly apparent at small momenta. The exclusion principle alters the  $q = 0$  limits seen in the Bose case (Fig. 4), by virtue of the Fermi cancellation effect mentioned in the preceding section. For a Fermi system described by a Slater-Jastrow

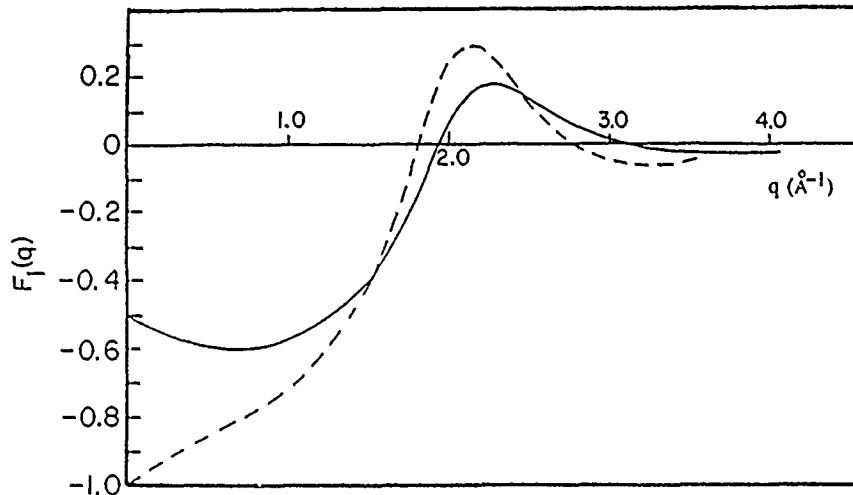


Fig. 4. Test of (36'). Form factor  $F_1(q)$  for creation of a particle out of the condensate, in HNC/0 (solid curve) and Silver's (dashed curve) approximations, for liquid  ${}^4\text{He}$  at equilibrium density, described by an optimized Jastrow wave function. Static structure function of (36') was evaluated in HNC/0 approximation.

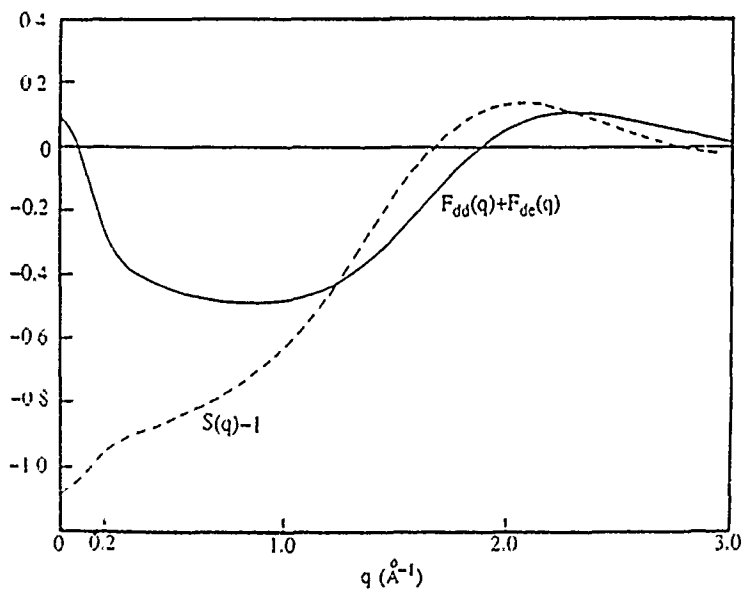


Fig. 5. Test of (36) Sum of form factors  $F_{dd}(q) + F_{dc}(q)$  (solid curve) compared with overshoot of static structure function  $S(q)$  (dashed curve), for liquid  ${}^3\text{He}$  at equilibrium density, described within a Jastrow-FHNC/0 approximation.

wave function, this cancellation phenomenon guarantees, at  $q = 0$ , the properties  $X_{de}(q) = X_{ee}(q) = -1$  and, consequently,  $S(q) = 0$  and  $F_{dd}(q) + F_{de}(q) = 0$ . The latter properties are (approximately) reflected in our numerical results for  $S(q)$  and  $F_{dd}(q) + F_{de}(q)$ . However, one does see, in Fig. 5, slight deviations from the correct limiting value of zero, which result from use of the FHNC/0 approximation. The standard FHNC approximants (/0, /4, etc.) are known to disobey the Fermi cancellation rules as a result of the neglect or inconsistent treatment of elementary diagrams.<sup>7</sup>

Fig. 6 shows the momentum distributions  $n(p)$  and  $n_{DI}(p)$  and tests the replacement (35) [equivalent to (32)]. The strength factor associated with both of distributions is  $n_0 = 0.2212$ . The two functions are seen to have very similar behavior, but their magnitudes differ typically by 10-15%.

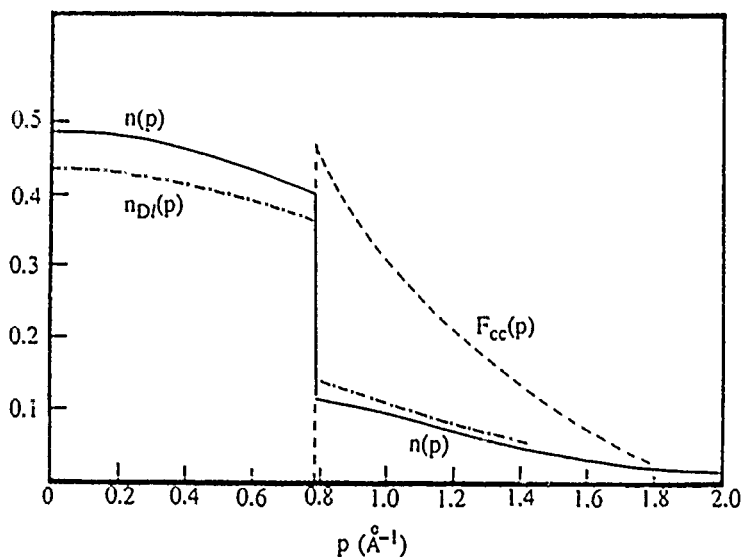


Fig. 6. Test of (35) and (37). Momentum distribution functions  $n(p)$  (solid curve) and  $n_{DI}(p)$  (dot-dashed curve) of liquid  ${}^3\text{He}$  at equilibrium density, described within a Jastrow-FHNC/0 approximation. Dashed curve shows circular-exchange function  $F_{cc}(p)$ .

According to (37), the Pauli exclusion corrections to  $n(p, q)$  of the circular type, involving  $\nu^{-1}\theta(k_F - p) - F_{cc}(p)$ , are entirely ignored in Silver's treatment - even the trivial kinematic statistical effect of the first term is absent. The form factor  $F_{cc}(p)$ , evaluated in FHNC/0 approximation, is shown in Fig. 6 as the dashed line. This function vanishes inside the Fermi sea, jumps to a height of about 0.5 at the Fermi surface, and decreases slowly in magnitude with further increase of the wave number  $p$ . In general one may therefore expect such statistical effects to be important. On the other hand, we note that their net contribution to  $n(p, q)$  of (27) is proportional to the strength factor  $n_0$ , which is only about 0.2 in liquid  ${}^3\text{He}$ .

In brief, an initial application of the microscopic theory of the density-matrix elements  $\rho_2(r_1 r_2 r'_1)$  has documented significant quantitative deficiencies of the simple estimate proposed by Silver. We should point out, however, that the final-state corrections evaluated in Silver's theory of deep-inelastic scattering at high momentum and energy transfers may be insensitive to the errors we have noted, and, in particular, to the behavior of the sum of form factors  $F_{dd}(q) + F_{de}(q)$  at small  $q$ . This possibility is currently under investigation.<sup>12</sup>

## FURTHER WORK

We have not reported numerical data on the non-separable terms  $n^{(2)'}(\mathbf{p}, \mathbf{q})$  and  $n^{(3)'}(\mathbf{p}, \mathbf{q})$  of (27), nor on the integral term in (29) involving the three-point function  $F_1(\mathbf{r}_1 \mathbf{r}_2 \mathbf{r}'_1)$ . While these more complicated objects may all be calculated from quantities generated in the FHNC/0 or HNC/0 treatment, their detailed evaluation will be deferred until a scaling or interpolation procedure<sup>13,14</sup> has been implemented for the incorporation of elementary-diagram corrections. At the same time, the Jastrow ansatz will be supplemented by triplet correlations. Work in these directions is currently in progress.<sup>15</sup>

It is worth mentioning that some HNC/0 results for the quantity  $F_1(\mathbf{r}_1 \mathbf{r}_2 \mathbf{r}'_1)$  were presented in Ref. 8., results which demonstrate the failure of the HNC/0 treatment to fulfill the condition  $\rho_2(\mathbf{r}_1 \mathbf{r}_2 \mathbf{r}_1) = \rho^2 g(r_{12})$  and thereby provide another reminder of the necessity of including effects of elementary diagrams.

While our derivation of the decomposition (27) for the Fermi generalized momentum distribution was predicated on the Slater-Jastrow choice for the wave function  $\Psi$ , the corresponding decomposition (28) for the Bose system (derived here as a limiting case of the Fermi result) was originally obtained for very general  $\Psi$ , including the exact ground-state wave function.<sup>8</sup> Indeed, Ref. 8 contains a general asymptotic analysis of the full Bose two-body density matrix in configuration space, as well as the restricted version  $\rho_2(\mathbf{r}_1 \mathbf{r}_2 \mathbf{r}'_1)$  considered here.

A more detailed presentation of some of the results of this contribution may be found in a longer article.<sup>16</sup> Further studies along the same lines will be concerned with the full Fermi two-body density matrix.

This research was supported in part by the Spanish CICyT under its sabbatical program, by the Condensed Matter Theory Program of the Division of Materials Research of the U. S. National Science Foundation under Grant No. DMR-8519077, and by the Theoretical Physics Institute of the University of Minnesota. We thank Richard Silver for many informative discussions and Fernando Arias de Saavedra and Enrique Buendia for furnishing the numerical data for our analysis. JWC is grateful to the Army Research Office, Durham, for providing travel funds.

## REFERENCES

1. R. N. Silver, in *Condensed Matter Theories*, Vol. 3, ed. J. S. Arponen, R. F. Bishop, and M. Manninen (Plenum, New York, 1988), p. 131; R. N. Silver, *Phys. Rev. B* **37**, 3794 (1988); R. N. Silver, *Phys. Rev. B* **38**, 2283 (1988).
2. M. L. Ristig and J. W. Clark, *Phys. Rev. B* **14**, 2875 (1976).
3. M. L. Ristig, *Nucl. Phys. A* **317**, 163 (1979).
4. M. L. Ristig, in *From Nuclei to Particles*, Proceedings of the International School of Physics "Enrico Fermi", Course LVII, Varenna 1981, ed. A. Molinari (North Holland, Amsterdam, 1982), p. 340.
5. S. Fantoni, *Nuovo Cimento A* **44**, 191 (1978).
6. J. W. Clark, *Nucl. Phys. A* **328**, 587 (1979).
7. J. W. Clark, in *Progress in Particle and Nuclear Physics*, Vol. 2, ed. D. H. Wilkinson (Pergamon, Oxford, 1979), p. 89.
8. M. L. Ristig and J. W. Clark, *Phys. Rev. B*, in press.
9. E. Feenberg, *Theory of Quantum Fluids* (Academic, New York, 1969).
10. D. Schiff and L. Verlet, *Phys. Rev.* **160**, 208 (1967).
11. K. E. Kürten and J. W. Clark, *Phys. Rev. B* **30**, 1342 (1984).
12. R. N. Silver, private communication.

13. Q. N. Usmani, B. Friedman, and V. R. Pandharipande, Phys. Rev. B 25, 4502 (1982); Q. N. Usmani, S. Fantoni, and V. R. Pandharipande, Phys. Rev. B 26, 6123 (1982); M. Puorskari and A. Kalos, Phys. Rev. B 30, 152 (1984); E. Manousakis, V. R. Pandharipande, and Q. N. Usmani, Phys. Rev. B 31, 7022 (1985); M. F. Flynn, Phys. Rev. B 33, 91 (1986).
14. A. Fabrocini and S. Rosati, Nuovo Cimento D1, 567 (1982); D1, 615 (1982); M. Viviani, E. Buendia, A. Fabrocini, and S. Rosati, Nuovo Cimento D8, 561 (1986); M. Viviani, E. Buendia, S. Fantoni, and S. Rosati, Phys. Rev. B 38, 4523 (1988); S. Rosati, M. Viviani, and E. Buendia, contribution to this volume.
15. F. Arias, E. Buendia, and M. Viviani, private communication.
16. M. L. Ristig and J. W. Clark, to be published.

ABNORMAL OCCUPATION, TIGHTER-BOUND COOPER PAIRS and HIGH  $T_c$   
SUPERCONDUCTIVITY

M. de Llano\*

Physics Department  
North Dakota State University  
Fargo, North Dakota, 58105

and

J. P. Vary

Physics Department  
Iowa State University  
Ames, Iowa 50011

Talk presented at "XIII International Workshop on Condensed-Matter Theories", Campos do Jordão, SP, BRAZIL, Aug. 1989, to be published by PLENUM PRESS

The classic Cooper electron-pair problem is generalized via a Fermi sea having two concentric surfaces, rather than the familiar sphere of a perfect (interactionless) fermion gas. Substantially tighter-bound pairs are obtained for fixed phonon coupling with the BCS model interaction, no matter how weak. This will admit increased transition temperatures for superconductivity in the BCS theory and beyond, and suggests that *designing* materials having multiply-connected Fermi surfaces with maximal interior area will yield larger  $T_c$  values.

INTRODUCTION

The Cooper electron pair problem<sup>1</sup> is vitally central to the Bardeen-Cooper-Schrieffer (BCS) microscopic theory of superconductivity<sup>2</sup>. It consists in a Schrödinger equation for two particles of opposite momenta and spins being scattered by a particular attractive interaction *only* into one-electron plane wave (PW) states just above the spherical Fermi sea occupied by the PW orbitals of the other  $N - 2$  background electrons in the  $N$ -electron system. PW states are used for simplicity, instead of Bloch states. The well-known resulting eigenvalue equation for the pair energy  $E_0$  is then

$$1 = V \sum_{\mathbf{k}}' \frac{1}{2E(\mathbf{k}) - E_0} \longrightarrow V \int_{E_F}^{E_F + \hbar\omega_D} d\mathcal{E} \frac{g(\mathcal{E})}{2\mathcal{E} - E_0} \quad (1)$$

\*A travel grant from US Army Research Office is gratefully acknowledged.

where  $E(k) = \hbar^2 k^2 / 2m$  are the unperturbed single-particle energies and  $V > 0$  is the strength of the effective attractive electron-electron interaction induced by the electron-phonon coupling. This is nonzero only within a very thin shell of thickness  $\hbar\omega_D$  above the Fermi surface of energy  $E_F = \hbar^2 k_F^2 / 2m$ ,  $k_F$  being the Fermi sphere radius; it is the so-called "BCS model interaction". Here,  $\hbar\omega_D$  is the maximum energy possible for an ionic lattice phonon, and is typically  $10^{-3}$  to  $10^{-2}$  times smaller than  $E_F$ . The prime over the summation sign means restriction to those PW states such that  $E_F < E(k) < E_F + \hbar\omega_D$ , i.e., to states that are unoccupied. The integral involves the free-electron density of states  $g(\mathcal{E}) \propto \mathcal{E}^{1/2}$ , which can in turn be factored out from the integral as a constant  $g(\mathcal{E}_F)$  due to the smallness of  $\hbar\omega_D/E_F$ . This leaves an elementary integral to be performed that gives a logarithm. Solving for the eigenvalue  $E_0$  then yields

$$E_0 = 2E_F - \frac{2\hbar\omega_D}{e^{2/g(E_F)V} - 1} \equiv 2E_F - \Delta_0 \xrightarrow{V \rightarrow 0} 2E_F - 2\hbar\omega_D e^{-2/g(E_F)V} \quad (2)$$

Putting  $\epsilon_0 \equiv E_0/2E_F$  and  $\nu \equiv \hbar\omega_D/2E_F$ , the first equation can be rearranged to read

$$e^{-2/g(E_F)V} = \frac{\epsilon_0 - 1}{\epsilon_0 - 1 - 2\nu} \quad (3)$$

The lhs (a constant for fixed coupling and density of states) and rhs of this equation are displayed, for the special but typical case  $2\nu = 10^{-3}$ , in Figure 1 as function of  $\epsilon \equiv 1 - \Delta_0/2E_F$ , where  $\Delta_0$  is the pair binding energy. We see that  $\epsilon_0$  differs *very little* from unity (and hence  $\Delta_0/2E_F$  from zero) for all but the largest values of the coupling parameter  $\lambda \equiv g(E_F)V/2$ . Since (3) results from solving a two-body Schrödinger equation (in momentum representation), its validity is *not* limited to weak coupling, unless regarded as a Bethe-Goldstone equation (ladder approximation) treatment of the many-fermion problem, which is exact only for small  $k_F\lambda$ .

Also restricted to weak coupling is the BCS *many*-electron theory<sup>2</sup>. In this formalism a temperature-dependent energy gap  $\Delta(T)$  emerges, which for  $T = 0$  is found to be

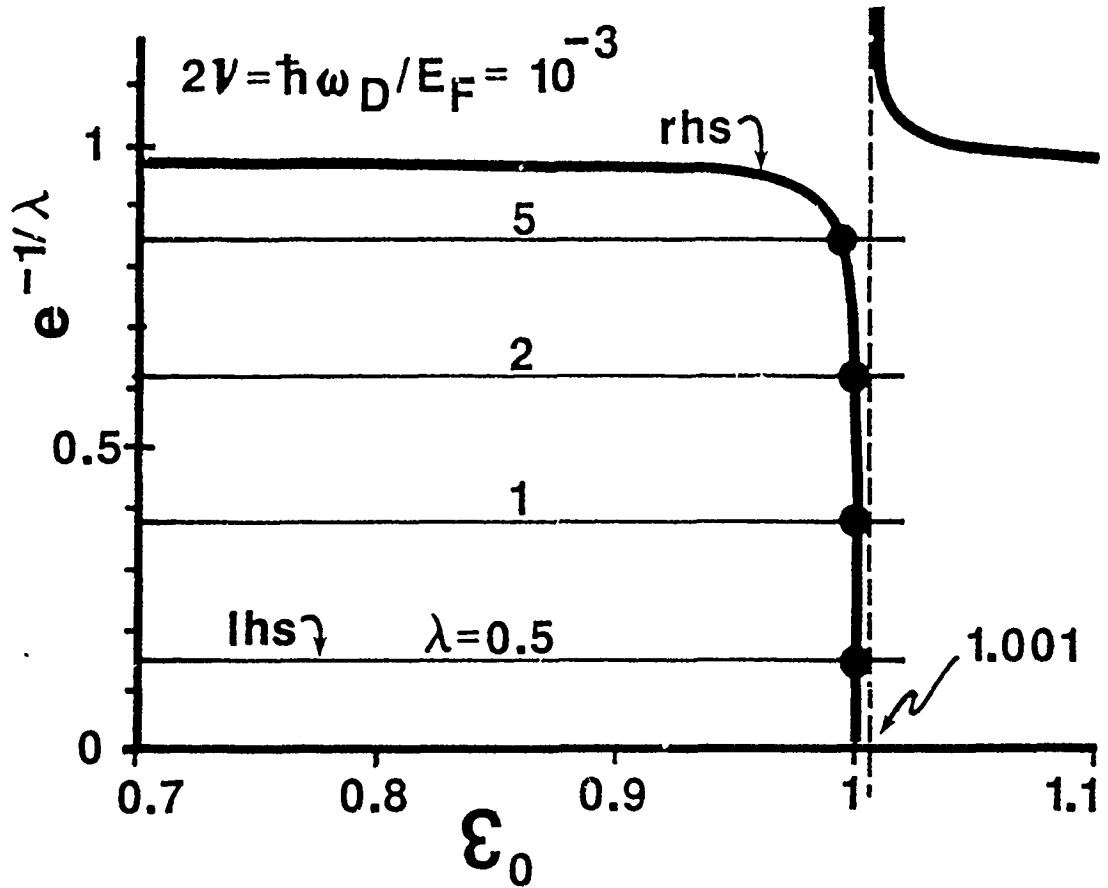


Fig. 1. Graphical solution of Eq.(3) for  $2\nu = 10^{-3}$  and several values of the coupling parameter  $\lambda$  as indicated.

$$\Delta(0) \equiv \Delta_0^{\text{BCS}} = \frac{\hbar\omega_D}{\sinh[1/\lambda]} \xrightarrow{\lambda \rightarrow 0} 2\hbar\omega_D e^{-1/\lambda}, \quad (4)$$

i.e., identical to the weak-coupling limit of the Cooper pair binding energy  $\Delta_0$  in (2). The "normal metal" to "superconductor" transition temperature  $T_c$  is then determined by the vanishing of  $\Delta(T)$ , or  $\Delta(T_c) = 0$ , whose solution is the celebrated relation

$$\Delta_0^{\text{BCS}} = \pi e^{-\gamma} kT_c \approx 1.76kT_c \quad (5)$$

where  $\gamma \approx 0.577$  is the Euler constant. Combining (4) and (5) we have

$$T_c = 1.13 \Theta_D e^{-1/\lambda}, \quad (6)$$

where  $\Theta_D \equiv \hbar\omega_D/k$  is the Debye temperature. For elemental superconductors measured  $T_c$  values range from a very low  $3.25 \times 10^{-4}$  K for Rh to 9.26 K for Nb. Since  $\Theta_D$  is proportional to an appropriately averaged sound speed  $\bar{c}$  for the lattice, and since  $\bar{c} \propto M_{\text{ion}}^{-1/2}$ , with  $M_{\text{ion}}$  the mass of the lattice ions, we see that  $T_c \propto M_{\text{ion}}^{-1/2}$ . This is known as the *isotope effect*, observed for many elemental superconductors but *not* for the new copper-oxide high- $T_c$  materials. Since  $\Theta_D \sim 10^2$  K, (6) severely limits  $T_c$  to a few degrees K with acceptable values of  $\lambda$ . Other  $T_c$  formulas<sup>3</sup>, beginning with the MacMillan<sup>4</sup> formula based on strong-coupling Migdal-Eliashberg theory<sup>5</sup>, give values of  $T_c$  as high as around 40 K. Indeed, a recent realistic tight-binding calculation with the Eliashberg equations gave Weber<sup>6</sup>  $T_c$  values between 30 to 40 K for the copper-oxide superconductors  $\text{La}_{2-x}(\text{Ba,Sr})_x\text{CuO}_4$ , which have empirical  $T_c$  values in the range 30 to 36 K. But for  $\text{YBa}_2\text{Cu}_3\text{O}_7$  with observed  $T_c = 95$  K Weber and Mattheiss, using similar techniques, were not able to extract a  $T_c$  larger than about 30 K. Furthermore, the observed value of the exponent  $\alpha$  in the formula  $T_c \propto M_{\text{ion}}^{-\alpha}$  is about 0.18 for the lanthanum-based copper oxide just cited, and 0 for the yttrium-based copper oxide.

We show how the restriction to low  $T_c$ 's, exemplified by (6) and traceable to the  $e^{-1/\lambda}$  factor in the Cooper pair problem (2), can be surmounted through a *generalized Fermi sea*. And, moreover, a negligibly weak isotope effect is then possible, even with a phonon-mediated interaction.

The fact that (quasi) electron-pair binding occurs for arbitrarily weak attraction---as well as the non-perturbative (essential singularity in  $V$ ) property of the energy  $\Delta_0$  needed to break up a Cooper pair---occurs even for one-body potential well problems<sup>8</sup> in two-dimensions (2D). Recalling that  $g(\mathcal{E}) = \text{const}$  in 2D, it is then clear why the Cooper pair problem behaves like a 2D quantum system, a fact which may be pivotal in understanding the superconductivity of the *layered* copper-oxide ceramics.

#### ABNORMAL OCCUPATION

The all-important Fermi sea assumed in the Cooper problem is appropriate to the perfect Fermi gas Slater determinant ground state wave

function for  $N$  particles enclosed in a volume  $\Omega$ ,

$$\Phi = (N!)^{-1/2} \det_{n_k} \left[ \Omega^{-1/2} e^{i\mathbf{k}_i \cdot \mathbf{r}_j} \right], \quad (7)$$

with  $i, j = 1, 2, \dots, N$ , and  $n_k^0 = \theta(k_F - k)$  the unit step function,  $\theta(x) \equiv \frac{1}{2}[1 + \text{sgn}(x)]$ . For an interacting system the most general occupation scheme consistent with the Pauli principle, however, is merely

$$n_{\mathbf{k}} = 0 \text{ or } 1, \quad \sum_{\mathbf{k}} n_{\mathbf{k}} = N. \quad (8)$$

We have raised the general question<sup>9</sup> of what the optimum scheme might be for a *non-ideal*, fully-interacting many-fermion assembly in any dimension. After all, Fermi surfaces for many materials are known which contrast drastically with the familiar Fermi sphere. Overhauser<sup>10</sup>, for example, has considered multiply-connected Fermi seas associated with both charge and spin density wave states. These states break the translation symmetry and will not concern us here. Indeed, as early as 1950 Fröhlich<sup>11</sup> had already contemplated a departure from the simple Fermi sphere, with ordinary PW orbitals. He took a spherical shell concentric upon, but disjointed from, an interior sphere, of occupied electronic states, and used this with his new electron-phonon hamiltonian in (second-order) perturbation theory to find a lower energy state, *if* the coupling exceeded a certain critical value. This behavior, however, sharply differs from the empirical fact that superconducting critical temperatures can be arbitrarily small, a drawback eventually circumvented by the (infinite-order) treatment<sup>1</sup> of Cooper with the standard Fermi sea. More recently, in an infinite meson-nucleon system a transition from a Fermi sphere to a Fermi "shell" [cf. below, Eq. (10)] distribution has been interpreted as a possible phase transition from "nuclear" to "quark" matter within a relativistic Hartree-Fock (HF) treatment<sup>12</sup>. The (first-order) transition is signalled by a large jump at high densities in the resulting low-temperature specific heat. Finally, abnormal occupation in a finite nucleus has been discovered in <sup>24</sup>Mg, in constrained HF calculations<sup>13</sup> (with good total angular momentum and its projection), using a realistic effective two-nucleon interaction based on the Reid soft-core potential.

Within the (nonrelativistic) plane-wave Hartree-Fock (PWHF)

approximation with many-fermion hamiltonian  $H$  we originally showed<sup>9</sup> that for a simple one-dimensional system under a sufficiently attractive (but non-collapsing in the thermodynamic limit), short-ranged, two-body interaction  $v_{12}$ , lower HF total energies

$$\begin{aligned} \mathcal{E}_{\text{HF}}[n_k] &\equiv \langle \phi | H | \phi \rangle \\ &= \sum_k E(k) n_k + \frac{1}{2} \sum_{k_1 k_2} \{ \langle k_1 k_2 | v_{12} | k_1 k_2 \rangle - \langle k_1 k_2 | v_{12} | k_2 k_1 \rangle \} n_{k_1} n_{k_2} \end{aligned} \quad (9)$$

emerge for some particle densities  $N/\Omega = k_F^3/3\pi^2$ , with a generalized Fermi sea defined by

$$\begin{aligned} n_k &= \theta(k - \beta k_F) \theta(\gamma k_F - k) \\ \gamma^3 - \beta^3 &= 1, \quad \gamma > \beta \geq 0, \quad \gamma \geq 1. \end{aligned} \quad (10)$$

This corresponds to a spherical shell in  $k$ -space of inner and outer radii  $\beta k_F$  and  $\gamma k_F$ , respectively. In other words, it was established that  $\mathcal{E}_{\text{PWHF}}[n_k] < \mathcal{E}_{\text{PWHF}}[n_k^0]$  for a range of densities, and in a manner reminiscent of a (first-order) gas-liquid phase transition. Any lowering of the total HF energy at fixed density comes entirely from the last (exchange) term in (9), since the first (kinetic energy) term can only increase for any  $n_k$  other than a spherical Fermi sea, while the second (direct) term is unchanged if the interaction is local, as then that matrix element is independent of the summation indices for PW states. The search for lower-energy, abnormally occupied Slater PW determinants for a wide variety of pair-interaction cases was subsequently extended<sup>14</sup> to three dimensions (3D), and to a much larger class of abnormal occupation schemes  $n_k$ . Moreover, starting from a very-many-shell structure modeling the general distribution (8), random-search and random-walk numerical techniques<sup>14</sup> established the "single-shell" distribution (10) as the optimum one in numerous cases. In still further work<sup>15</sup> it was proved, for example, that any hard-core plus square-well two-body potential prefers abnormal occupation, no matter how weak the attraction. This potential has been employed<sup>16</sup> to model liquid-<sup>3</sup>He semi-realistically. Finally, several many-boson systems were also found<sup>17</sup> which prefer abnormal occupation.

Summarizing, even at the PWHF level of approximation, Fermi seas more general than the usual spherical sea are favored for sufficiently strong

interparticle coupling. A possible physical rationale<sup>18</sup> for this is the appearance, as coupling is increased, of "particle clusterings" of some kind, since abnormal occupation precludes *small-k* states, meaning suppression of particle orbits with *large* spatial extensions.

#### TIGHTER-BOUND COOPER PAIRS

Robustly tighter bound Cooper pairs are possible, for any coupling strength, with abnormal occupation. We suggest that when suitably incorporated into the BCS-Bogoliubov<sup>19</sup>-Anderson<sup>20</sup>-Gor'kov<sup>21</sup>-Migdal-Eliashberg<sup>5</sup> formalisms, this may yet provide a comprehensive understanding of *both* low- and high- $T_c$  superconductivity, perhaps in terms of the phonon mechanism alone. The term "normal" is here used in the sense of Landau's Fermi liquid theory, since a key assumption for a first-principles derivation by Klein<sup>22</sup> of Landau's theory is that the lowest-energy single-particle states be occupied, i.e., that the familiar finite-temperature Fermi distribution holds for the single-particle spectra, instead of some *other*, more general, distribution.

Guided by our PWHF studies<sup>9,14,17</sup> we employ the model (10) merely as an illustration. This particular occupation scheme is a definite step beyond the perfect Fermi gas picture, and suffices to uncover an instability in the Fermi-sphere-induced Cooper pair. The two surfaces in (10) are situated at energies  $E_1 \equiv \beta^2 E_F \equiv (\gamma^3 - 1)^{2/3} E_F \geq 0$  and  $E_2 = \gamma^2 E_F \geq E_F$ . The parameter  $\gamma$  is presumably characteristic of the fully-interacting *many-body* system, and can later be fixed, within a BCS-like theory, e.g., variationally, with respect to the total superconducting ground-state energy. The integral in (1) now becomes

$$1 \approx V \left\{ g(E_1) \int_{E_1 - \hbar\omega_D}^{E_1} \frac{d\mathcal{E}}{2\mathcal{E} - E} + g(E_2) \int_{E_2}^{E_2 + \hbar\omega_D} \frac{d\mathcal{E}}{2\mathcal{E} - E} \right\}, \quad (11)$$

provided that  $E_1$  is significantly larger than  $\hbar\omega_D$  (as was verified *post hoc*). Scattering is now allowed by the BCS model interaction in the vicinity of *both* surfaces. Performing the integrals makes solving for  $e^{-2/g(E_F)V}$  easier than for the new eigenvalue  $E$ . Putting  $E/2E_F \equiv \epsilon$  and  $\hbar\omega_D/2E_F \equiv \nu$ , Eq. (11) leads to a transcendental equation for  $\epsilon$  which, in

the 3D application presented here, is

$$e^{-1/\lambda} \equiv e^{-2/g(E_F)\nu} = \left[ \frac{\epsilon - (\gamma^3 - 1)^{2/3} + 2\nu}{\epsilon - (\gamma^3 - 1)^{2/3}} \right]^{(\gamma^3 - 1)^{1/3}} \left[ \frac{\epsilon - \gamma^2}{\epsilon - \gamma^2 - 2\nu} \right]^\gamma. \quad (12)$$

Both quantities in the square brackets must be non-negative to ensure that the lhs of (12) be real.

We have carried out a numerical search for values of  $\epsilon$  and  $\gamma$  satisfying (12), such that  $\gamma > 1$  and  $\epsilon_0 > \epsilon \equiv 1 - \Delta/2E_F$ , with  $\Delta$  positive, for a wide range of  $(\lambda, \nu)$  values. However, a better feeling for the solutions of our model is obtained from Fig. 2, where both sides of Eq. (12)

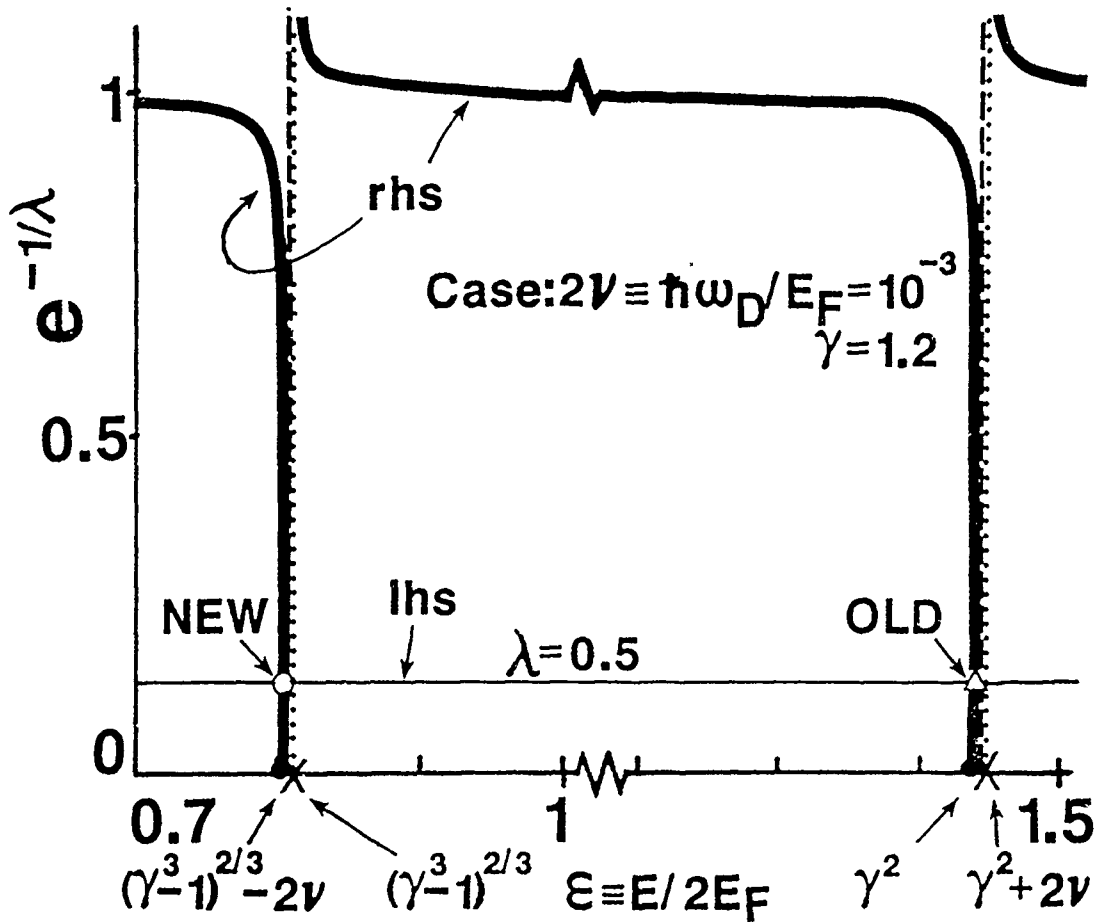


Fig. 2. Typical case illustrating graphical solution of Eq. (12).

are plotted for the case specified by  $\lambda = 0.5$ ,  $2\nu = 10^{-3}$ , and  $\gamma = 1.2$ . The lhs then equals  $\approx 0.135$ . The rhs of (12) gives rise to the full thick

curves shown; the dashed curves correspond to negative quantities inside both square brackets of (12) and so are not relevant. The two zeros (poles) are designated by dots (crosses) on the  $\epsilon$ -axis. They are labeled by their real values, for any  $\gamma \geq 1$  and  $2\nu$ , which for the specific case just cited are respectively equal to 0.808259, 0.809259, 1.440 and 1.441. The dot-to-cross distances have been exaggerated somewhat in the figure, for clarity. The lowest energy eigenvalue occurs from the projection of the intersection marked "NEW" and indicated by an open circle: it is a (quasi) bound state since  $\epsilon < 1$  and moreover, by inspection,  $\epsilon < \epsilon_0 (= 1 - 10^{-3} = 0.999)$ . The intersection marked "OLD" and indicated by an open triangle is now an *unbound* level in the pair continuum, and becomes the ordinary Cooper bound state (2) or (3) as  $\gamma \rightarrow 1$ , when the open circle intersection is pushed leftwards outside the  $\epsilon > 0$  region. The reason for tighter-bound Cooper pairs with abnormal occupation is almost trivial: an interior Fermi surface allows for *lower* kinetic energy electron pairs with roughly the same potential energy. As in the usual Cooper pair case, the new, tighter-bound Cooper pair solution will survive, no matter how weak the coupling  $V$ , since smaller coupling merely lowers the horizontal line marked "lhs". More interesting, however, is that these tighter-bound Cooper pairs can lead to transition temperatures  $T_c$  with a *robust* contribution of order  $T_F$  ( $\sim 10^4$  to  $10^5$  K), in addition to a much weaker "isotope-effect" contribution of order  $\Theta_D$  ( $\sim 10^2$  K), as we now discuss.

#### HIGH-TEMPERATURE SUPERCONDUCTIVITY

In the weak-coupling limit ( $\lambda \equiv g(E_F)V/2 \ll 1$ ) the intersection marked "new" in Fig. 2 will correspond to

$$1 - \Delta/2E_F \equiv \epsilon = (\gamma^3 - 1)^{2/3} - 2\nu - \eta, \quad (13)$$

with  $0 < \eta \ll 1$ . Inserting the last member of this into (12) and expanding about  $\eta = 0$  gives  $\eta \approx 2\nu e^{-1/\beta\lambda}$ . Recalling (5), (13) leads to

$$T_c \approx 1.13 (1 - \beta^2)T_F + 1.13 (1 - e^{-1/\beta\lambda}) \Theta_D + \dots, \quad (14)$$

where  $\beta \equiv (\gamma^3 - 1)^{1/3}$  is the radius (in units of  $k_F$ ) of the *inner* Fermi surface of the abnormal distribution (10). We found that typically  $\beta$  ranged from about 0.7 to about 0.9, so that  $1 - \beta^2$  ranges from 0.2 to 0.5.

Thus  $T_c$  values well in excess of room temperatures ( $\sim 300$  K) are possible without invoking stronger electron-phonon coupling, nor unconventional interaction mechanisms. The latter, however, are not ruled out in principle. We also note that in (14) only  $\Theta_D$  depends on  $M_{\text{ion}}^{-1/2}$  so that the isotope effect, if present, will be  $10^2$  to  $10^3$  times weaker, since  $\Theta_D/T_F \approx 10^{-3}$  to  $10^{-2}$ .

## CONCLUSIONS

Tighter-bound Cooper pairs will arise by generalizing the assumed Fermi sea for the occupied background electrons, without invoking either stronger electron-phonon coupling in the BCS interaction nor unconventional interaction mechanisms. The calculations performed in 3D can straightforwardly be done in any dimensionality as only the form of  $g(\mathcal{E})$  (which is absorbed into  $\lambda$  anyway), and the  $\beta - \gamma$  relation (10), will change.

Multiple-surfaced Fermi topologies can lead to  $T_c$ 's tied not to the Debye temperature  $\Theta_D$  ( $\sim 10^2$  K) as in normal-occupation BCS theory, but rather to the Fermi temperature  $T_F$  ( $\sim 10^4$  to  $10^5$  K). They also lead to the absence (or extreme weakness) of an isotope effect, but, as before, this neither proves nor disproves the presence of an electron-phonon interaction mechanism.

If more were known about multiply-connected Fermi surfaces and how to manipulate them, perhaps one could design materials (most probably compounds) having *interior* Fermi surfaces which, allowing for Cooper pairs with smaller kinetic energies, would result in higher  $T_c$  values.

## ACKNOWLEDGEMENTS

This work was supported in part by the U.S. Department of Energy under Contracts Nos. DE-FG02-87ER40371, Division of High Energy and Nuclear Physics. We wish to acknowledge discussions with Professors O. Civitarese, J.R. Clem, D. Cox, Christina Keller, M. Luban, H.G. Miller, S.A. Moszkowski, O. Rojo, M. Saraceno, B.D. Serot, V.V. Tolmachev and R.N. Zitter.

## REFERENCES

1. L.N. Cooper, Phys. Rev. 104, 1189 (1956)
2. J. Bardeen, L.N. Cooper and J. Schrieffer, Phys. Rev. 108, 1175 (1957)
3. P.B. Allen and B. Mitrović, Sol. State Phys. 37, 1 (1982)
4. W.L. McMillan, Phys. Rev. 167, 331 (1968)
5. A.B. Migdal, Sov. Phys.-JETP 7, 996 (1958); G. M. Eliashberg, *ibid* 11, 696 (1960)
6. W. Weber, Phys. Rev. Lett. 58, 1371 (1987)
7. W. Weber and L.F. Mattheiss, Phys. Rev. B 37, 599 (1988)
8. L.D. Landau and I.M. Lifshitz, *Quantum Mechanics*, (Pergamon, London, 1977) p. 163
9. M. de Llano and J.P. Vary, Phys. Rev. C 19, 1083 (1979)
10. A.W. Overhauser, in *Highlights of Condensed-Matter Theory*, Proc. of the Intl. School of Phys. "E. Fermi", Course LXXXIX, ed. by F. Bassoni *et al* (North-Holland, Amsterdam, 1985)
11. H. Fröhlich, Phys. Rev. 79, 845 (1950)
12. C.J. Horowitz and B.D. Serot, Phys. Lett. 109B, 341 (1982)
13. R.M. Quick and H.G. Miller, Phys. Rev. C 34, 1458 (1986)
14. M. de Llano, A. Plastino and J.G. Zabolitzky, Phys. Rev. C 20, 2418 (1979)
15. V.C. Aguilera-Navarro, R. Belehrod, M. de Llano, M. Sandel and J.P. Vary, Phys. Rev. C 22, 1260 (1980)
16. T.W. Burkhardt, Ann. Phys. (N.Y.) 47, 516 (1968)
17. V.C. Aguilera-Navarro, R. Barrera, J.W. Clark, M. de Llano and A. Plastino, Phys. Lett. 80 B, 327 (1979); Phys. Rev. C 25, 560 (1982); M.C. Cambiaggio, M. de Llano, A. Plastino and L. Szybisz, Rev. Mex. Fís. 28, 91 (1981)
18. S.A. Moszkowski, priv. comm.
19. N.N. Bogoliubov, Sov. Phys. (J.E.T.P.) 34, 41 (1958); N.N. Bogoliubov, V.V. Tolmachev and D.V. Shirkov, *A New Method in the Theory of Superconductivity* (Consultants Bureau, Inc., N.Y., 1959)
20. P.W. Anderson, Phys. Rev. 112, 1900 (1958)
21. L.P. Gor'kov, Sov. Phys. JETP 9, 1364 (1959)
22. A. Klein, Phys. Rev. 121, 957 (1961)

## THE FOUNDATION OF THE NUCLEAR SHELL MODEL<sup>†</sup>

W. H. Dickhoff and P. P. Domitrovich

Department of Physics, Washington University,  
St. Louis, Missouri 63130, USA

A. Polls and A. Ramos

Departament d'Estructura i Constituents de la Matèria,  
Universitat de Barcelona, E-8028 Barcelona, Spain

**Abstract:** The nuclear shell model exists now for forty years. The notion of independent particle motion which is at the basis of this simple picture of nuclei has recently been challenged by new experimental data. Nevertheless, a considerable amount of experimental data has successfully been interpreted over the years in terms of this picture. On a microscopic level, the success of the shell model has been linked to the strong short-range repulsion in the nuclear interaction by introducing the concept of the healing of the relative wave function of two nucleons. Recent calculations of the effective interaction in nuclear matter are discussed which demonstrate that this concept of healing is not valid but instead particles scatter at all energies in the medium. It will be argued that the success of the shell model picture should instead be linked to the validity of the quasi-particle picture as used by Landau for liquid  $^3\text{He}$ . Calculations of the spectral function for  $^{16}\text{O}$  are discussed which demonstrate the essential difference between a finite nucleus and nuclear matter. The finiteness of a nucleus ensures that a relevant single-particle basis has shell structure, implying that there is an energy window in nuclei related to the difference between particle and hole energies in which this quasi-particle picture can be applied.

### I. INTRODUCTION

The simplest version of the shell model considers nucleons bound in some attractive well moving independently from each other. This well can be thought of as being generated by the average interaction a nucleon experiences with the other

<sup>†</sup>This research was supported by the Condensed Matter Theory Program of the Division of Materials Research of the U.S. National Science Foundation under Grant No. DMR-8519077 (at Washington University) which also provided computer time for the calculations which were partly performed at the Pittsburgh Supercomputer Center. A travel grant from the U.S. Army Research Office is gratefully acknowledged. Additional support was provided in part by NATO under Grant No. RG 85/0684 and in part by CAYCIT Grant No. PB85-0072-C02-00 (Spain).

nucleons in the system. Since this average interaction is obviously attractive, nucleons can be assigned single-particle (sp) quantum numbers of a spherical well. When an average spin-orbit interaction is included, this nuclear shell model can account for all observed magic numbers as well as a number of other experimental data. This is essentially the picture as it has been published 40 years ago.<sup>1,2</sup> It has been very difficult to link this mean field picture of the nucleus and the strong repulsion present in the nucleon-nucleon (NN) interaction on a microscopic level. Historically, Brueckner<sup>3</sup> suggested to convert the bare interaction into a renormalized interaction (G matrix) which includes any number of interactions (ladder diagrams) between the particles in the medium, similar to the corresponding T matrix in free space. This G matrix is obtained by solving the Bethe-Goldstone equation.<sup>4</sup> This interaction has played an important role in the efforts to reconcile the strong interaction at short distance with the tranquil picture of nucleons moving in simple sp orbits. In ref. 5 the concept of healing of the relative wave function is introduced as an explanation for the validity of the shell model. This healing property results from the fact that the conventional solution of the Bethe-Goldstone equation does not allow scattering for energies below  $2\varepsilon_F$  as a consequence of the Pauli principle and is therefore purely real.

One of the purposes of this contribution is to show that this analysis must be improved and extended. This new analysis will rely on explicit calculations which have been performed recently for nuclear matter.<sup>6</sup> In this work the short-range correlations of the Reid soft core interaction were carefully treated and the resulting sp properties were studied in detail. This study is also relevant for finite nuclei since short-range correlations should be similar in finite and infinite systems for the same bare interaction. It will be shown that the concept of healing as discussed in the literature has no strict validity since the particles in the medium do scatter at all energies. In sec. 2 of this contribution the results of these calculations which employ the Green's function method will be reviewed and its implications for the nuclear shell model indicated. Special attention will be paid to the nucleon spectral function and the relevance of the quasi-particle concept. In sec. 3 the modifications of these results due to the finiteness of the system will be discussed. Results for calculations of the spectral function for  $^{16}\text{O}$  will illustrate the usefulness of the quasi-particle idea for finite nuclei and its relation to the success of the simple shell model.

## 2. SHORT-RANGE CORRELATIONS AND SINGLE-PARTICLE PROPERTIES

In ref. 6 the original idea of Brueckner how to treat the influence of short-range correlations, is embedded in a Self-Consistent Green's Function (SCGF) approach. The ladder equation is solved with inclusion of both particle-particle (pp) as well as hole-hole (hh) propagation. The connection between this interaction and the resulting sp properties is made by calculating the resulting self-energy. This self-energy can then be used to calculate the sp propagator or the particle and hole spectral functions in nuclear matter. In principle, this requires a self-consistent solution in which the full dressing of the sp propagator is included in the determination of the ladder correlations. At present this self-consistency has been established in ref. 6 for the quasi-particle energy which corresponds to the inclusion of only the real on-shell part of the self-energy in the self-consistency procedure.

$$\varepsilon(k) = \frac{k^2}{2m} + \text{Re } \Sigma(k, \varepsilon(k)) \quad . \quad (1)$$

When this average self-consistency is achieved the complete energy and momentum dependence of the self-energy can be studied. This requires knowledge of the imaginary

part of the self-energy above but also below the Fermi energy. It is this last contribution which has never been considered in the conventional treatment using the Bethe-Goldstone equation which only considers pp propagation in the ladder equation. Including hh propagation one naturally treats the coupling of sp degrees of freedom to 2h1p and more complicated states and therefore one obtains an imaginary contribution to the self-energy below  $\epsilon_F$ . A Green's function procedure automatically treats hh propagation on the same footing as pp propagation. Recently, this hh propagation (to all orders) has also been shown<sup>7</sup> to be the crucial link in connecting the coupled ladder self-energy problem with the description of pairing, going even beyond the conventional BCS description.<sup>8</sup>

Including hh propagation in the ladder equation implies that the resulting interaction is complex not only for energies above  $2\epsilon_F$  but also below. This conflicts with the notion of healing which has been related to the G matrix being purely real for energies below  $2\epsilon_F$  in the case of the Bethe-Goldstone equation.<sup>5</sup> Obviously, collisions do take place in the correlated system at any energy. This statement must be regarded as general for a normal Fermi liquid. The validity of shell model concepts in finite nuclei can therefore not be linked to this healing property of the relative wave function.

Calculations have been performed for the central part of the  ${}^3S_1 - {}^3D_1$  channel of the Reid soft core potential.<sup>9</sup> This avoids the strong pairing instability<sup>10</sup> in the deuteron channel and allows a careful study of the influence of short-range correlations on the sp self-energy.<sup>6</sup> The self-energy of a nucleon contains all the information necessary to obtain occupation probabilities, quasi-particle strength and broadening features which alternatively can be visualized in terms of hole and particle spectral functions. Results for the hole spectral function are given in Fig. 1 for  $k = 0.828, 1.258, 2.220,$  and  $4.376 \text{ fm}^{-1}$  at a density corresponding to  $k_F = 1.4 \text{ fm}^{-1}$ . Results for the particle spectral function are given in Fig. 2 for the same momenta. Clearly one observes the increasing validity of the quasi-particle concept when  $k$  approaches  $k_F$  since the peak of the spectral function becomes sharper the closer the momentum is to  $k_F$ . This holds for momenta below  $k_F$  (Fig. 1) as well as for momenta above  $k_F$  (Fig. 2). One observes therefore in this actual calculation which uses a strongly repulsive NN interaction at short distances, that the notion of quasi-particles is valid in exactly the same sense as it has been used by Landau in his description of Fermi liquids.<sup>11</sup> In an infinite system this concept is strictly valid only for the Fermi momentum. For other momenta one observes therefore that the further the momentum value is removed from  $k_F$  the more the quasi-particle peak is broadened.

For momenta close to  $k_F$  most of the hole strength is under the quasi-particle peak when  $k$  is smaller than  $k_F$ . For  $k = 1.258 \text{ fm}^{-1}$  83% of the hole strength is under the peak whereas 3% is found at lower energies. The occupation of this momentum in the correlated ground state is obtained by integrating the hole spectral function up to  $\epsilon_F$  and therefore corresponds to 86%. The remaining strength is moved beyond the Fermi energy and belongs to the particle spectral function shown in Fig. 2. The remaining 14% of the strength is smeared out over a very large energy domain which is intimately connected with the character of the interaction which couples sp degrees of freedom to very high-lying 2p1h etc. states. This removal of sp strength to high energy is observed for all momenta by the same amount (see Fig. 2) emphasizing the short-range nature of the effect. The jump in the momentum distribution at  $k_F$  is equal to the strength of the quasi-particle pole at  $k_F$  and a value of 0.83 is obtained here. The inclusion of tensor correlations is expected to decrease this value further by a few percent.<sup>12</sup>

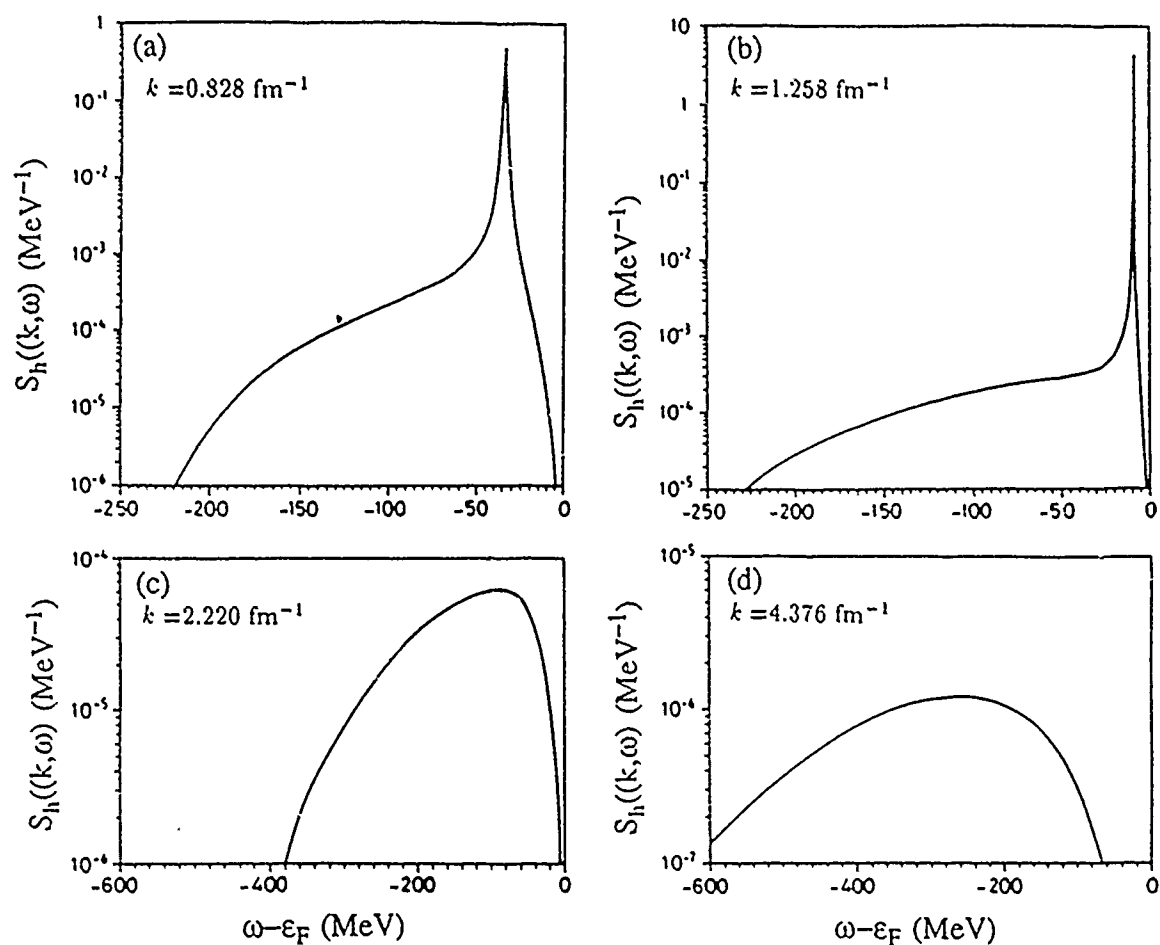


Fig. 1. Hole spectral functions at  $k_F = 1.4 \text{ fm}^{-1}$  for  $k = 0.828, 1.258, 2.220,$  and  $4.376 \text{ fm}^{-1}$ .

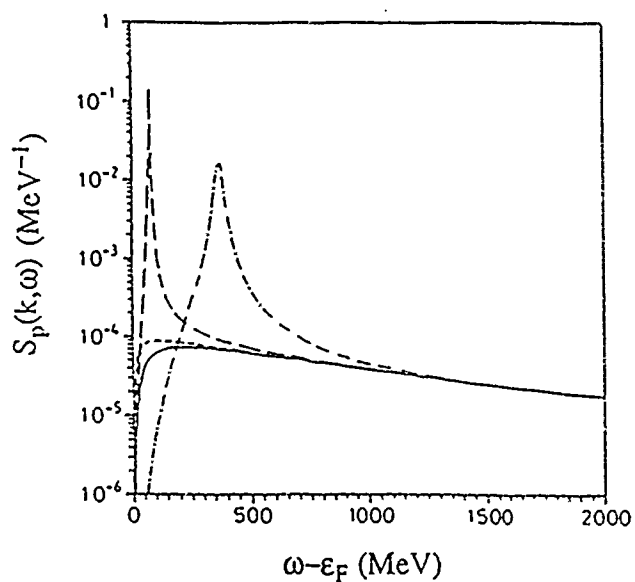


Fig. 2. Particle spectral functions at  $k_F = 1.4 \text{ fm}^{-1}$  for  $k = 0.828$  (solid),  $1.258$  (short dashed),  $2.220$  (long dashed), and  $4.376 \text{ fm}^{-1}$  (dot dashed).

These and other results are more fully discussed in ref. 6 together with the calculational details. One can conclude from these results that even though there is strong scattering in the medium, the concept of a quasi-particle picture is still extremely useful in exactly the same way as it has been used in Landau's Fermi liquid theory<sup>11</sup> for  $^3\text{He}$ . For a normal Fermi liquid this validity of the quasi-particle concept is almost exclusively a phase space effect related to the presence of  $2p1h$  and  $2h1p$  states around the Fermi surface which can mix with  $sp$  states. The strength of the quasi-particle pole is then a good measure of the correlations, the closer to 1 the more the system can be described in terms of a mean field picture.

The role of short-range correlations should be similar in finite nuclei and infinite nuclear matter at the corresponding density. These results have therefore direct bearing on the situation in finite nuclei and depletion effects due to short-range correlations are inevitable.<sup>13</sup> From the present results one can also infer that the missing  $sp$  strength is not just "around the corner"; it is removed to very high energies as a consequence of the short-range correlations. This effect of the short-range correlations and its consequences have not been properly considered in Brueckner type calculations.

### 3. FINITE NUCLEI AND IMPLICATIONS FOR THE SHELL MODEL

Presently, the breakdown of the mean field picture is an experimental reality. Combined analysis of  $(e,e'p)$  reactions<sup>14</sup> together with absolute charge density distribution measurements<sup>15</sup> indicates that the occupation of the  $3s_{1/2}$  proton shell in  $^{208}\text{Pb}$  is  $80 \pm 10\%$ . This should be compared to the theoretical results of refs. 13,16 and 17. Direct analysis of  $(e,e'p)$  cross sections with shell model momentum distributions suggests that the discrete low energy transitions carry about 50% of the hole strength.<sup>18,19</sup> This would imply that 30% of the hole strength is at even higher energies in the  $A-1$  nucleus and cannot be detected. The analysis of ref. 16 for the neutron states in  $^{208}\text{Pb}$  indicates that about 73% of the hole strength is found at low energy for such states with occupation numbers corresponding to 0.85. Assuming similar results for protons this indicates a 20% discrepancy between this theoretical result and the experimental analysis

To address this question it is profitable to investigate the influence of low-lying excitations on the redistribution of  $sp$  strength directly in finite nuclei. One should keep in mind that the nuclear matter results discussed above indicate that somewhat more than 10% of the  $sp$  strength is at high energy. This result is due to a basic asymmetry between the influence of  $pp$  and  $hh$  contributions and should be taken into account in analyses like the one in ref. 16. The spectral functions in finite nuclei can be obtained directly by solving the Dyson equation in a suitable basis for the relevant nucleus. Results are reported here for  $^{16}\text{O}$ . First a Hartree-Fock (HF) basis is generated by solving the HF equations using the  $G$  matrix interaction  $G_{NM}^{\text{II}}$  which is a good local and static approximation of a  $^{16}\text{O}$   $G$  matrix.<sup>20</sup> As in any HF calculation a mean field is generated in which one can define fully occupied and completely empty  $sp$  states for this nucleus. The  $G$  matrix that is used here does not include any shell structure information since it is calculated originally for nuclear matter with a standard gap in the  $sp$  spectrum.<sup>21</sup>

To calculate the influence of low energy excitations on the distribution of  $sp$  strength the second order self-energy contribution calculated with this interaction is used to solve the Dyson equation.

$$g(\alpha, \beta; \omega) = g^{(0)}(\alpha, \beta; \omega) + \sum_{\gamma, \delta} g^{(1)}(\alpha, \gamma; \omega) \Sigma^{(1)}(\gamma, \delta; \omega) g(\delta, \beta; \omega) \quad (2)$$

The sp quantum numbers  $\alpha, \beta$ , etc. refer to the HF basis. The sums in Eq. (2) are restricted to HF states within 50 MeV of the Fermi energy of the HF calculation. This ensures that indeed the influence of low-lying 2p1h and 2h1p states on the redistribution of sp strength in a finite system is studied. Contributions from higher shells will eventually also lead to some form of double counting since these states have already been considered in the construction of the residual interaction. The presence of an explicit energy dependence in this second order self-energy contribution is responsible for the fragmentation of sp strength both above the Fermi energy by coupling to 2p1h states as well as below the Fermi energy by coupling to 2h1p states. This can be clearly seen by inspection of the explicit second order self-energy contribution

$$\begin{aligned} \Sigma^{(2)}(\gamma, \delta; \omega) = & \frac{1}{2} \sum_{\epsilon, \mu, \nu} \langle \gamma \mu | G_{N, N+1}^{\parallel} | \epsilon \nu \rangle \langle \epsilon \nu | G_{N, N+1}^{\parallel} | \delta \mu \rangle \\ & \times \left[ \frac{\theta(\epsilon - F) \theta(\nu - F) \theta(F - \mu)}{\omega - (\epsilon_{\epsilon} + \epsilon_{\nu} - \epsilon_{\mu}) + i\eta} + \frac{\theta(F - \epsilon) \theta(F - \nu) \theta(\mu - F)}{\omega - (\epsilon_{\epsilon} + \epsilon_{\nu} - \epsilon_{\mu}) - i\eta} \right] \quad (3) \end{aligned}$$

The solution to Eq. (2) has the form

$$g(\alpha, \beta; \omega) = \sum_n \frac{\langle \psi_0^A | a_{\alpha} | \psi_n^{A+1} \rangle \langle \psi_n^{A+1} | a_{\beta}^{\dagger} | \psi_0^A \rangle}{\omega - (E_n^{A+1} - E_0^A) + i\eta} + \sum_m \frac{\langle \psi_0^A | a_{\beta}^{\dagger} | \psi_m^{A-1} \rangle \langle \psi_m^{A-1} | a_{\alpha} | \psi_0^A \rangle}{\omega - (E_0^A - E_m^{A-1}) - i\eta} \quad (4)$$

The poles in this equation give the energies of the states in the  $A \pm 1$  systems which can couple to the ground state of the  $A$ -body system through the creation and annihilation operators  $a$  and  $a^{\dagger}$ , respectively. The residues at the poles for the diagonal sp propagator correspond to the spectroscopic factors for the corresponding transition from the ground state in the  $A$ -body system to the state  $n(m)$  in the  $A+1(A-1)$ -body system. The energies and residues in Eq. (4) are obtained by solving an energy dependent eigenvalue problem which can be derived from Eq. (2).<sup>22</sup>

In Fig. 3 results for the sp strength distribution are shown for the relevant  $s_{1/2}$  states in  $^{16}\text{O}$ . The results are smeared by distributing the strength of each peak by 0.5 MeV. In the HF picture, the lowest  $s_{1/2}$  state has full occupation, *i.e.*, a spectroscopic factor of 1.0 to one state in the  $A-1$  nucleus. This result is also typical for Brueckner-Hartree-Fock calculations in which the energy dependence of the  $G$  matrix is treated explicitly. When no hh contributions in the ladder equation are included the resulting self-energy is real below the Fermi energy and therefore leads to HF like hole states. The next  $s_{1/2}$  state is completely empty and has a spectroscopic factor of 1.0 to one state in the  $A+1$  system. Including dynamic correlations in this second order self-energy calculation still leads to a concentration of the  $2s_{1/2}$  strength in one peak as shown in Fig. 3. In contrast the  $1s_{1/2}$  strength (represented by all the other peaks in the figure) is completely fragmented with most of its strength below the Fermi energy leading in this case to an occupation of 96%. The remaining 4% is located at higher energy shown by the smaller peaks to the right of the  $2s_{1/2}$  peak.

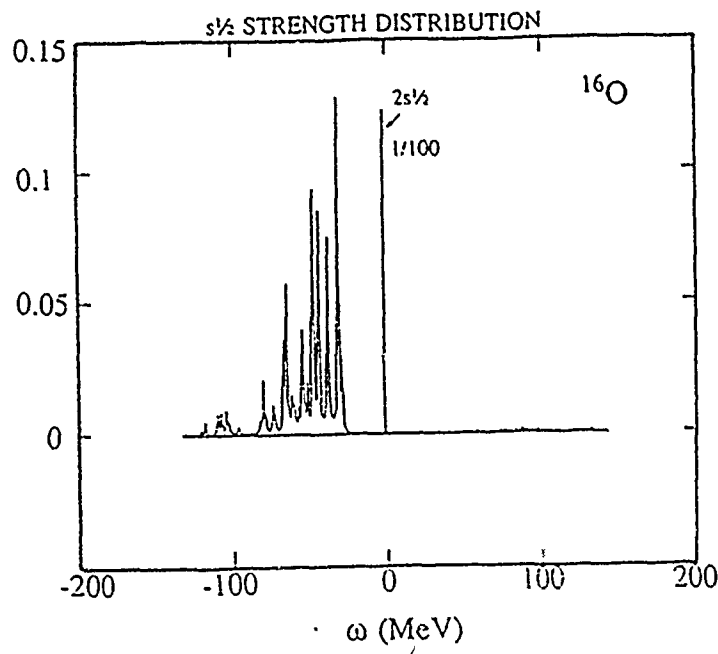


Fig. 3. Distribution of  $s_{1/2}$  strength in  $^{16}\text{O}$  as a function of energy. The  $2s_{1/2}$  strength is located mainly in one peak reduced here by a factor of  $1/100$ . The rest of the  $2s_{1/2}$  strength is not shown. All other peaks correspond to strongly fragmented  $1s_{1/2}$  strength. Note that a small portion of  $1s_{1/2}$  strength is also found above the Fermi energy.

This calculation therefore has the same typical features that one encounters in nuclear matter. For  $sp$  states which are close to the Fermi energy the dynamic coupling in the self-energy results in one strong peak which carries less than but of the order of 100% of the strength. In a finite nucleus like  $^{16}\text{O}$  this is particularly obvious since there are no  $2p_{1h}$  or  $2h_{1p}$  states in the immediate vicinity of the  $2s_{1/2}$  energy and the strength remains mainly concentrated in one state since more complicated states are too far away in energy. This feature emphasizes the important role of the finiteness of the system. It leads automatically to a finite  $ph$  energy gap which results in a larger window of validity of the quasi-particle approximation in finite nuclei. For the  $1s_{1/2}$  state one observes a strong fragmentation since its energy (in HF) is located in an energy interval where (in this case) many  $2h_{1p}$  are located and it becomes relatively easy to mix with such more complicated states. The same result is observed in infinite systems for momenta far from the Fermi momentum. Experimental results on finite nuclei by means of the  $(e,e'p)$  reaction show a smooth  $1s_{1/2}$  strength distribution for proton knock-out of  $^{16}\text{O}$ .<sup>23</sup> Recent  $(p,2p)$  and  $(p,pn)$  experiments on  $^{16}\text{O}$  show the same feature.<sup>24</sup> Clearly the knock-out of an  $1s_{1/2}$  particle is possible for a broad range of energies.

The calculation gives similar results as discussed above for other orbitals. Particles in shells closer to the Fermi energy like the  $1p_{3/2}$  and the  $1p_{1/2}$  are found in large fractions in the low energy states of the  $A = 15$  system but do not carry 100% of the strength. On the other side of the Fermi energy most of the  $1d_{5/2}$ ,  $2s_{1/2}$  (see Fig. 3) and  $1d_{3/2}$  strength is found in the low energy states of the  $A = 17$  system. Unoccupied states which in HF are far removed from the Fermi energy show a similar fragmentation as the  $1s_{1/2}$  state on the other side of the Fermi energy.

These results are in sharp contrast with the mean field picture of nuclei. In an atom *e.g.*, where the Hartree-Fock approximation works very well, all hole states have a well defined energy and carry 100% of the strength. The situation in a nucleus

therefore resembles much more that in liquid  ${}^3\text{He}$  and in nuclear matter as discussed in sec. 2. Nuclear single-particle excitations as observed near the Fermi energy must therefore be reinterpreted as quasi-particle or quasi-hole excitations which carry a considerable amount of sp strength. Present experimental results put the nucleus somewhere in between atoms and liquid  ${}^3\text{He}$  as far as the strength of correlations are concerned. States which are far away from the Fermi energy in mean field are located at energies at which a considerable number of  $2p1h$  or  $2h1p$  states are found. The strength of the nuclear interaction is such that considerable mixing between these degrees of freedom occurs leading to the appearance of sp strength in a broad energy range.

The experimentally observed smooth distribution of hole strength<sup>18,19,23,24</sup> further emphasizes the non-linear aspects of the problem of calculating the sp propagator. The present calculation uses HF sp propagators in the calculation of the second order self-energy contribution. However, also these intermediate  $2h1p$  and  $2p1h$  states are not good eigenstates (see Eq. (3)) and are broadened themselves. This effect can be incorporated by using self-consistent sp propagators in the calculation of the self-energy in the same non-linear fashion as the HF problem is solved. This self-consistent formulation is necessary to explain the observed experimental results of smooth hole strength distributions. This observation suggests that it is not very realistic to obtain information on the widths of such strength distributions from nuclear matter calculations. The role of the ph gap in a finite system in the fragmentation of sp strength should be explicitly treated.

The results obtained here for  ${}^{16}\text{O}$  do not yet include the effect of short-range and tensor correlations on the sp propagator but instead emphasize the role of the finiteness of the system with its shell structure and surface. These calculations show that up to 5% of strength (using second order self-energy) can be found in tiny fragments below the Fermi energy as a result of the coupling of sp states to low-lying  $2h1p$  states. Taking the global effect of short-range correlations (as discussed in sec. 2) into account and adding another 5% depletion effect due to tensor correlations,<sup>12,17</sup> one expects about 20% of the sp strength to be located above  $\epsilon_F$  for normally occupied states. Still, most of the remaining strength for these valence hole states should be found in discrete peaks and not much more than 10% at lower energies (higher excitation energy in the  $A-1$  system) according to the present theoretical results. This is in reasonable agreement with the results of ref. 16, but disagrees with the present analysis of the  $(e,e'p)$  experiment<sup>18,19</sup> which assigns about 50% of the hole strength to discrete states at low energy and from a combined analysis together with charge density distributions<sup>15</sup> leads to 80% occupation for the  $3s_{1/2}$  state in  ${}^{208}\text{Pb}$ .

From the results discussed here and in sec. 2 one can conclude that the success of the conventional shell model is related to the success of the quasi-particle picture for nuclear systems and the finiteness of the nucleus which extends the window of the validity of this picture. In a Fermi liquid this picture pertains strictly to the Fermi momentum and energy. Since particle-hole excitations start already at zero excitation energy, there is immediately this broadening effect when one moves away from the Fermi surface. In contrast to this, a finite particle-hole excitation energy exists in nuclei since these systems are confined in space which leads to discrete single-particle energies. For this reason there is a broader validity of the quasi-particle picture in nuclei and the shell model makes sense when it is not pushed beyond its window of validity. Finally, one should also remember the difficulty to explain the experimental charge density distribution of nuclei<sup>25</sup> when a mean field picture is employed. From partially occupied  $s_{1/2}$  states in a nucleus one obtains an automatic reduction of the central charge density which can qualitatively explain the experimental data.

The conclusion one can draw from the above discussion is that a marriage of the idea of Brueckner to treat short-range correlations and the notion of quasi-particles employed by Landau both developed already in the fifties, leads to a fascinating picture of the nucleus as a correlated many-body system and also provides a basis for a theoretical foundation of the nuclear shell model in the presence of strong interactions. Present experimental and theoretical evidence suggests that nuclei are considerably more correlated than atoms and the mean field picture for nuclei is not valid.

#### REFERENCES

1. O. Haxel, J. H. D. Jensen, and H. E. Suess, *Phys. Rev.* 75 (1949) 1766.
2. M. Goeppert-Mayer, *Phys. Rev.* 75 (1949) 1969.
3. K. A. Brueckner, C. A. Levinson and H. M. Mahmoud, *Phys. Rev.* 95 (1954) 217.
4. H. A. Bethe and J. Goldstone, *Proc. Roy. Soc. A*238 (1957) 1531.
5. L. C. Gomes, J. D. Walecka and V. F. Weisskopf, *Ann. Phys.* 3 (1958) 241.
6. A. Ramos, A. Polls, and W. H. Dickhoff, *Nucl. Phys. A* in press; in *Condensed Matter Theories*, vol. 3, ed. J. S. Arponen, R. F. Bishop and M. Manninen (Plenum, New York, 1987) p. 319.
7. W. H. Dickhoff, *Phys. Lett.* 210B (1988) 15.
8. J. Bardeen, L. N. Cooper and J. R. Schrieffer, *Phys. Rev.* 108 (1957) 1175.
9. R. V. Reid, *Ann. Phys.*50 (1968) 411.
10. W. H. Dickhoff, *Condensed Matter Theories Vol.4*, ed. J. Keller (Plenum, New York, 1989) in press.
11. L. D. Landau, *Soviet Phys.*8 (1958) 70.
12. S. Fantoni and V. R. Pandharipande, *Nucl. Phys.* A427 (1984) 473.
13. V. R. Pandharipande, C. N. Papanicolas and J. Wambach, *Phys. Rev. Lett.* 53 (1984) 1133.
14. E. N. M. Quint *et al.*, *Phys. Rev. Lett.* 58 (1987) 1088.
15. J. M. Cavedon *et al.*, *Phys. Rev. Lett.* 49 (1982) 978.
16. C. Mahaux and R. Sartor, *Nucl. Phys.* A493 (1989) 157.
17. O. Benhar, A. Fabrocini and S. Fantoni, preprint.
18. E. N. M. Quint, Ph.D. Thesis (University of Amsterdam, 1988).
19. L. Lapikás, preprint NIKHEF (1989).
20. P. Czerski, W. H. Dickhoff, A. Faessler and H. Müther, *Nucl. Phys.* A427 (1984) 224.
21. W. H. Dickhoff, *Nucl. Phys.* A399 (1983) 287.
22. P. P. Domitrovich and W. H. Dickhoff, to be published.
23. J. Mougey, *Nucl. Phys.*A335 (1980) 35.
24. W. J. McDonald *et al.*, *Nucl. Phys.* A456 (1986) 577.
25. B. Frois and C. Papanicolas, *Ann. Rev. Nucl. Part. Sci.* 37 (1987) 133.

# QUANTUM MOLECULAR DYNAMICS SIMULATION OF ELECTRON BUBBLES IN A DENSE HELIUM GAS

Rajiv K. Kalia and P. Vashishta

Materials Science Division, Argonne National Laboratory, Argonne, IL 60439, USA

S. W. de Leeuw

Universiteit van Amsterdam, Amsterdam, The Netherlands

John Harris

Institut für Festkörperforschung der Kernforschungsanlage, D-5170 Jülich, West Germany

## 1. INTRODUCTION

In recent years, mixed quantum-classical systems consisting of excess electrons interacting with classical many-body systems at finite temperatures have been studied extensively with computer-simulation techniques<sup>1</sup>. The simulation methods for these systems include the path integral Monte Carlo<sup>1</sup> or molecular dynamics<sup>2</sup> and dynamical simulated annealing<sup>3</sup>. The latter can only provide the ground-state static properties of the quantum particles. The path integral approach has been used successfully to calculate the equilibrium properties, but the study of time correlation functions<sup>4</sup> is not reliable at long times. However, the recently developed quantum molecular dynamics method, which deals directly with the time-dependent Schrödinger equation, contains all the dynamical information for quantum particles.

## 2. QUANTUM MOLECULAR DYNAMICS METHOD

Quantum molecular dynamics method<sup>5</sup> provides the real-time dynamics of quantum and classical particles in mixed systems at finite temperatures through the numerical solutions of the time-dependent Schrödinger equation for quantum particles and Newton's equations of motion for classical particles. To understand this technique, consider a quantum particle of mass  $m$  described by the wave function,  $\psi(\mathbf{r},t)$ , interacting with a classical system of  $N$  particles with masses  $M_i$  and positions  $\{\mathbf{R}_i(t)\}$ . For the quantum particle we have

$$i \frac{\partial \psi(\vec{r}, t)}{\partial t} = \left( -\frac{\nabla^2}{2m} + V(\vec{r}) \right) \psi(\vec{r}, t); \quad V(\vec{r}) = \sum_{i=1}^N v(\vec{r} - \vec{R}_i) \quad (1)$$

where  $v$  is the interaction potential between the quantum and classical particles and we use atomic units,  $\hbar = e = 1$ . In the Born-Oppenheimer approximation, the positions of the classical particles evolve from Newton's equations of motion:

$$M_i \ddot{\vec{R}}_i = -\nabla_i U(\{\vec{R}_i\}) - \nabla_i \int d\vec{r} |\psi(\vec{r}, t)|^2 v(\vec{r} - \vec{R}_i) \quad (2)$$

where  $U$  is the potential energy for the classical particles. Choosing a small time step  $\Delta t$ , the solution of Eq. (1) can be written as<sup>6</sup>

$$\psi(\vec{r}, t + \Delta t) = e^{i\Delta t \nabla^2/4m} e^{-i\Delta t V} e^{i\Delta t \nabla^2/4m} \psi(\vec{r}, t) + O[(\Delta t)^3] \quad (3)$$

Equation (3) is solved with fast Fourier transform (FFT) techniques<sup>6</sup>. First, note

$$e^{i\Delta t \nabla^2/4m} \psi(\vec{r}, t) = \sum_{\vec{k}} \psi(\vec{k}, t) e^{-i\Delta t k^2/4m} e^{i\vec{k} \cdot \vec{r}} \quad (4)$$

which means multiplying the Fourier transform of  $\psi(\vec{r}, t)$ , i. e.,  $\psi(\vec{k}, t)$  with  $\exp(-i\Delta t k^2/4m)$ , followed by an inverse FFT. Next, the outcome of Eq. (4) is multiplied by  $\exp(-i\Delta t V)$ . Finally, the FFT of the resultant of the last step is multiplied with  $\exp(-i\Delta t k^2/4m)$  and then the inverse FFT is taken. These three steps are repeated to obtain the time evolution of the wave function. The classical equations of motion can be integrated numerically with one of several available algorithms<sup>7</sup>.

For systems with broken symmetry due to the presence of surfaces or an external electric field, the use of periodic boundary conditions in the broken-symmetry direction is inappropriate and so the first and third steps in the time-stepping operation in Eq. (3) cannot be executed with the FFT method. For these physical situations a new QMD algorithm<sup>8</sup> has been developed.

### 3. AN EXCESS ELECTRON IN A DENSE HELIUM GAS

An injected electron in a sufficiently dense helium gas tends to localize in the form of a bubble as a result of the strongly repulsive electron-helium interaction<sup>9</sup> at short and intermediate distances. Recently we investigated the electron bubble formation using the QMD scheme<sup>10</sup>. For the electron in helium problem, the helium particles interact with each other via a two-body Lennard-Jones

potential with parameters  $\epsilon = 10.22\text{K}$  and  $\sigma = 2.576 \text{ \AA}$ , and with the electron via a pseudopotential<sup>9</sup>.

The QMD simulations<sup>10</sup> were performed at 77K for reduced helium densities  $n = \rho\sigma^3 = 0.1, 0.17,$  and  $0.25$  which correspond to  $\rho = 0.61, 1.0,$  and  $1.46 \times 10^{22} \text{ cm}^{-3}$ . Systems with  $n = 0.1$  and  $0.17$  contained 512 helium atoms while the simulations at the highest helium density were carried out with 64 and 140 particles. These gave similar results though the smaller system showed evidence of finite-size effects. The electron wave packet was propagated with fast Fourier transforms on  $32^3$  grid points and with time step,  $\Delta t$ , in the range of  $0.2 - 0.5 \text{ a.u.}$  The total energy was conserved to better than  $0.1\%$  over  $10^6$  time steps. Some simulations with  $64^3$  grid points gave identical results. Classical molecular dynamics for helium atoms was performed in the canonical ensemble<sup>11</sup>.

#### 4. RESULTS

Figure 1 shows the electron-helium radial distribution function,  $G(r)$ , measured relative to the center-of-mass of the electron wave packet for  $n = 0.25$ . At this high helium density, there are no helium atoms up to  $r \sim 12 \text{ a.u.}$  and this excluded-volume effect is an indication of an electron bubble. The excluded volume is also present at  $n = 0.17$ . The shape parameter<sup>10</sup> for the electron bubble indicates that the bubble is spherical. From the excluded-volume region in  $G(r)$  we estimate the size of the bubble to be  $\sim 12 \text{ a.u.}$  At the lowest density,  $n = 0.1$ ,  $G(r)$  does not display the excluded-volume behavior as the wave packet de-localizes.

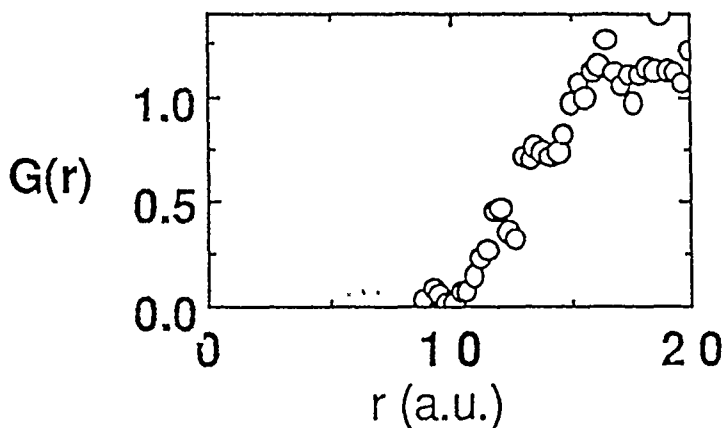


Figure 1: Electron-helium radial distribution function,  $G(r)$ , for  $n = 0.25$ .

Next, let us examine the time variation of the extent of the self-trapped electron. At  $n = 0.17$ , the participation ratio remains small and almost constant over the entire simulation, indicating that the electron is localized. The behavior is quite similar at  $n = 0.25$ , but very different at  $n = 0.10$ . Figure 2 shows the participation ratio,  $p(t) = (\Omega \int dr |\psi(r,t)|^4)^{-1}$ , normalized to the volume of the MD

cell for  $n = 0.1$ . This simulation was started by expanding the length scale of the final configuration of the  $n = 0.17$  run to a value corresponding to  $n = 0.1$  and projecting out the new electron ground state, which corresponds to an almost spherical bubble. Therefore the participation ratio starts

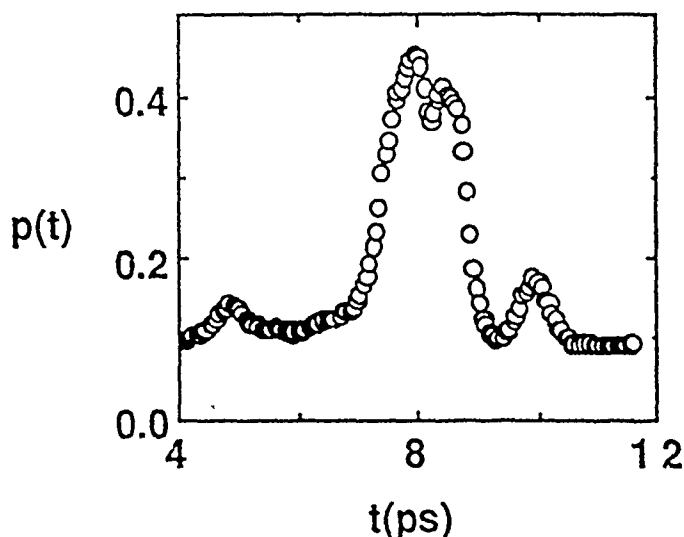


Figure 2: Participation ratio for  $n = 0.1$  as a function of time.

out at a value determined primarily by the bubble size at  $n = 0.17$  scaled by the increase in the cell size in changing the system density from  $n = 0.17$  to  $0.1$ . It is observed that the bubble quickly expands to a volume that is a sizeable fraction of the cell volume. After 4 ps the electron wave packet undergoes large expansions and contractions and finally after 8 ps the wave packet occupies almost the entire volume of the cell. This expansion indicates de-localization of the electron that is very likely limited by the size of the system. The wave packet attempts to find a region of the cell where the helium density is less. Thus, as the simulation proceeds, the wave packet localizes again temporarily because of thermal fluctuation in the system. This partial localization and de-localization is expected to continue indefinitely.

Figure 3 shows the current-current correlation function of the electron,  $\chi''(\omega)$ , for  $n = 0.25$  and  $0.1$  obtained by Fourier transforming the time correlation function  $\langle \nabla \psi_t \cdot \nabla \psi_0 \rangle$  and taking the configurational average within the Franck-Condon<sup>6</sup> approximation. For  $n = 0.25$ ,  $\chi''(\omega)$ , which is simply related to the optical absorption spectrum, displays a significant structure which

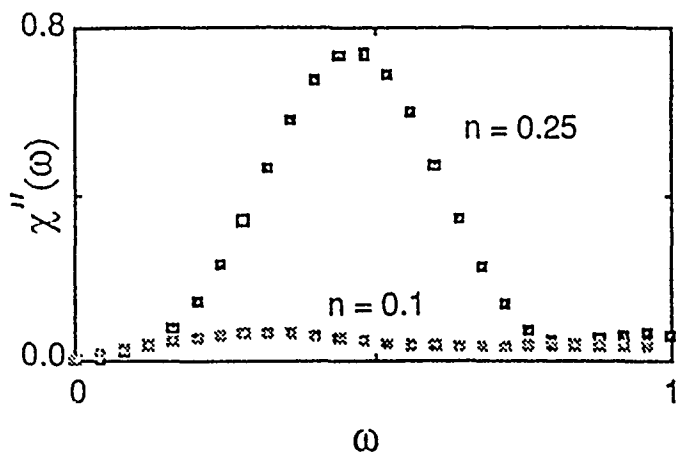


Figure 3: Imaginary part of the current-current correlation function as a function of energy in electron volts for helium densities  $n = 0.25$  and  $0.1$ . The peak at  $n = 0.25$  is due to intra-bubble transitions.

shifts to a lower energy as the helium density is reduced to  $0.17$ . These peaks are present throughout the simulations. At  $n = 0.1$ , when the wave packet is delocalized, the structure disappears and only a background is observed.

At  $T = 77\text{K}$  we have also calculated<sup>8</sup> the electron mobility at a helium density of  $1.25 \times 10^{22} \text{ cm}^{-3}$ . Applying an electric field of  $2.6 \times 10^5 \text{ volt/cm}$  in the  $x$  direction, it is observed that the electron drifts with a velocity of  $(2.2 \pm 0.5) \times 10^4 \text{ cm/s}$ . The applied field is small since it does not produce any noticeable changes in  $G(r)$ . From this simulation we obtain the electron mobility to be  $(0.08 \pm 0.02) \text{ cm}^2/\text{volt-s}$  which is in good agreement with the extrapolated experimental value<sup>12</sup> ( $0.1 \text{ cm}^2/\text{volt-s}$ ).

## 5. CONCLUSION

In this paper we have presented the QMD simulation technique for studying the dynamics of quantum particles in mixed systems at finite temperatures. This technique is applied to simulate the behavior of an excess electron in helium gas at  $77\text{K}$ . It is found that the electron localizes in the form of a nearly spherical bubble of approximately  $7 \text{ \AA}$  in radius above a critical density of  $0.6 \times 10^{22} \text{ cm}^{-3}$ . The bubble possesses quasi bound excited states and intra-bubble dipole transitions between these states give rise to a pronounced structure in the optical absorption spectrum. Below the critical density the electron percolates through the helium gas and displays a featureless excitation spectrum.

## ACKNOWLEDGEMENTS

We would like to thank L. H. Yang, M. H. Degani, and J. P. Rino for useful discussions. This work was supported by the U. S. DOE, BES-Materials Sciences Contract No. W-31-109-ENG-38. One of us (R.K.K) would also like to

acknowledge grants of CPU time on the MFE Cray 2 at Livermore through a Grand Challenge proposal. R. K. K. and P. V. would like to acknowledge partial travel support from the U. S. Army Research Office.

## REFERENCES

- 1) B. J. Berne and D. Thirumalai in Annual Review of Physical Chemistry, vol 37, eds. H. L. Strauss, G. T. Babcock, and C. Bradley Moore, (Annual Reviews Inc. Palo Alto, 1986) pp. 401-424.
- 2) M. Parrinello and A. Rahman, J. Chem. Phys. **80**, 860 (1984).
- 3) R. Car and M. Parrinello, Phys. Rev. Lett. **55**, 2471 (1985).
- 4) J. D. Doll and D. L. Freeman, J. Phys. Chem. **92**, 3278 (1988) .
- 5) A. Selloni, P. Carnevali, R. Car, and M. Parrinello, Phys. Rev. Lett. **59**, 823 (1987).
- 6) M. D. Feit, J. A. Fleck, and A. Steiger, J. Comp. Phys. **47**, 412 (1982) .
- 7) A. Rahman, Correlation Functions and Quasiparticle Interactions in Condensed Matter, ed. J. Woods Halley, (Plenum, N.Y., 1978) pp. 417-433.
- 8) R. K. Kalia, P. Vashishta, and S. W. de Leeuw, J. Chem. Phys. **90**, 6802 (1989).
- 9) N. R. Kestner, J. Jortner, M. H. Cohen, and S. A. Rice, Phys. Rev. **140**, A56 (1965).
- 10) R. K. Kalia and J. Harris, to be published.
- 11) S. Nosé, Mol. Phys. **52**, 255 (1984) .
- 12) A. Bartels, Appl. Phys. **8**, 59 (1975) .

## QUANTUM LIQUID FILMS: A GENERIC MANY-BODY PROBLEM

E. Krotscheck<sup>†</sup>, J. L. Epstein<sup>†</sup>, and M. Saarela<sup>‡</sup>

<sup>†</sup>Center for Theoretical Physics, Department of Physics,  
Texas A&M University, College Station, Texas 77843.

<sup>‡</sup>Department of Theoretical Physics, University of Oulu,  
Linnanmaa, SF-90570 Oulu 57, Finland.

This contribution reports on recent progress in the investigation of the structure and excitations of quantum liquids adsorbed to a solid surface, the states of impurity atoms in such films, and the interaction between them. The subtitle of my talk is "*A Generic Many-Body Problem*", it indicates that I will, to some extent, emphasize the methodological aspect of the problem.

We start the microscopic description of a many-body system of  $N$  particles in a given volume  $\Omega$  in an external potential with an empirical Hamiltonian

$$H = \sum_{i=1}^N \left\{ -\frac{\hbar^2}{2m} \nabla_i^2 + U_{sub}(r_i) \right\} + \frac{1}{2} \sum_{1 \leq i < j \leq N} v(|r_i - r_j|). \quad (1)$$

To be specific, we consider a system of  $^4\text{He}$  atoms at zero temperature. Ideally, one would like to solve the Schrödinger equation for this Hamiltonian. But, even with substantial computational resources, this is only possible only for a few systems with simple geometries and simple interactions. Therefore, we must resort to approximations. However, obvious physical consequences of the exact problem are not necessarily satisfied by an approximate theory.

A microscopic theory must be able to deal with the short-ranged repulsion between particles and include the long-ranged correlations correctly. Considering  $N$  particles in a given volume  $\Omega$ , the theory must also be able to *decide* whether particles fill the given volume uniformly, or only a part of it. There may be a regime of average densities  $N/\Omega$  where *both* states are possible. This is where the *pressure* of the uniform phase is negative, but the *compressibility* is positive. However, if the uniform phase is diluted to the density point where the compressibility becomes negative, the theory for the uniform phase should cease to have solutions. In other words, the theory must describe the response of the system to long wavelength excitations correctly.

The correct treatment of the bulk phase is prerequisite to determining whether a system of particles will or will not be adsorbed to a substrate. The requirement of the correct inclusion of short- and

long-ranged correlations is needed when we consider the structure of the adsorbed atoms. Heuristically, one would think of the  $^4\text{He}$  atoms as hard spheres. These spheres would first form a layer closest to the surface, then, as their number is increased, a second layer, and so on. Eventually, the zero-point motion of the atoms will win over the attraction to the substrate, and far from the substrate the  $^4\text{He}$  particles will behave as if they are in the bulk. Next, we add some attraction to the "hard spheres", which is strong enough to form a many-body bound state. The particles will wish to stick together even when the attractive substrate is not there. In the presence of the attractive substrate, it is not clear whether the plane geometry (i.e. a geometry that is translationally invariant in the directions parallel to the surface) is energetically favourable. The question is to what extent the liquid will "wet" the surface. Formally, we again encounter the problem of stability against long-wavelength excitations.

Summarizing the above qualitative arguments, we find that, in order to adequately describe the physics discussed above, the many-body theory to be used must at least qualitatively implement the following features:

- The theory must describe short-ranged correlations in order to account for a layer-structure of the adsorbed liquid.
- The theory must include long-ranged correlations in order to give us the right geometry.
- Finally, our theoretical description of the system should be flexible enough to take any symmetry breaking fully into account.

These physical requirements translate into the simple *dictum* that a theory should be internally consistent such that it has only *stable* solutions. Phrased in the formal language of many-body theory, our theory must contain a self-consistent description of short- and long ranged correlations, which is accomplished by a self-consistent summation of ring- and ladder diagrams. For simpler systems like the bulk liquid one may get away with simpler theories for a while, but eventually the "crimes" will catch up and lead to unphysical predictions like a negative compressibility. Even if numerical comparison with experiments look good, it is clear that something is *fundamentally wrong* with such a theory.

Of course, everything we do should eventually be compared with experiments. Unfortunately, quantities that can be calculated easily are often hard to measure and vice versa. From the way the experiments are done, ground-state energy measurements are difficult. Neutron scattering experiments probing the liquid surface are difficult since the penetration depth of the neutron is about  $100 \text{ \AA}$ , whereas the surface width of  $^4\text{He}$  is of the order of  $10 \text{ \AA}$ . If one is interested in exploring the layer structure, one has to look for experiments that are sensitive to the surface structure. Therefore, it may also be necessary to extend the theory in order to address the quantities that can be measured more easily.

Going back to the formal problem of a self-consistent summation of ring- and ladder diagrams, it has been known for some time that this goal is accomplished by both the optimized hypernetted-chain<sup>1</sup> (HNC/EL) and the parquet-diagram<sup>2</sup> theory, which ultimately lead to the same equations to be solved<sup>3</sup>. Here we adopt the HNC/EL version of the theory since it is more widely developed and can more easily be tested by variational Monte-Carlo calculations. One starts with a variational *ansatz* for the ground-state wave function of the  $N$  particle system of  $^4\text{He}$  atoms with coordinates  $r_1, \dots, r_N$ :

$$\Psi_0(\mathbf{r}_1, \dots, \mathbf{r}_N) = \exp \frac{1}{2} \left\{ \sum_{1 \leq i \leq N} u_1(\mathbf{r}_i) + \sum_{1 \leq i < j \leq N} u_2(\mathbf{r}_i, \mathbf{r}_j) \right\}. \quad (2)$$

The one-body function  $u_1(\mathbf{r})$  describes the spatial structure of the system, and the two-body function  $u_2(\mathbf{r}_i, \mathbf{r}_j)$  describes the short- and long-ranged correlations between pairs of particles. These functions are determined by minimization of the ground-state energy-expectation value  $E_0$ .

$$\frac{\delta E_0}{\delta u_1(\mathbf{r})} = 0, \quad \frac{\delta E_0}{\delta u_2(\mathbf{r}_i, \mathbf{r}_j)} = 0. \quad (3)$$

In many cases the calculation of the variational energy expectation value  $E_0$  cannot be performed exactly. Using *approximate* energy functionals may, of course, render the Euler equations (3) meaningless. It is therefore important to use an energy functional that has meaningful stationary points under the variational problems (3). It has been known for some time that the HNC hierarchy of approximations has meaningful variational minima. To show that the HNC/EL equations also provide a correct description of the short- and the long ranged correlations, we give the HNC/EL equations for the homogeneous Bose liquid<sup>4</sup>. These equations are most conveniently formulated in terms of the pair correlation function  $g(r)$ , and the static structure function  $S(k) = 1 + \rho \int d^3r [g(r) - 1] e^{i\mathbf{k} \cdot \mathbf{r}}$ :

$$S(k) = \left\{ \sqrt{1 + \frac{4m\rho}{\hbar^2 k^2} \tilde{V}_{ph}(k)} \right\}^{-\frac{1}{2}} \quad (4)$$

with

$$V_{ph}(r) = g(r)v(r) + \frac{\hbar^2}{m} |\nabla \sqrt{g(r)}|^2 + [g(r) - 1]w_I(r). \quad (5)$$

The "induced interaction"<sup>5</sup>  $w_I(r)$  is most conveniently represented in Fourier-space:

$$\tilde{w}_I(k) = -\frac{\hbar^2 k^2}{4m\rho} [2S(k) + 1][1 - S^{-1}(k)]^2 \quad (6)$$

(The three-dimensional Fourier-transform is denoted by a tilde). It is worth noting here that

$$V_{ph}(|\mathbf{r} - \mathbf{r}'|) = \frac{\delta^2 E_0}{\delta \rho_1(\mathbf{r}) \delta \rho_1(\mathbf{r}')}, \quad (7)$$

where the variational derivative is taken for constant  $u_2(\mathbf{r}, \mathbf{r}')$ . In Eq. (4) we recover the RPA expression for the static form factor. The HNC/EL theory supplements the RPA with a microscopic theory of the particle-hole interaction  $V_{ph}(r)$ .

An alternative way to formulate the Euler-Lagrange equation is<sup>5</sup>

$$\left[ -\frac{\hbar^2}{m} \nabla^2 + v(r) + w_I(r) \right] \sqrt{g(r)} = 0. \quad (8)$$

Eq. (8) is the Boson-version of the Bethe-Goldstone equation, in which the bare interaction has been supplemented by the "induced interaction"  $w_I(r)$ .

Eqs. (4) and (8) are algebraically equivalent, they merely suggest different iteration paths for the determination of the optimal  $g(r)$ . The self-consistent solution of Eqs. (4-6) takes three Fourier transforms per iteration, compared with two Fourier transforms per iteration for the solution of the

HNC equations with a parametrized Jastrow function  $u_2(r)$ . Thus, the efficiency of the optimization algorithm makes the use of a parametrized trial function completely pointless. The same is true for three-body correlations and for the Fermion version of the HNC/EL approach.

Returning to the physics, we see that the HNC/EL theory includes both the ring and the ladder diagrams exactly, and the mixed diagrams approximately<sup>2</sup>. In particular, Eq. (4) shows that the theory has, as required, no *uniform* solution with negative compressibility, c.f. Eq. (7). The appropriate symmetry breaking (a droplet or a plane surface geometry, for example) is put into the wave function (1) by including a one-body function  $u_1(\mathbf{r})$  and breaking the translational invariance of  $u_2(r_1, r_j)$ . If system is, within the assumed geometry, stable against small perturbations, then the theory has solutions. We conclude that the HNC/EL theory satisfies all the minimum requirements that are needed to deal with the problem of a quantum liquid surface.

The simplest symmetry breaking that can be treated with reasonable computational effort is the plane surface or the spherical geometry. The HNC/EL equations for the inhomogeneous system are straightforward generalizations of Eqs. (4-6), the equations and the algorithm for their iterative numerical solution has been given in Ref. 6.

The physical system considered here is a number of helium atoms interacting via the Aziz potential<sup>7</sup>. The atoms are adsorbed to a substrate which is described by an external field  $U_{sub}(z)$ . A simple form for  $U_{sub}(z)$  is the potential obtained by averaging Lennard-Jones interactions between helium and substrate atoms over a half space<sup>8</sup>. One obtains

$$U_{sub}(z) = \epsilon \left[ \frac{1}{15} \left( \frac{s}{z} \right)^9 - \left( \frac{s}{z} \right)^3 \right]. \quad (9)$$

Given the substrate potential, the two-body interaction, and the surface coverage

$$n = \int dz \rho_1(z), \quad (10)$$

the physical problem is completely defined. In our geometry, all two-body quantities depend on the distances  $z_i$  of both particles from the substrate, and their separation  $r_{\parallel}$  parallel to the surface. The Euler equations for the <sup>4</sup>He background were solved numerically in the HNC approximation, specifying only the surface coverage  $n$ . Some typical examples of density profiles are shown in Fig. 1. Most remarkable are the strong density-oscillations of the <sup>4</sup>He-background, which are due to the geometric core-exclusion between the <sup>4</sup>He particles.

It was already pointed out that a direct measurement of the surface profile by neutron scattering experiments is very difficult. It also turns out that the energy per particle does not depend strongly on the layer structure of the system<sup>9</sup>, and the chemical potential has only a weak modulation, c.f. Fig. 2.

One might expect that the sound velocity exhibits a stronger dependence on the layer structure of the surface, but the analysis of our theoretical calculations and the experiments shows that the third sound velocity  $c_3$  (or the derived quantity  $mc_3^2$ ) depends strongly on the underlying substrate potential (Fig. 3) which makes conclusions on the structure of the film very difficult.

So far, we have seen that it is difficult to probe the layer structure of an adsorbed <sup>4</sup>He film directly. A moderately easy probe of the surface structure is a <sup>3</sup>He impurity. Experimental interest focusses presently on the following areas:

Fig. 1: The density  $\rho_1(z)$  of the background film of  $^4\text{He}$  atoms (dotted lines) and of the  $^3\text{He}$  impurity,  $\rho_1^I(z)$  (solid lines) are shown for surface coverages of  $n = 0.15, 0.20, 0.25, 0.30,$  and  $0.35$   $^4\text{He}$  atoms/ $\text{\AA}^2$ . The  $^4\text{He}$  densities of all films shown are virtually identical within the first layer, whose density maximum is about  $0.08$  atoms/ $\text{\AA}^3$ . The  $^3\text{He}$  impurity density is normalized such that  $\int dz \rho_1^I(z) = 1$ .

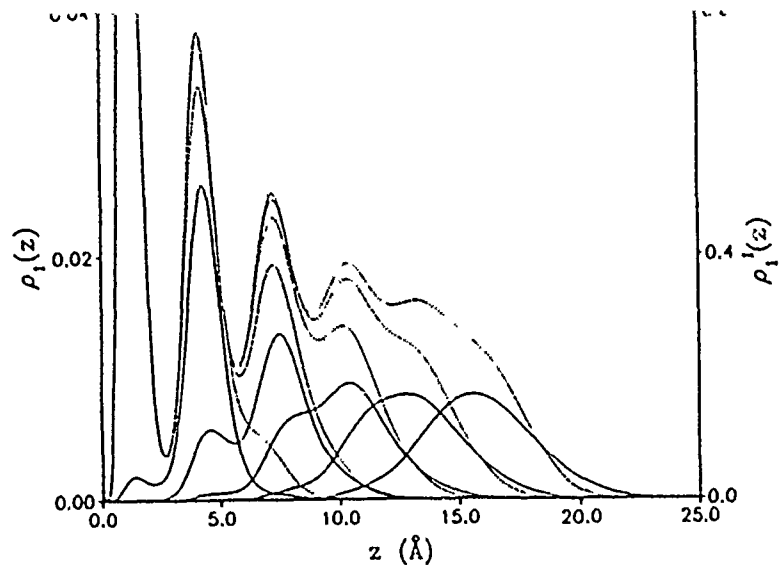
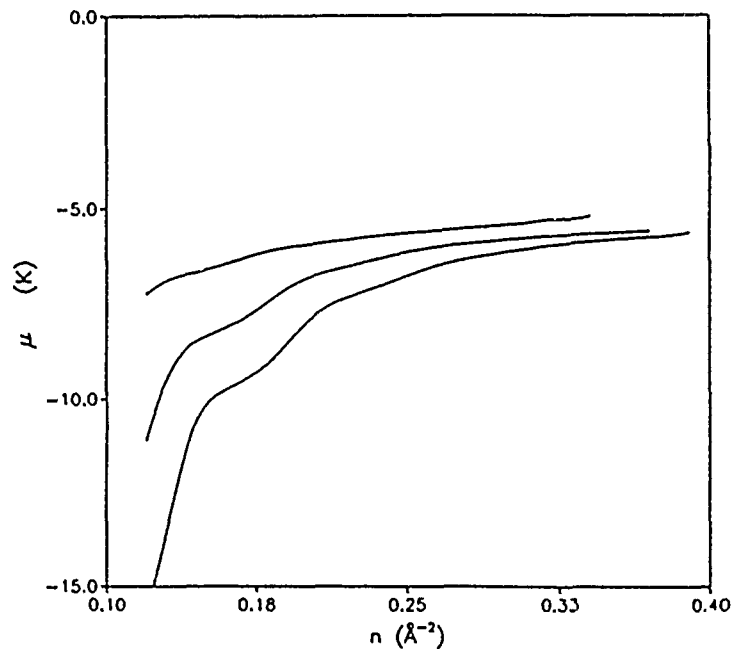


Fig. 2: The chemical potential  $\mu$  of  $^4\text{He}$  atoms is shown, as a function of the surface coverage  $n$ , for three different substrate potentials of different strength. The upper curve corresponds to a weakly attractive glass substrate, the lowest one to graphite, and the middle curve to a potential of average strength.

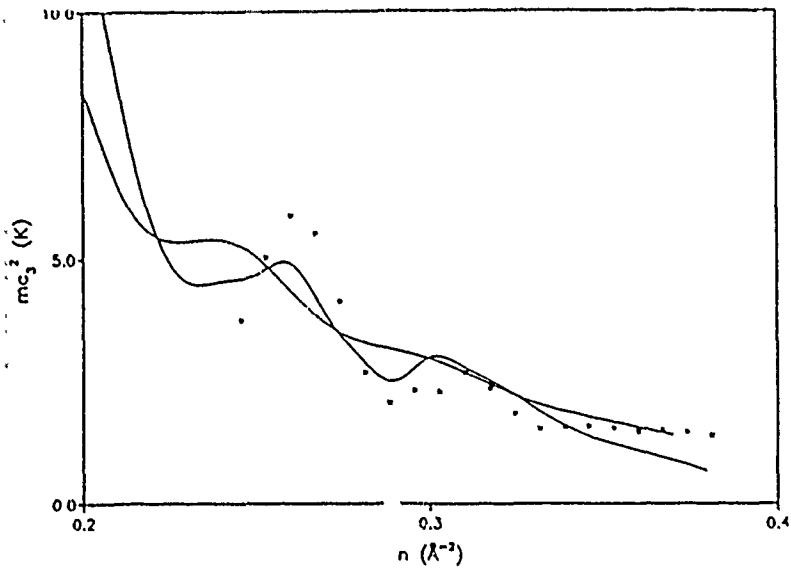


- (a) Measurements of the binding energy and the specific heat of  $^3\text{He}$  impurities<sup>11</sup>, and
- (b) Measurement of magnetic properties of  $^3\text{He}$  impurities adsorbed to  $^4\text{He}$  surfaces<sup>12</sup>.

Qualitatively, one should expect the following effects:

- For a *thin* film of  $^4\text{He}$  atoms (one or two layers thick), the substrate potential dominates, and the  $^3\text{He}$  impurity atom will be in the outermost layer.
- For a *thick* film of  $^4\text{He}$  atoms (five or more layers), the larger zero-point motion of the  $^3\text{He}$  impurity will dominate, and the impurity atom will appear to “swim” on the  $^4\text{He}$  background.
- If the outermost layer of the  $^4\text{He}$  film is full, it will be hard for the  $^3\text{He}$  impurity to move. The “backflow” effect and hence the effective mass of the impurity atom will be large.
- If the outermost layer of the  $^4\text{He}$  film is incomplete, the backflow, and hence the effective mass, will be smaller.

Figure 3:  $mc_3^2$  for the medium (weakly oscillating curve) and the strong (strongly oscillating curve) substrate potential are compared with the experimental data of Maynard and Chan (Ref. 10, crosses). See Ref. 9 for details on the analysis of the experiments and the calculational procedures.



The last two points also depend on how deep the impurity atom penetrates into the  $^4\text{He}$  surface.

The above experimental situations require the development of three levels of theoretical tools.

- (a) Single-impurity theories aim at the calculation of impurity binding-energy and effective mass. The static correlations between particles determine if and how many bound states the impurity particle can have at the surface, and whether it penetrates to the substrate. The calculation of the (complex) self-energy of the impurity particle gives access to the specific heat and the mobility.
- (b) Mixture films in the dilute limit correspond to a system of *two* static impurities<sup>13</sup>. To the extent that the concentration of the impurities is small, one can ignore all higher-order correlations between the impurity particles and possible dynamic effects due to momentum-dependent correlations.
- (c) A theory for two-component systems is needed for large "impurity" concentrations. This enables us to study the structure of quantum-liquid interfaces.

Formally, impurities may be added to the system by extending the wave function to include impurity-background and impurity-impurity correlation functions  $u_1^I(r^I)$ ,  $u_2^{IB}(r_i^I, r_i)$ , and  $u_2^{II}(r_i^I, r_j^I)$ . For Fermion impurities, the wave function is multiplied with a Slater determinant to ensure the antisymmetry with respect to exchange. To include a momentum dependence, one may either add a "backflow" function to the one-impurity correlations, or calculate the self-energy in CBF perturbation theory. The variational wave function of a system of  $N$   $^4\text{He}$ -background atoms and one  $^3\text{He}$  impurity of momentum  $q$  is

$$\Psi_q(r^I, r_1, \dots, r_N) = \exp \left\{ \frac{1}{2} u_1^I(r^I) + iq \cdot r^I + \sum_{j=1}^N \left[ \frac{1}{2} u_2^{IB}(r^I, r_i) + i \alpha_q(r^I, r_i) \right] \right\} \Psi_0(r_1, \dots, r_N). \quad (11)$$

$\alpha_q(r^I, r_i)$  is the backflow correlation function<sup>14</sup> describing the current of  $^4\text{He}$  atoms flowing around the moving impurity. The functions  $u_1^I(r^I)$ ,  $u_2^{IB}(r^I, r_i)$ , and  $\alpha_q(r^I, r_i)$  are determined by minimizing the energy  $E_q$  of the system, consisting of the  $^4\text{He}$ -background and an impurity particle with momentum  $q$ .

$$\frac{\delta E_q}{\delta u_1^I(r^I)} = 0, \quad \frac{\delta E_q}{\delta u_2^{IB}(r^I, r_i)} = 0, \quad \frac{\delta E_q}{\delta \alpha_q(r^I, r_i)} = 0. \quad (12)$$

The total energy of the whole system can then be written as

$$E_q = E_0 + \epsilon_0 + \frac{\hbar^2 q^2}{2m_H}, \quad (13)$$

where  $E_0$  is, as above, the ground state energy of the  $^4\text{He}$  background system,  $\epsilon_0$  is the binding energy of an impurity with zero momentum, and  $m_H$  is the so-called hydrodynamic effective mass. It is the contribution to the effective mass arising from the interaction of the impurity particle with the background.

Similarly, the variational wave function for two impurity Fermions with coordinates  $r_1^I, r_2^I$  is

$$\begin{aligned} \Psi_{N+2}^{II}(r_1^I, r_2^I; r_1, \dots, r_N) = \exp \frac{1}{2} \left\{ u_1^I(r_1^I) + u_1^I(r_2^I) + u_2^{II}(r_1^I, r_2^I) + \right. \\ \left. + \sum_{1 \leq i \leq N} [u_2^{IB}(r_1^I, r_i) + u_2^{IB}(r_2^I, r_i)] \right\} \Psi_0(r_1, \dots, r_N) \Phi(1, 2), \end{aligned} \quad (14)$$

where  $\Phi(1, 2)$  is a 2-particle Slater determinant. We leave out the backflow correlations since we will consider only small momenta of the  $^3\text{He}$  impurities. The only new unknown function is the impurity-impurity correlation function  $u_2^{II}(r_1^I, r_2^I)$ , which is again determined by minimization of the total energy.

Instead of describing the further manipulations in detail (see Refs. 15-17), let us turn to the results of our calculations. The solid lines in Fig. 1 show the impurity density in comparison with the background density. We see that the  $^3\text{He}$  particle is, as predicted, inside the outermost  $^4\text{He}$  layer for our calculation of a double-layer system. As the thickness of the background increases, the  $^3\text{He}$  particle is pushed outward into the low-density regime of the film.

A more instructive picture is given by considering the distribution of  $^4\text{He}$  particles in the vicinity of the impurity. Figs. 4 and 5 show the  $^4\text{He}$  density assuming that the  $^3\text{He}$  atom is located at  $(x, y) = (0, 0)$ , i.e. the quantity

$$\rho^B(z, r_{\parallel}) = \int a z^I \rho^{IB}(r^I, r), \quad (15)$$

where  $\rho^{IB}(r^I, r)$  is the impurity-background two-body density. For the very thin film we see that the  $^3\text{He}$  atom is located within the outermost layer, whereas for the thick film, the  $^4\text{He}$  background is only modestly deformed.

We have carried out extensive calculations for the static ground state of one  $^3\text{He}$  impurity on a family of  $^4\text{He}$  backgrounds ranging from a double layer ( $n = 0.12 \text{ \AA}^{-2}$ ) to a system of about five helium layers ( $n = 0.35 \text{ \AA}^{-2}$ ). The hydrodynamic effective mass has been calculated using the uniform limit<sup>1</sup> for the Euler-equation for the backflow function  $\alpha_q(r^I, r_i)$ . In this limit, one obtains a closed-form expression for the effective mass which is identical to a second-order approximation for the self-energy in terms of the emission and re-adsorption of ripplons and phonons. Our theoretical description of the first layer should not be considered very realistic<sup>5</sup>, but the uncertainty in the description of the first layer does not seriously affect our conclusions. This part of the system has a very high density and the impurity hardly penetrates (c.f. Fig. 1). Effectively, the impurity atom "sees" the first layer as a solid.

Our results are compared in Fig. 6 with the experimental results of Refs. 11. We find that the hydrodynamic mass is somewhat lower than the experimental mass. We notice, however, that the

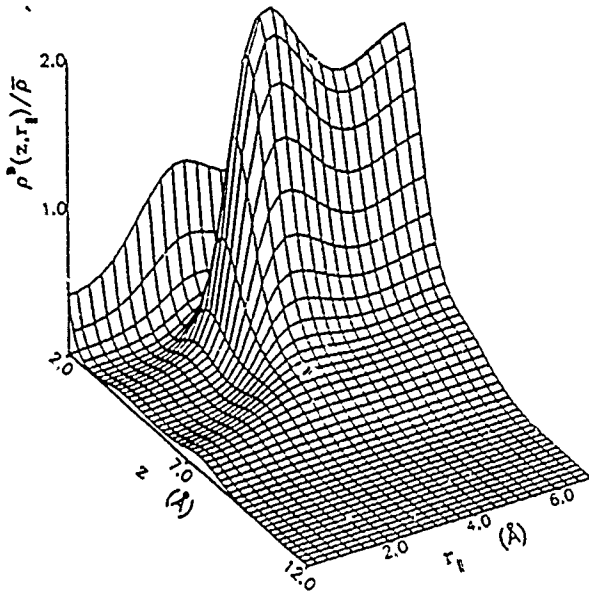


Fig. 4. The density of  $^4\text{He}$  atoms in the vicinity of the  $^3\text{He}$  impurity,  $\rho^B(z, r_{\parallel})$ , is shown for the double layer background film with a surface coverage of  $n = 0.15\text{\AA}^{-2}$ . The density is normalized to the *calculated* bulk equilibrium density,  $\bar{\rho}^{HNC}$ .

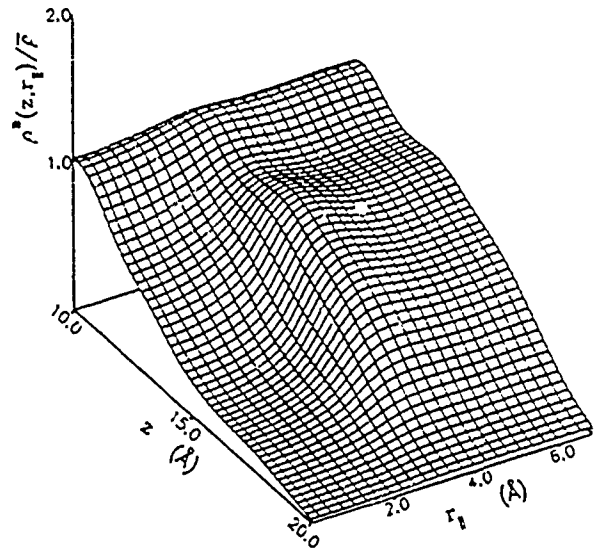


Fig. 5. Same as Fig. 4 for the background films with the largest surface coverage  $n = 0.35\text{\AA}^{-2}$ .

experiment has not been done in the dilute limit, but for a  $^3\text{He}$  density of 0.3 layers. Therefore we must include the effects of the quasiparticle interaction between the  $^3\text{He}$  atoms.

The interaction between  $^3\text{He}$  impurities is intelligently discussed in terms of a *local* effective interaction  $V_{eff}(\mathbf{r}, \mathbf{r}')$ . This effective interaction includes both the direct Van der Waals force between the impurities and the exchange of ripplons and phonons through the  $^4\text{He}$  background. It can be obtained by generalizing the theory of the impurity-impurity interaction<sup>11</sup> to the inhomogeneous case. In the case of a dilute system of impurities, we may take the impurity-impurity interaction as an effective interaction between any two  $^3\text{He}$  atoms for a *finite* impurity population ("quasiparticle interaction"). The relation to Landau's Fermi-Liquid theory in two dimensions<sup>18</sup> is drawn in momentum space by identifying

$$\begin{aligned} f_c(q_{\parallel}) + f_{\sigma}(q_{\parallel})\sigma_1 \cdot \sigma_2 &\equiv V(0+) - \frac{1}{2}V(q_{\parallel})(1 + \sigma_1 \cdot \sigma_2) \\ &= \int dz_1 dz_2 d^2 r_{\parallel} \rho_1^I(z_1) \rho_1^I(z_2) V_{eff}(z_1, z_2, r_{\parallel}) \left[ 1 - \delta_{\sigma_1, \sigma_2} e^{i q_{\parallel} \cdot r_{\parallel}} \right], \end{aligned} \quad (16)$$

with the quasiparticle interaction. Given the interaction (16), we can calculate the Fermi-Liquid parameters of the two-dimensional Fermi liquid,<sup>18</sup>

$$\begin{aligned} N(0)f_c(|\mathbf{q}_1 - \mathbf{q}_2|) &= \sum_{m=0}^{\infty} F_m^c \cos(m\phi) \\ N(0)f_{\sigma}(|\mathbf{q}_1 - \mathbf{q}_2|) &= \sum_{m=0}^{\infty} F_m^{\sigma} \cos(m\phi), \end{aligned} \quad (17)$$

where  $\phi$  is the angle between  $\mathbf{q}_1$  and  $\mathbf{q}_2$ , and  $N(0) = m^*/\pi h^2$  the density of states at the Fermi surface.

From these, we obtain the magnetic susceptibility  $\chi(0)$ , in units of the susceptibility of the free two-dimensional Fermi gas,  $\chi_{30}$ ,

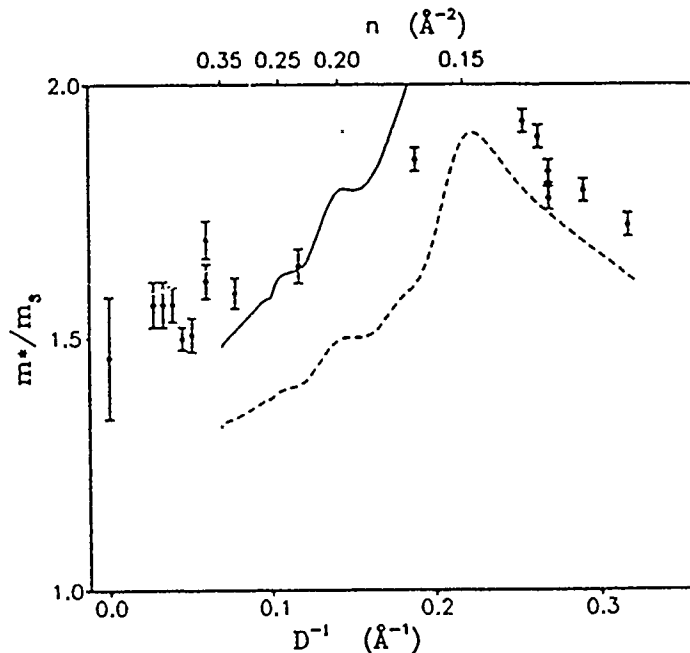
$$\chi(0)/\chi_{30} = (m_H/m_3)(1 + F_1^s/2)/(1 + F_0^s) \quad (18)$$

and the total effective mass

$$m^* = m_H(1 + F_1^s/2). \quad (19)$$

Figure 6 (solid line) shows the total effective mass  $m^*$  calculated from Eq. (19). For one active layer of  $^4\text{He}$  the hydrodynamic mass is about  $1.8 m_3$ , in reasonable agreement with both the data of Refs. 11 and the conclusion of Ref. 12 with their thinnest  $^4\text{He}$  film. In this regime the correction due to the quasiparticle interaction becomes quite sizable with increasing  $^3\text{He}$  concentration, but it is difficult to make a quantitative statement due to both the high density of the background and the rapid variation of the effective mass.

Fig. 6: The calculated effective mass  $m^*$  is shown in units of the bare  $^3\text{He}$  mass  $m_3$  as a function of the inverse film thickness  $D^{-1}$  (dashed line). The circles with error bars are the experimental data of Refs. 11. The upper scale shows the surface coverage corresponding to the film thickness  $D$ . The dashed line shows the hydrodynamic effective mass  $m_H$  for 0.3 layers of  $^3\text{He}$ .



For all cases with thicker  $^4\text{He}$  films, the accuracy of our theoretical prediction is quite satisfactory. The microscopic theory predicts a hydrodynamic mass that is consistent with the estimate  $m_H/m_3 = 1.26 \pm 0.15$  given by Valles *et al.* (Ref. 12), but below the results of Refs. 11. The agreement with the latter data is improved when the corrections due to the quasiparticle interaction are included. The quasiparticle interaction between  $^3\text{He}$  atoms in the surface gives a density-dependent correction to the effective mass. The contribution is about 10% for the case of 0.3 layers of  $^3\text{He}$ .

There are slight oscillations of the  $^3\text{He}$  effective mass as a function of the thickness of the underlying film. A weak plateau is seen around  $D^{-1} \approx 0.1 \text{ \AA}^{-1}$ . This coincides with the regime where the third liquid layer is formed. Thus, we conclude that the impurity effective mass has weak layer structure, but that these oscillations damp out rather fast. The effect of the migration of the impurity atom into the surface is much stronger than the modification of the backflow for different degrees of filling of the last layer so that it would be much harder to observe fluctuations of the  $^3\text{He}$  effective mass for very thick films.

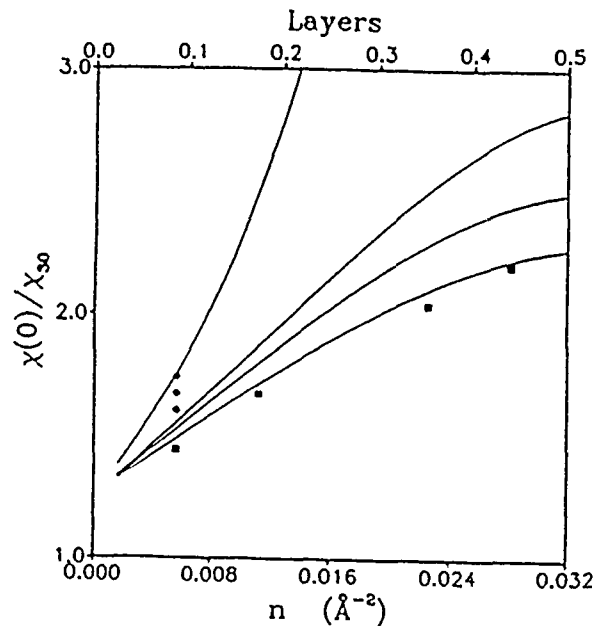
A comparison of the theoretical and the experimental magnetic susceptibility ratio  $\chi(0)/\chi_{30}$  is shown in Fig. 7. Here we have taken a hydrodynamic mass of  $1.26 m_3$ , which gives the best fit to experimental

refer to a much smaller  $^3\text{He}$  coverage. We find a quite satisfactory agreement between theory and experiment.

The agreement is not quite so good for smaller  $^4\text{He}$  coverages. This is partly due to the fact that no attempt was made to re-adjust the effective mass. One must also be concerned about the accuracy of the theoretical description when the  $^3\text{He}$  impurity penetrates into a regime of higher  $^4\text{He}$  density, where HNC methods are intrinsically less accurate. However, HNC-type microscopic theories are, while using modest computational resources, quite capable of giving at least a semi-quantitative picture of the structure of complicated systems like the ones discussed here.

Finally, we stress that the good agreement between the experimental results and our calculation has been obtained with a *static, momentum-dependent* quasiparticle interaction. The calculation of the magnetic susceptibility involves phase-space integrals of the quasiparticle interaction over momenta between  $q = 0$  and  $q = 2k_F$ . Therefore, with increasing impurity density one probes the *momentum-dependence* of the quasiparticle interaction. We believe that measurements of the type of Ref. 12 are extremely useful to enhance our theoretical understanding of the quasiparticle interaction in liquid  $^3\text{He}$ .

Fig. 7: Magnetic susceptibility  $\chi/\chi_{30}$  of the  $^3\text{He}$  film as a function of areal density  $n$  in atoms/ $\text{\AA}^2$ , for  $^4\text{He}$  coverages between 0.15 atoms/ $\text{\AA}^2$  (uppermost curve), and 0.30 atoms/ $\text{\AA}^2$  (lowest curve). Solid squares: experimental data<sup>12</sup> for a surface coverage of 9.5  $^4\text{He}$  layers. Circles: experimental data<sup>12</sup> for a  $^3\text{He}$  density of 0.088 layers, for  $^4\text{He}$  coverages of 2.8, 3.4, 4.75, and 5.24 atoms/ $\text{\AA}^2$ .



I hope that I have succeeded in this contribution to present the study of quantum liquid surfaces as an exciting field for both experimental and theoretical research. Let me conclude by highlighting the most interesting physical and conceptual aspects of this field of research:

- Physically, one is able to construct very clean two-dimensional Fermi systems and investigate these systems over a wide regime of densities. This is in contrast to bulk  $^3\text{He}$ , where experiments can be performed only in a narrow regime around the equilibrium density. By carrying out measurements on  $^3\text{He}$  impurity films over a large density regime, one should be able to *measure the momentum dependence of the quasiparticle interaction*.
- Conceptually, quantum liquid films are many-body systems where state-of-the-art many-body theory is necessary for a thorough microscopic understanding. At this time I do not intend to suggest that

quantum liquid films be studied with other many-body methods. But looking back at the obvious requirements that must be satisfied by a theory in order to successfully deal with such systems, it may be worth asking

Can your favorite many-body theory deal (in principle and in practice) with these systems ?

#### Acknowledgements

This paper was written while one of us (EK) enjoyed the hospitality of the Theoretical Physics Institute at the University of Minnesota in Minneapolis. The work was supported, in part, by the National Science Foundation under Contract PHY-8806265 and the Robert A. Welch foundation under Grant A-1111. Participation in this workshop has been made possible by a travel grant from the U.S Army research office. Stimulating discussions with C. E. Campbell are gratefully acknowledged.

#### References

1. E. Feenberg, *Theory of Quantum Fluids* (Academic, New York, 1969).
2. A. D. Jackson, A. Lande and R. A. Smith, Phys. Rep. 86, 55 (1983); A. D. Jackson, A. Lande and R. A. Smith, Phys. Rev. Lett. 54, 1469 (1985).
3. E. Krotscheck, A. D. Jackson, and R. A. Smith, Phys. Rev. A33, 3535 (1986).
4. C. E. Campbell and E. Feenberg, Phys. Rev. 188, 396 (1969).
5. L. J. Lantto and P. J. Siemens, Phys. Lett. 68B, 308 (1977).
6. E. Krotscheck, G.-X. Qian, and W. Kohn, Phys. Rev. B31, 4245 (1985).
7. R. A. Aziz, V. P. S. Nain, J. C. Carley, W. L. Taylor and G. T. McConville, J. Chem. Phys. 70, 4330 (1979).
8. M. W. Cole, D. R. Frankl, and D. L. Goodstein, Rev. Mod. Phys 53, 199 (1981).
9. J. L. Epstein and E. Krotscheck, Phys. Rev. B37, 1666 (1988).
10. J. D. Maynard and M. H. W. Chan, Physica 109-110B, 2090 (1982)
11. X. Wang and F. M. Gasparini, Phys. Rev. B38, 11245 (1988); B. K. Bhattacharyya, M. J. DiPirro, and F. M. Gasparini, Phys. Rev. B30, 5029 (1984).
12. J. M. Valles, Jr., R. H. Higley, R. B. Johnson, and R. B. Hallock, Phys. Rev. Lett 60, 428 (1988)
13. J. C. Owen, Phys. Rev. Lett. 47, 586 (1981).
14. J. C. Owen, Phys. Rev. B23, 2169 (1981).
15. E. Krotscheck, M. Saarela, and J. L. Epstein, Phys. Rev. B38, 111 (1988).
16. E. Krotscheck, M. Saarela, and J. L. Epstein, Phys. Rev. Lett. 61, 1728 (1988).
17. J. L. Epstein, E. Krotscheck, and M. Saarela, preprint (1989).
18. S. M. Havens-Sacco and A. Widom, J. Low Temp. Phys. 40, 357 (1980).

Invited talk delivered at the XIII. International Workshop on Condensed Matter Theories held at Campos do Jordão, Brazil, August 1989.

ON THE ROLE OF ELECTRON-MEDIUM COUPLING IN HIGH TEMPERATURE SUPERCONDUCTORS\*#

F. B. Malik

Physics Department, Southern Illinois University,  
Carbondale, Illinois, 62901, U.S.A.

ABSTRACT

The effective Hamiltonian for a pair of Fermion derived from the basic many body Hamiltonian allows for the interaction of a pair with its medium in a number of ways e.g., once via the mean field and another via the pairing part of the interaction. The two state model developed earlier has been solved in a better approximation. The model has then been applied to calculate pairing energy, critical temperature, coherence length and critical field for  $\text{YBa}_2\text{Cu}_3\text{X}_{7-\delta}$  with  $X = \text{O, S, Cl, F, Br, I}$ . The model can account for the general trend and magnitude of these observables, particularly the very large value of the critical field. Using a model Hamiltonian of Frölich type, the electron-phonon coupling strength is estimated. The electron-phonon coupling strength for our particular system is more than an order of magnitude larger than the one in normal superconductors. The Eliashberg dimensionless coupling parameter  $\lambda$  is found to be about 2.0 to 3.0.

1. INTRODUCTION

Transition from a normal state, be it a conductor or a semiconductor or a perovskite, to a superconducting state involves a phase transition. Whereas, electrons in a normal state behave like incoherent Fermions, the formation of Boson-like coherent pairs is a necessary criterion for a superconducting state. Near critical temperature,  $T_c$ , one has, therefore, two types of states of a system, one representing incoherent Fermion and the other coherent quasi boson like pairs. A set of coupled equation commensurate with this situation has been derived<sup>1,2</sup> and the zeroeth order solution has been successful in predicting the trend of  $T_c$  in  $\text{Y-Ba-Cu-O-X}$  with  $X = \text{O, S, Cl}$  and  $\text{F}$ .

\*A travel grant from the U. S. Army Research Office is thankfully acknowledged.

#Dedicated to Professor Don Lichtenberg in appreciation of his human qualities and contribution to physics.

The key to the pairing has been assumed to be the formation of doubly ionized negative ion  $X^{2-}$ . Qualitatively, one, therefore, expects that the substitution by Br and I both of which form negative ions should give rise to superconducting behavior and this has recently been confirmed<sup>3</sup>). In sections 2, we present a better approximation of the two state model and calculate  $T_c$ , energy gap, coherence length and the critical field. In section 3 we discuss the relation of the calculated energy gap to electron-phonon coupling constant using an interaction similar to the one proposed by Frölich. Hamiltonian containing this interaction has been diagonalized using the method of Huang and Rys<sup>5</sup>. We estimate the electron-phonon coupling strength in a simple model and present there a discussion of the Eliashberg coupling constant.

## 2. THE THEORY

As noted in ref. 1, the equation for a pair of Fermion in state  $\alpha$  in a medium is given by

$$[\theta(i) + \theta(j) + V(i,j) - \epsilon_\alpha] \phi_\alpha(i,j) + (1/2) \sum_{\beta=1}^n \int dk dl \phi_\beta^*(k,l) W \phi_\alpha(i,j) \phi_\beta(k,l) = 0 \quad (1)$$

where  $V(i,j)$  is the effective two-electron interaction obtained by integrating over all lattice coordinates  $R$ , of the bare electron-electron and electron-lattice interaction  $h_{ee}$  and  $h_{e-x}$ , respectively.

$$V(i,j) = \langle h_{ee}(ij) + h_{e-x}(R,ij) \rangle_R \quad (2)$$

$\theta(i)$  is the effective one body operator which could be bare kinetic energy or an effective one-body interaction.  $W$  is given by

$$W = [V(i,k) (1-X(i,k)) + V(i,l) (1-X(i,l)) + V(j,k) (1-X(j,k)) + V(j,l) (1-X(j,l))] \quad (3)$$

$X(i,j)$  is the exchange operator transposing all coordinates  $i$  and  $j$ .  $\phi$  is an antisymmetric function.  $W$  is the average potential generated by pairs other than  $\phi_\alpha$ . In case all the pair functions are replaced by  $2 \times 2$  determinants of single particle orbitals, (1) reduces to the set of Hartree-Fock equation. Above critical temperature the total electronic wave function  $\psi_F$  is given by properly ordered permutation  $P$  of Fermion type of pair function

$$\psi_F = (1/\sqrt{2n!}) \sum_P \epsilon^P \phi_{\alpha_1}(1,2) \dots \phi_{\alpha_n}(2n-1,2n) \quad (4)$$

Below critical temperature  $\psi_S$  is a linear combination of Schafroth pair functions<sup>6</sup>) and leads to condensation necessary for superconductivity

$$\psi_S = C_n \sum_P (-1)^P [\phi(1,2)\phi(3,4)\dots\phi(2n-1,2n)] \quad (5)$$

Because of the difference between these two types of wavefunctions, the average potential seen by a pair i.e., the terms containing  $W$  in (1), differs significantly in two cases. That might result in a change in total energy signaling a phase transition. Near critical temperature we expect significant components of both types of states to be present and the total wavefunction may be written as

$$\chi = A_1 \psi_F + A_2 \psi_S \quad (6)$$

Thus, near critical temperature, one is to diagonalize the matrix

$$\begin{pmatrix} H_{11} & H_{12} \\ H_{21} & H_{22} \end{pmatrix} \quad (7)$$

where  $H_{ii}$  ( $i=1,2$ ) contains diagonal matrix elements in states 1, identified as Fermion like states and in state 2, identified as quasi-Boson like states.  $H_{12} = H_{21}^*$  are the coupling terms.  $H_{ii}$  is a sum of two terms,  $\epsilon_i$  containing effective average field seen by a pair and  $\epsilon_{ii}$ , the interaction between a pair. The coupling term  $H_{ij}$  contains at least the effective two body interaction  $V(i,j)$  but might also take into account the difference in mean field in two cases.

The diagonalization of (7) leads to

$$E_{\pm} = \frac{1}{2} (H_{11} + H_{22}) \pm \frac{1}{2} \sqrt{(H_{11} - H_{22})^2 + 4|H_{12}|^2} \quad (8)$$

$E_-$ , being lower in energy, is to be identified with the superconducting state and  $E_+$  with the normal state. Since  $(H_{11} - H_{22})^2$  and  $|H_{12}|^2$  are, respectively, of the order of a few eV and a few tens of meV, it is reasonable to assume  $4|H_{12}|^2 \ll |H_{11} - H_{22}|^2$ . Then

$$E_- \cong H_{22} - \frac{|H_{12}|^2}{H_{11} - H_{22}} = H_{22} - \frac{|H_{12}|^2}{\epsilon_1 - \epsilon_2 + \epsilon_{11} - \epsilon_{22}} \quad (9)$$

$\epsilon_{11} - \epsilon_{22}$  is usually much less than  $(\epsilon_1 - \epsilon_2)$ . Therefore,

$$E_- \cong \epsilon_2 + \epsilon_{22} - \frac{|H_{12}|^2}{\epsilon_1 - \epsilon_2} \quad (10)$$

∴ Pairing energy in the superconducting state  $\Delta E$

$$\Delta E = (E_- - \epsilon_2) = \epsilon_{22} - \frac{|H_{12}|^2}{\epsilon_1 - \epsilon_2} \quad (11)$$

Both  $\epsilon_{22}$  and  $|H_{12}|^2$  involve integration over all lattice coordinates and represent a coupling between electrons and the medium. These depend on various parameters of media or lattice and are collectively denoted by  $\kappa$ .

Since this is a zero-temperature theory one can relate  $\Delta E$  to  $T_c$  using the relation<sup>7,8</sup>

$$(\pi/\gamma)kT_c = \Delta E \quad (12)$$

(Here  $k$  and  $\gamma$  are, respectively, Boltzmann and the exponential of Euler constants and  $\pi/\gamma \cong 1.764$ ). Assuming  $|H_{12}|^2$  to depend on mass of ion  $X$  as  $1/\sqrt{M}$ , we may write

$$T_C = a(\kappa) - b(\kappa)/\sqrt{M(\epsilon_2 - \epsilon_1)} \quad (13a)$$

$$\approx a(\kappa) - b(\kappa) \Delta W \quad (13b)$$

Using  $T_C = 93^\circ\text{K}$  and  $90^\circ\text{K}$  for  $X = 0$  and  $S$ , respectively, we find  $a(\kappa) = 31^\circ\text{K}$  and  $b(\kappa) \approx 2521^\circ\text{K}$ . Since  $\Delta W$  for  $0$  and  $S$  are very close, we expect them to have similar  $T_C$  which is, indeed, the case. As noted in refs. 1 and 2, the superconducting state in this system is identified with the localization of electron pairs in forming doubly ionized negative ion,  $X^{2-}$  and the normal state with singly ionized negative ion,  $X^{1-}$ . In table 1 we have compared calculated  $T_C$  with the observed ones. For  $X = \text{Br}$  and  $\text{I}$ , we provide theoretical estimates using a range of electron affinities of  $\text{Br}^-$  and  $\text{I}^-$ . The theory can reproduce the trend.

There is some uncertainty about the validity of (12) in this type of superconductors. Nevertheless, we have used it to calculate the gap parameter and tabulated them in table 2. The measurements for the oxygen case is in accord with the calculated number but indicate that the constant of proportionality between  $\Delta$  and  $T_C$  is about twice the one in (12).

Coherence length  $\zeta_0$  is related gap parameter by

$$\zeta_0 = \hbar V_F / \pi \Delta \quad (14)$$

where  $V_F$  is the velocity near Fermi surface. Assuming the  $V_F$  in this type of superconductors is close to those in type II superconductors, we may determine this from  $\text{Nb}_3\text{Sn}$  ( $T_C = 18^\circ\text{K}$ ,  $\zeta_0 = 50 \text{ \AA}$ ). Calculated values are tabulated and compared with data in table 2.

Since  $\Delta$  and  $\zeta_0$  for this type of superconductors are, respectively, substantially larger and smaller than those in type I and II superconductors, we may call these type III superconductors. The large  $\Delta$  and small coherence length are indicative of very strong coupling between pairs and the environment and the coherence is more localized. Thus, the BCS approximation of a constant weak coupling between a pair of electron via phonons is invalid for these materials.

The difference between the total energy of the normal and superconducting states is related to critical field  $H_C$  by  $H_C^2/8\pi =$  energy difference per unit volume

$$H_C^2/8\pi = \frac{1}{2\rho} \times \sqrt{(H_{11} - H_{22})^2 + 4|H_{12}|^2} \quad (15)$$

where  $\rho$  is the number of electrons per unit volume. We have used (8) to get the energy difference per pair between the normal and the superconducting state.

Assuming that  $(\epsilon_{11} - \epsilon_{22}) \ll (\epsilon_1 - \epsilon_2)$  we get

$$\begin{aligned} (H_C^2/8\pi) (2/\rho) &\approx \left| (\epsilon_1 - \epsilon_2) + \frac{2|H_{12}|^2}{\epsilon_1 - \epsilon_2} \right| \\ &= \left| (\epsilon_1 - \epsilon_2) - 2(\pi/\gamma)k b(\kappa) \Delta W \right| \\ &\approx |\epsilon_1 - \epsilon_2| \end{aligned} \quad (16)$$

The last approximation is valid since the second term is of the order of a few tens of meV but  $|(\epsilon_1 - \epsilon_2)|$  is about 5 to 10eV. Eq. (16) is an important result and is very different from the expression obtained in the Schafroth or BCS theory. In latter two cases instead of (15), one has<sup>9</sup>  $(H_c^2/8\pi)(2V/\rho_E) = \Delta^2$ . Thus, the theory predicts that critical field in this types of superconductors is much larger than that in type I superconductors. We may estimate  $\rho$  from normal superconductors e.g., tin which has a  $T_c = 3.73^\circ\text{K}$  and  $H_c = 306$  Gauss. Noting the  $\rho$  per meV =  $\rho_E/V$ , we get  $\rho = 10^{18}/\text{cm}^3$  from the tin data. Calculated critical field using this, is noted and compared to the observed value in table 2. The theory can account for the large critical field seen in high  $T_c$  superconductors.

### 3. EFFECTIVE COUPLING STRENGTH IN A FROHLICH MODEL

Describing the medium and the electrons, respectively, by Boson operators,  $b_k$  and Fermion operators  $a_k$  we may write the Hamiltonian for a linear coupling between the two as follows

$$H = \sum_{\lambda} \epsilon_{\lambda} a_{\lambda}^{\dagger} a_{\lambda} + \sum_{\vec{k}} \hbar\omega(\vec{k}) [b_{\vec{k}}^{\dagger} b_{\vec{k}} + \frac{1}{2}] + \sum_{\lambda, \vec{k}} a_{\lambda}^{\dagger} a_{\lambda} [v(\vec{k}, \lambda) b_{\vec{k}} + v(\vec{k}, \lambda) b_{\vec{k}}^{\dagger}] \quad (17)$$

This is basically the Hamiltonian proposed by Fröhlich<sup>4</sup> and used in the Eliashberg<sup>11</sup> formalism. Taking  $v(\vec{k}, \lambda)$  to be the matrix element of  $(\hat{\epsilon} \cdot \nabla V)$  where  $\hat{\epsilon}$  and  $V$  are, respectively, unit polarization vector and potential at lattice sites, one may define a dimensionless coupling parameter  $\lambda$  within the framework of Eliashberg formalism. The averaged electron-phonon interaction  $\alpha^2(\omega)$ , averaged electron-phonon matrix elements  $\langle g^2 \rangle$  and the dimensionless coupling constant  $\lambda$  are related as follows:

$$\lambda = 2 \int \alpha^2(\omega) F(\omega) d\omega / \omega \quad (18)$$

$$\frac{N(0) \langle g^2 \rangle}{2M} = \int_0^{\infty} \omega \alpha^2(\omega) F(\omega) d\omega \quad (19)$$

In the above  $F(\omega)$  is phonon density of states, and  $N(0)$  is electronic density of state at the Fermi energy and  $M$  is the atomic mass. In case  $\alpha^2 = \text{constant}$ , as suggested by McMillan<sup>14</sup>

$$\lambda = \frac{N(0) \langle g^2 \rangle}{M \langle \omega^2 \rangle} = 2\alpha^2 \int F(\omega) \omega^{-1} d\omega \quad (20)$$

$$\text{with } \langle \omega^2 \rangle \equiv \int F(\omega) \omega d\omega / \int F(\omega) \omega^{-1} d\omega \quad (21)$$

Evaluation of  $\alpha^2$  and  $\langle g^2 \rangle$  require a knowledge of  $\lambda$  and either  $\langle \omega^2 \rangle$  or  $\langle \omega^{-1} \rangle$ .

$\lambda$  can be determined from observed  $T_c$ . For small and moderate values of  $\lambda$ , McMillan's relation holds<sup>14</sup>

$$T_c = K \exp\left[-\frac{1.04(1+\lambda)}{\lambda - \mu^*(1+0.62\lambda)}\right] \quad (22)$$

Here  $\mu^*$  is McMillan's Coulomb parameter and  $K$  is either logarithmic average phonon frequency  $\omega_{\log}/1.2$  or Debye temperature  $T_D/1.45$ .

For very large  $\lambda$  i.e.  $\lambda >$  five times (phonon frequency)<sup>2</sup>, Allen and Dyne's<sup>13</sup> relation holds

$$T_c = 0.180(1 + 2.60 \mu^*)^{-1/2} \lambda^{1/2} \quad (23)$$

Implication of (23) is that there is no upper limit of  $T_c$ .  $\lambda$ , is not expected to be very large for the 1-2-3 superconductors. Since  $\omega_{\log}$  is not very well known, we can estimate  $\lambda$  using  $K = T_D/1.45$ . For X = oxygen  $T_c = 93$ , and  $T_D = 812$  (ref. 16). Calculated values for  $\lambda$  are 1.38, 1.89, 2.09, 2.45 and 2.81 for  $\mu^* = 0, 0.10, 0.13, 0.18$  and  $0.22$ , respectively. Thus,  $\lambda$  is estimated to be between 2 and 3. Both  $\alpha^2$  and  $\langle g^2 \rangle$  can be evaluated once phonon spectra become available.

One may, however, follow a different approach noting that the Hamiltonian (17) can be diagonalized exactly following the method of Huang and Rys<sup>5,12</sup>. The expression for diagonalized energy  $E$  is given by

$$E_\lambda(n, k) = \epsilon_\lambda - \Delta_\lambda + \sum_k \hbar\omega(\vec{k}) \left[ n_k + \frac{1}{2} \right] \quad (24)$$

with

$$\Delta_\lambda = \sum_R |v(\vec{k}, \lambda)|^2 \hbar\omega(\vec{k}) \quad (25)$$

$v(\vec{k}, \lambda)$  could take various forms, including the matrix element of  $(\epsilon.VV)$ . We can, however, make a simple estimation of the electron-phonon coupling strength by setting  $v(\vec{k}, \lambda) = g \hbar\omega(k)$ . In this case<sup>28</sup>

$$\Delta_\lambda = g_\lambda^2 \sum_k \hbar\omega(k) \quad g_\lambda^2 k T_D \quad (26)$$

Using the observed values of  $\Delta \approx 32 \text{ meV}^{15}$  and  $50 \text{ meV}^{17}$  and a Debye temperature<sup>16</sup>  $T_D = 812^\circ \text{ K}$ , we get  $g^2 \approx 0.46$  and  $0.71$ , respectively.

Both (23) and (25) in conjunction with (12) imply that there is, in principle, no limit of  $T_c$ . The key to high  $T_c$  is strong electron-phonon coupling as suggested by Fröhlich<sup>4</sup>.

Since the model should be valid for type I and II superconductors, we can calculate  $g^2$  for those cases. In Table 3, we have compared effective coupling strength  $g^2$  for type I, II and III superconductors. The electron-phonon coupling in high  $T_c$  superconductors is two orders of magnitude larger than that in type I superconductors. It is about an order of magnitude larger than that in type II superconductors.

#### 4. CONCLUDING REMARKS

Although in this analysis, particularly in section 3, one has mentioned electron-phonon coupling, the theory outlined in section 2 does not restrict superconductivity to effective pairing caused by electron-phonon coupling case only. IN FACT, ANY MECHANISM THAT MAKES EFFECTIVE INTERACTION (2) ATTRACTIVE AND ALLOWS TO FORM SCHAFFROTH'S PAIR

COULD GIVE RISE TO SUPERCONDUCTIVITY. A coupled electron pair in a singlet state and with opposite momenta is usually the lowest energy state in many potential wells. Hence, it is natural to use this coupling scheme along with the coherence state condition for superconducting states. One can form such a state in many ways e.g., by surrounding a pair of electrons by positively charge ions. Given the right condition, that system could also exhibit superconducting behavior, even though no electron-phonon coupling is directly involved. There is no upper limit of  $T_c$  and a strong electron-phonon or electron-environment interaction is a necessary requirement for high  $T_c$ , as noted by Fröhlich<sup>4</sup>).

#### REFERENCES

1. P. Haapakosi and F. B. Malik, Condensed Matter Theories, ed. J. Keller (Plenum Publishing Corp. 1989) Vol. 4., p. 311.
2. P. Haapakoski, A. Kallio and F. B. Malik, Phys. Lett A. (submitted).
3. Yu. A. Osip'yan, O. V. Zharikov, G. V. Novikov, N. S. Sidorov, V. I. Kulakov, L. V. Sipavina, R. K. Nikolaer and A. , Promov, Pis'ma Zh. Eksp. Teor. Fiz 49, 61 (1989) [Eng. Trans. 49, (1989)].
4. H. Fröhlich, Proc. Roy. Soc. (Lond.) A215, 291 (1952).
5. K. Huang and A. Rys, Proc. Roy. soc. (Lond.) A204, 406 (1950).
6. M. R. Schafroth, Phys. Rev. 96, 1442 (1954).
7. J. Bardeen, L.N. Cooper and J. R. Schrieffer, Phys. Rev. 108, 1175 (1957).
8. B. Mühlischlegel, Z. Physik 155, 313 (1959).
9. J. M. Blatt, Theory of Superconductivity (Academic Press, New York 1964).
10. R. J. Cana et al. Phys. Rev. Lett. 58, 1676 (1987).
11. G. M. Eliashberg, Zh. Eksp. Teor. Fiz., 38, 966 (1960) (Eng. JETP 11, 696 (1960)) and 39, 1437 (1960) (Eng. JETP 12, 1000 (1961)).
12. C. B. Duke and G. D. Mahan, Phys. Rev. 139A, 1965 (1965).
13. P. B. Allen and R. C. Dynes, Phys. Rev. B 12, 905 (1975).
14. W. L. McMillan, Phys. Rev. 167, 331 (1968).
15. Z. Schlesinger, R. T. Collins, D. L. Kaiser and F. Holtzberg, Phys. Rev. Lett. 59, 1958 (1987).
16. M. De Llano, Private Communication.
17. M. D. Kirk et al. Phys. Rev. B 35, 8850 (1987).
18. Robert C. Weast ed., Handbook of Chemistry and Physics (Chemical Rubber Co., Cleveland. 60th edition 1979).
19. M. K. Wu et al. Phys. Rev. Lett. 58, 908 (1987).
20. R. N. Bhargara, S. P. Herko and W. N. Osborne, Phys. Rev. Lett. 59, 1468 (1987).
21. X. R. Meng et al. Solid State Comm. 64, 325 (1987).
22. P. K. Davies et al. Solid Sate comm. 64 1441 (1987).
23. I. Felner et al. Phys. Rev. B 36, 3923 (1987).
24. J. R. Kirtley et al. Phys. Rev. B 35, 8846 (1987).
25. Z. Schlesinger, R. T. Collins, D. L. Kaiser and F. Holtzberg, Phys. Rev. Lett. 59 (1987).
26. M. Kirk et al. Phys. Rev. B 35, 8850 (1987).
27. R. J. Cara et. al. Phys. Rev. Lett. 58, 1676 (1987).  
C. B. Duke, F. B. Malik and F. W. K. Firk, Phys. Rev. 157, 879 (1987).

Table 1: Calculated  $T_c$  (col. 5), are compared to observed one (col. 6). Electron affinities in col. 2 and for O and S in col. 3 are taken from ref. 18. Electron affinities for  $F^-$  and  $Cl^-$  are theoretical calculation and Br and I are estimation. (a), (b), (c), (d), (e) and (f) are refs. 19-23 and 3, respectively.

X	e.a(x)(eV)	ea(x <sup>-</sup> )eV	$\Delta W$	$T_c(\text{cal.})^\circ K$	$T_c(\text{expt})^\circ K$
O	1.47	-8.73	-0.02451	93	93 <sup>a</sup>
F	3.45	-4.81	-0.02778	102	159 <sup>b</sup> 140 <sup>c</sup> 80 to 89 <sup>d</sup>
S	2.07	-5.51	-0.02332	90	90 <sup>e</sup>
Cl	3.61	-6.11	-0.01739	75	72 <sup>e</sup>
Br	3.36	-6.00	-0.01202	61	- 75 <sup>f</sup>
		-5.00	-0.01346	65	
		-4.00	-0.01528	70	
I	3.06	-6.00	-0.00979	56	- 50 <sup>f</sup>
		-5.00	-0.01100	59	
		-4.00	-0.01259	63	

Table 2: Calculated gap  $\Delta$  (col.2), coherence length  $\zeta_0$  (col. 4), critical field (col. 6) are compared with respective observed values, in columns 3, 5 and 6.(a), (b), (c), and (d) are, respectively, ref. 24-27.

X	$\Delta(\text{cal.})$ MeV	$\Delta(\text{expt})$ MeV	$\zeta_0(\text{calc.})\text{\AA}$	$\zeta_0(\text{exp})\text{\AA}$	$H_\psi(\text{cal.})G$	$H_c(\text{exp})0_e$
O	14	15-23 <sup>a)</sup> 32 <sup>b)</sup> -50 <sup>c)</sup>	10	-22 <sup>d)</sup>	25 x 10 <sup>3</sup>	(10±2 <sup>d)</sup> 10 <sup>3</sup>
F	16	-	9	-	-	-
S	14	-	10	-	-	-
Cl	11	-	12	-	-	-
Br	11	-	13-15	-	-	-
I	10	-	15-17	-	-	-

Table 3: Coupling strength  $g^2$  in some type I, II and III superconductors.

Substance →	Al	Re	Sn	Nb	Y-Ba-Cu-O
$T_c$ in °K	1.16	1.69	3.72	9.22	93.00
$k \times$ debye Temperature (meV)	36.9	35.8	17.20	23.90	70.06
$g^2$	0.003	0.004	0.019	0.037	0.46 to 0.71

## BAYM-KADANOFF THEORY MADE EVEN PLANAR

Roger Alan Smith

Center for Theoretical Physics  
Physics Department  
Texas A&M University  
College Station, TX 77843

### INTRODUCTION

In the last workshop in this series, I presented some results obtained by expressing the Baym-Kadanoff algorithm[1-2] in the language of the parquet theory[3-14]. That paper[15] showed (i) that the parquet theory is not a conserving theory in the sense of the Baym-Kadanoff theory, (ii) applied the Baym-Kadanoff theory in this form to some simple self-energy diagrams, and (iii) observed that none of the resulting vertex functions was antisymmetric. This contribution presents some new results obtained using the same formalism. The main result is a proof that any set of diagrams which is both conserving and antisymmetric under exchange of the outgoing legs must include all parquet diagrams obtained using the bare interaction as well as an infinite number of irreducible diagrams.

### NOTATION

The notation has been changed slightly since the last workshop, so a definition of terms is in order. The diagrammatic constructs of interest are the two-body Green's function and the single-particle self-energy. Diagrams for the two-body Green's function are to be written in terms of one-body Green's functions which use the self-energy; hence explicit inclusion of self-energy insertions in the diagrams for the two-body Green's function should be avoided. The lowest-order contribution to the two-body vertex is taken to be the bare interaction and its exchange; the terms in the two-body Green's function which are just the direct and exchange products of two one-body Green's functions are not included in this category. A direct diagram is one in which the line of propagators entering one side at the bottom ultimately can be traced through to the same side as it goes out the top.

$$\begin{aligned}
\Gamma &= V + S + U - C + L + R \\
S &= \Gamma \textcircled{\textcircled{S}} (V + U + C + L + R) \\
U &= \Gamma \textcircled{\textcircled{D}} (V + S + C + L + R) \\
C &= \Gamma \textcircled{\textcircled{C}} (V + S + U) \\
L &= \Gamma \textcircled{\textcircled{L}} (V + S + U) \\
R &= \Gamma \textcircled{\textcircled{R}} (V + S + C + L + R).
\end{aligned} \tag{1}$$

The apparent asymmetry in these equations arises from the fact that some diagrams generated by the  $\textcircled{\textcircled{S}}$ ,  $\textcircled{\textcircled{D}}$ , and  $\textcircled{\textcircled{L}}$  operations could be generated in several different ways. The equations, as written, guarantee that each such diagram will be generated but once. A more symmetric set of equations, which is equivalent, is written in the form [12,14,16]

$$\begin{aligned}
\Gamma &= I + S + U + T \\
S &= (\Gamma - S) \textcircled{\textcircled{S}} \Gamma \\
U &= (\Gamma - U) \textcircled{\textcircled{D}} \Gamma \\
T &= B + \Gamma \textcircled{\textcircled{L}} (I + S + U + B) + (I + S + U + B) \textcircled{\textcircled{D}} \Gamma + \Gamma \textcircled{\textcircled{L}} (I + S + U + B) \textcircled{\textcircled{D}} \Gamma \\
B &= (I + S + U) \textcircled{\textcircled{D}} (I + S + U + B),
\end{aligned} \tag{2}$$

where

$$\alpha \textcircled{\textcircled{D}} \beta = \alpha \textcircled{\textcircled{C}} \beta + \alpha \textcircled{\textcircled{L}} \textcircled{\textcircled{D}} \beta. \tag{3}$$

Each form has its utility; eq. 2 is more symmetric, but it also has two operations explicitly on the right-hand side.

A convenient way to compute the single-particle self-energy  $\Sigma$  is to take some approximation for the exact vertex  $\tilde{\Gamma}$ , add an interaction  $V$  using the operation  $\textcircled{\textcircled{S}}$ , and then close off the two right-hand lines with a one-body propagator. If  $\tilde{\Gamma}$  is antisymmetric, the self-energy can be computed from the direct part of  $\Gamma$  by

$$\Sigma = d(\Gamma \textcircled{\textcircled{S}} V) + e(\Gamma \textcircled{\textcircled{S}} V), \tag{4}$$

where the direct and exchange lines contributions are formed by applying the two operations illustrated in fig. 2.

If  $\tilde{\Gamma}$  is not antisymmetric, then

$$\Sigma = d(\tilde{\Gamma} \textcircled{\textcircled{S}} V). \tag{5}$$

The exact theory and the parquet theory both have an antisymmetric  $\tilde{\Gamma}$ , so that  $\Gamma = \tilde{\Gamma}$  and eq. 4 is appropriate. However, the Baym-Kadanoff algorithm generates an approximate vertex which is not necessarily antisymmetric.

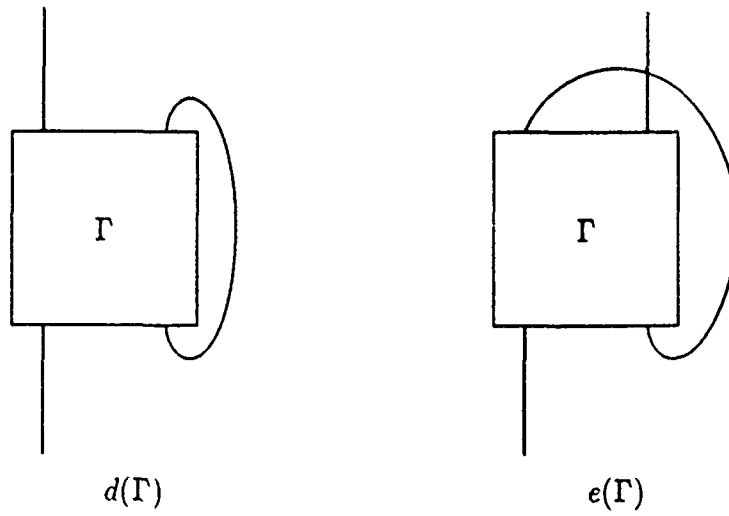


Fig. 2: Forming the self-energy  $\Sigma$ .

### BAYM-KADANOFF THEORY

The Baym-Kadanoff (BK) algorithm takes an approximation to the self-energy  $\Sigma$  which is taken to be constructed diagrammatically from one-body Green's functions which use the same  $\Sigma$ . The source of the approximate  $\Sigma$  need not be specified; it could be computed from some approximate vertex using eqs. 4 or 5, but it need not be. The conserving vertex is obtained as the functional derivative of the self-energy with respect to a weak external two-point non-local perturbation. The one-body Green's function is itself a functional of this interaction, and the functional derivative of the one-body Green's function can be expressed back in terms of the functional derivative of the self-energy with respect to this small non-local perturbation. We note that any self-energy contribution can always be expressed in the form of fig. 2, where the  $\Gamma$  may be irreducible. The algorithm, in the parquet notation, proceeds in two stages.

First, one generates a two-body kernel

$$\tilde{\Xi} = \Sigma', \quad (6)$$

where the prime denotes the functional derivative with respect to the Green's function. Careful inspection shows that  $\tilde{\Xi}$  can have both direct and exchange parts, but they cannot be of all reducibility types. Specifically, only reducibility types  $I$ ,  $S$ ,  $U$ ,  $\hat{I}$ ,  $\hat{S}$ ,  $\hat{C}$ ,  $\hat{L}$ ,  $\hat{R}$  and  $\hat{A}$  can come out of this operation. To show this, we first write

$$\begin{aligned} d(\alpha \otimes \beta) &= d(\alpha' \otimes \beta) + d(\alpha \otimes \beta') + \alpha \otimes \beta + \alpha \otimes \beta + \overline{\alpha \otimes \beta} \\ e(\alpha \otimes \beta) &= e(\alpha' \otimes \beta) + e(\alpha \otimes \beta') + \overline{\alpha \otimes \beta} + \overline{\alpha \otimes \beta} + \overline{\alpha \otimes \beta} \end{aligned} \quad (7)$$

The immediate functional derivatives are all of the types indicated. For computing  $\tilde{\Xi}$ ,  $\beta = V$ , so that  $\beta' = 0$ . The only remaining terms are the  $d(\alpha' \otimes \beta)$  or  $e(\alpha' \otimes \beta)$ . If  $\alpha$  is irreducible, then these terms are as well. If  $\alpha$  is reducible, then the functional derivative can be transformed using

$$\begin{aligned} d((\alpha \otimes \beta)' \otimes \gamma) &= d((\alpha' \otimes \beta) \otimes \gamma) + d((\alpha \otimes \beta') \otimes \gamma) + d((\alpha \otimes \beta') \otimes \gamma) \\ e((\alpha \otimes \beta)' \otimes \gamma) &= e((\alpha' \otimes \beta) \otimes \gamma) + e((\alpha \otimes \beta') \otimes \gamma) + e((\alpha \otimes \beta') \otimes \gamma). \end{aligned} \quad (8)$$

The last term on the right-hand sides of eq. 8 is always irreducible. The middle term can be expressed in reducible form using table 1. All of these table entries are in one of the stated categories.

Ⓢ	$d((\alpha \textcircled{\text{P}} \beta) \textcircled{\text{S}} \gamma)$		$d((\alpha \textcircled{\text{P}} \beta) \textcircled{\text{S}} \gamma)$	
Ⓢ	$\alpha \textcircled{\text{C}}(\tilde{\beta} \textcircled{\text{S}} \tilde{\gamma})$	$\alpha \textcircled{\text{U}}(\beta \textcircled{\text{S}} \gamma)$	$\alpha \textcircled{\text{T}}(\tilde{\beta} \textcircled{\text{S}} \tilde{\gamma})$	$\alpha \textcircled{\text{D}}(\beta \textcircled{\text{S}} \gamma)$
Ⓤ	$\alpha \textcircled{\text{C}}(\tilde{\gamma} \textcircled{\text{U}} \tilde{\beta})$	$\alpha \textcircled{\text{S}}(\beta \textcircled{\text{U}} \gamma)$	$\alpha \textcircled{\text{T}}(\tilde{\gamma} \textcircled{\text{T}} \tilde{\beta})$	$\alpha \textcircled{\text{S}}(\beta \textcircled{\text{D}} \gamma)$
Ⓢ	$\alpha \textcircled{\text{U}}(\gamma \textcircled{\text{C}} \tilde{\beta})$	$\alpha \textcircled{\text{S}}(\gamma \textcircled{\text{C}} \tilde{\beta})$	$\alpha \textcircled{\text{S}}(\gamma \textcircled{\text{D}} \tilde{\beta})$	$\alpha \textcircled{\text{U}}(\gamma \textcircled{\text{D}} \tilde{\beta})$
Ⓢ	$\alpha \textcircled{\text{S}}(\gamma \textcircled{\text{T}} \tilde{\beta})$	$\alpha \textcircled{\text{U}}(\gamma \textcircled{\text{T}} \tilde{\beta})$	$\alpha \textcircled{\text{D}}(\gamma \textcircled{\text{U}} \tilde{\beta})$	$\alpha \textcircled{\text{S}}(\gamma \textcircled{\text{U}} \tilde{\beta})$
Ⓢ	$\alpha \textcircled{\text{S}}(\beta \textcircled{\text{C}} \tilde{\gamma})$	$\alpha \textcircled{\text{T}}(\gamma \textcircled{\text{C}} \tilde{\beta})$	$\alpha \textcircled{\text{T}}(\gamma \textcircled{\text{D}} \tilde{\beta})$	$\alpha \textcircled{\text{S}}(\beta \textcircled{\text{T}} \tilde{\gamma})$

Table 1: Diagrams from the middle term of the right-hand sides of eq. 8.

The final case is the first term on the right-hand sides of eq. 5. These can be rearranged using the diagrams in fig. 3 which correspond to the right-hand sides of the identities

$$\begin{aligned}
d((\alpha \textcircled{\text{S}} \beta) \textcircled{\text{S}} \gamma) &= d(\alpha \textcircled{\text{S}}(\beta \textcircled{\text{S}} \gamma)) \\
d((\alpha \textcircled{\text{U}} \beta) \textcircled{\text{S}} \gamma) &= d(\alpha \textcircled{\text{S}}(\beta \textcircled{\text{U}} \gamma)) \\
d((\alpha \textcircled{\text{C}} \beta) \textcircled{\text{S}} \gamma) &= d(\alpha \textcircled{\text{S}}(\gamma \textcircled{\text{C}} \tilde{\beta})) \\
d((\alpha \textcircled{\text{T}} \beta) \textcircled{\text{S}} \gamma) &= d(\alpha \textcircled{\text{S}}(\gamma \textcircled{\text{T}} \tilde{\beta})) \\
d((\alpha \textcircled{\text{D}} \beta) \textcircled{\text{S}} \gamma) &= e(\alpha \textcircled{\text{S}}(\beta \textcircled{\text{C}} \tilde{\gamma})) \\
e((\alpha \textcircled{\text{S}} \beta) \textcircled{\text{S}} \gamma) &= e(\alpha \textcircled{\text{S}}(\beta \textcircled{\text{S}} \gamma)) \\
e((\alpha \textcircled{\text{U}} \beta) \textcircled{\text{S}} \gamma) &= e(\alpha \textcircled{\text{S}}(\beta \textcircled{\text{D}} \gamma)) \\
e((\alpha \textcircled{\text{C}} \beta) \textcircled{\text{S}} \gamma) &= d(\alpha \textcircled{\text{S}}(\gamma \textcircled{\text{D}} \tilde{\beta})) \\
e((\alpha \textcircled{\text{T}} \beta) \textcircled{\text{S}} \gamma) &= e(\alpha \textcircled{\text{S}}(\gamma \textcircled{\text{U}} \tilde{\beta})) \\
e((\alpha \textcircled{\text{D}} \beta) \textcircled{\text{S}} \gamma) &= e(\alpha \textcircled{\text{S}}(\beta \textcircled{\text{T}} \tilde{\gamma}))
\end{aligned} \tag{9}$$

These diagrammatic identities are equally valid if  $\alpha$  is replaced by  $\alpha'$ , and hence the first terms on the right-hand sides of eq. 8 can be transformed into the form of the left-hand sides of eq. 8. This process cannot go on indefinitely, since each time eq. 9 is used to make a transformation, the diagram  $\alpha$  is of lower order in perturbation theory.

The full BK conserving vertex is generated from  $\tilde{\Xi}$  by solving the equation

$$\tilde{X} = \tilde{\Xi} + \tilde{\Xi} \textcircled{\text{C}} \tilde{X} + \tilde{\Xi} \textcircled{\text{D}} \tilde{X} + \tilde{\Xi} \textcircled{\text{T}} \tilde{X}. \tag{10}$$

Sorting out the direct and exchange parts and doing some diagrammatic rearrangement, we cast the resulting components of the BK vertex in the form of eq. 2,

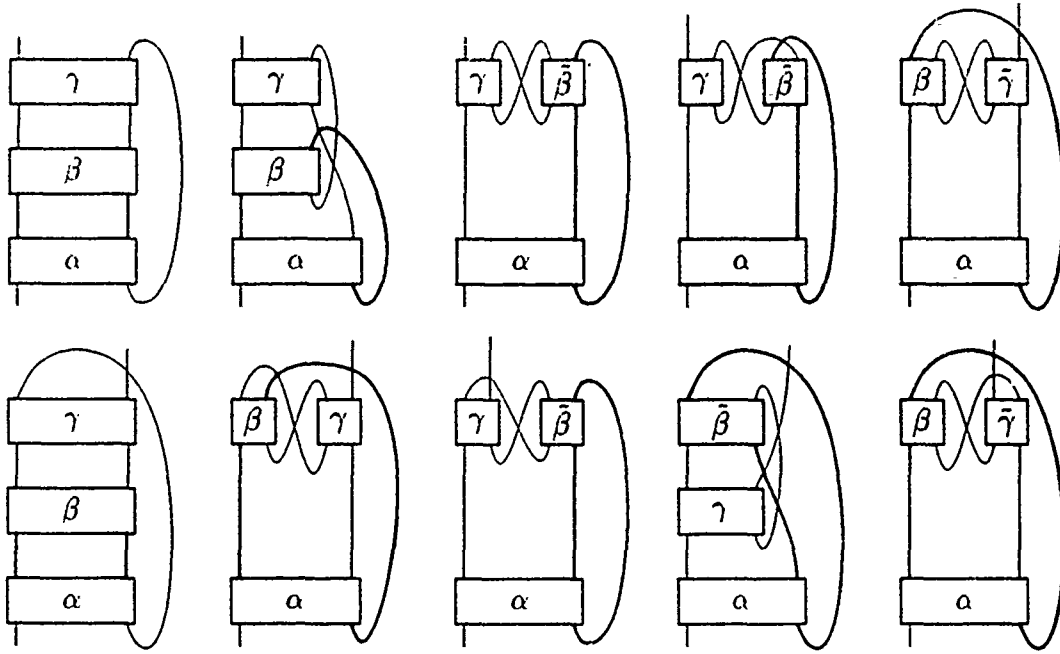


Fig. 3 Some diagrammatic rearrangements

obtaining exchange components

$$\begin{aligned}
 \hat{\Gamma}_X &= \hat{I}_X + \hat{S}_X + \hat{U}_X + \hat{T} \\
 \hat{I}_X &= \hat{I}_\Xi \\
 \hat{S}_X &= \hat{S}_\Xi \\
 \hat{U}_X &= (\hat{\Gamma}_X - \hat{U}_X) \circledast \hat{\Gamma}_X \\
 \hat{T}_X &= \hat{T}_\Xi
 \end{aligned} \tag{11}$$

and direct components

$$\begin{aligned}
 \Gamma_X &= I_X + S_X + U_X + T_X \\
 I_X &= I_\Xi \\
 S_X &= S_\Xi \\
 U_X &= U_\Xi \\
 T_X &= B_X + \hat{\Gamma} \circledast (I_X + S_X + U_X + B_X) + (I_X + S_X + U_X + B_X) \circledast \hat{\Gamma} \\
 &\quad + \hat{\Gamma} \circledast (I_X + S_X + U_X + B_X) \circledast \hat{\Gamma} \\
 B_X &= (I_X + S_X + U_X) \circledast (I_X + S_X + U_X + B_X)
 \end{aligned} \tag{12}$$

The  $\circledast$  operation in eq. 5 requires the Lindhard bubble to be dressed by  $\hat{\Gamma}$ .

These expressions for the conserving vertex basically can be easily understood: the self-consistency implicit in the BK algorithm is a t-channel operation as seen in eq. 10. Thus, the integral equations build the t-channel chains and vertex corrections, while the exchange channel is the u-channel. The s-channel diagrams can only come from the explicit functional differentiation with respect to the one-body

Green's function, since they can't be generated by a direct or exchange t-channel operation.

As we noted before, the vertex generated by the BK algorithm need not be antisymmetric; indeed, eq. 11 and eq. 12 show what the diagrammatic content actually is.

### CONSERVING AND ANTISYMMETRIC IS MORE THAN PARQUET

In this section, we prove that any approximation to the self-energy which is used to generate a vertex which is both antisymmetric and conserving and which includes the Hartree term must include a class of diagrams which includes all parquet diagrams generated from the bare interaction and a large class of irreducible diagrams. The key to this argument is that antisymmetry of the conserving vertex implies no need to distinguish between  $\Gamma$  and  $\hat{\Gamma}$ . This provides a significant constraint, since eq. 11 and eq. 12 then can be used to identify certain functional derivative results with the results of integral equations in the  $\textcircled{S}$  and  $\textcircled{T}$  channels.

At the Hartree-Fock level (Fock is included if Hartree is),  $I$  will include  $V$ . Now assume that all of the parquet terms are generated up to order  $n$  in perturbation theory by some set of self-energy diagrams. (A minimum set of self-energy diagrams can always be found by using the algorithm of the following section). The exchange channels (eq. 11) then generate  $U$  correctly to order  $n + 1$  using only the  $V$  in  $I$ , since all of the inputs are correct to order  $n$  and the first-order term is correct. The direct channels (eq. 12) generate  $T$  correctly to order  $n + 1$  for the same reason. Finally, we note that the functional differentiation of any diagram which produces  $\alpha\textcircled{\beta}$  also produces  $\alpha\textcircled{S}\beta$ , so that since  $U$  is correct to order  $n + 1$ , so must be  $S$ . But if all of the diagrams are correct to order  $n + 1$ , then they are correct to all orders. Hence all parquet diagrams must be generated.

As we argued previously, parquet is not conserving; a set of self-energy diagrams which generates parquet must also generate an infinite set of irreducible diagrams. As a consequence, parquet theory is not a sufficiently large class of diagrams to be both conserving and antisymmetric. We speculate that the only set of diagrams which satisfies both criteria is the complete set of diagrams.

### PARQUET DIAGRAMS GENERATE SELF-ENERGY DIAGRAMS

Here we present the algorithm which determines, for any reducible diagram  $\mu$ , the parquet diagram whose direct or exchange contribution to the self-energy gives  $\mu$  on functional differentiation with respect to the Green's function. It is convenient to use the notation of eq. 1 in this section. The first step is to determine whether the diagram is a member of the acceptable types  $\{S, U, \hat{S}, \hat{C}, \hat{L}, \hat{R}\}$ .

If so, then  $\mu = \alpha x \lambda$ , and the starting point is obtained by looking in tables 2-3.

In tables 2-3, the  $\rightarrow$  entries indicate that the direct diagram can be rearranged, and one should look up the transformed form.

$\lambda$	$a \textcircled{S} \lambda$	$a \textcircled{W} \lambda$
$V$	$d(\alpha \textcircled{S} V)$	$d(\alpha \textcircled{S} V)$
$\beta \textcircled{S} \gamma$	$\rightarrow (\alpha \textcircled{S} \beta) \textcircled{S} \gamma$	$d((\alpha \textcircled{S} \beta) \textcircled{S} \gamma)$
$\beta \textcircled{W} \gamma$	$d((\alpha \textcircled{W} \beta) \textcircled{S} \gamma)$	$\rightarrow (\alpha \textcircled{W} \beta) \textcircled{W} \gamma$
$\beta \textcircled{C} \gamma$	$d((\alpha \textcircled{C} \tilde{\gamma}) \textcircled{S} \beta)$	$d((\alpha \textcircled{C} \tilde{\gamma}) \textcircled{S} \beta)$
$\beta \textcircled{T} \gamma$	$d((\alpha \textcircled{T} \tilde{\gamma}) \textcircled{S} \beta)$	$d((\alpha \textcircled{T} \tilde{\gamma}) \textcircled{S} \beta)$
$\beta \textcircled{D} \gamma$	$e((\alpha \textcircled{C} \tilde{\gamma}) \textcircled{S} \beta)$	$e((\alpha \textcircled{C} \tilde{\gamma}) \textcircled{S} \beta)$

Table 2: The starting point for direct diagrams.

$\lambda$	$\overline{(\alpha \textcircled{S} \lambda)}$	$\overline{(\alpha \textcircled{C} \lambda)}$	$\overline{(\alpha \textcircled{D} \lambda)}$	$\overline{(\alpha \textcircled{T} \lambda)}$
$V$	$e(\alpha \textcircled{S} V)$	$d(\alpha \textcircled{S} V)$	$e(\alpha \textcircled{S} V)$	$e(\alpha \textcircled{S} V)$
$\beta \textcircled{S} \gamma$	$\rightarrow \overline{((\alpha \textcircled{S} \beta) \textcircled{S} \gamma)}$	$d((\alpha \textcircled{S} \tilde{\beta}) \textcircled{S} \tilde{\gamma})$	$e((\alpha \textcircled{S} \beta) \textcircled{S} \gamma)$	$e((\alpha \textcircled{S} \tilde{\beta}) \textcircled{S} \tilde{\gamma})$
$\beta \textcircled{W} \gamma$	$e((\alpha \textcircled{T} \tilde{\gamma}) \textcircled{S} \beta)$	$d((\alpha \textcircled{W} \tilde{\gamma}) \textcircled{S} \tilde{\beta})$	$e((\alpha \textcircled{T} \tilde{\gamma}) \textcircled{S} \beta)$	$\rightarrow \overline{((\alpha \textcircled{T} \beta) \textcircled{T} \gamma)}$
$\beta \textcircled{C} \gamma$	$d((\alpha \textcircled{D} \beta) \textcircled{S} \tilde{\gamma})$	$\rightarrow \overline{((\alpha \textcircled{C} \beta) \textcircled{C} \gamma)}$	$\rightarrow \overline{((\alpha \textcircled{D} \beta) \textcircled{C} \gamma)}$	$d((\alpha \textcircled{D} \tilde{\gamma}) \textcircled{S} \beta)$
$\beta \textcircled{T} \gamma$	$e((\alpha \textcircled{D} \beta) \textcircled{S} \tilde{\gamma})$	$\rightarrow \overline{((\alpha \textcircled{C} \beta) \textcircled{T} \gamma)}$	$\rightarrow \overline{((\alpha \textcircled{D} \beta) \textcircled{T} \gamma)}$	$e((\alpha \textcircled{W} \tilde{\gamma}) \textcircled{S} \tilde{\beta})$
$\beta \textcircled{D} \gamma$	$e((\alpha \textcircled{W} \beta) \textcircled{S} \gamma)$	$\rightarrow \overline{((\alpha \textcircled{T} \beta) \textcircled{C} \gamma)}$	$\rightarrow \overline{((\alpha \textcircled{W} \beta) \textcircled{D} \gamma)}$	$e((\alpha \textcircled{D} \tilde{\gamma}) \textcircled{S} \beta)$

Table 3: The starting point for exchange diagrams.

The second kind of entry is indicated by the first line: if  $\lambda$  is  $V$ , then we are really done, since then  $\alpha$  is the parquet diagram whose functional derivative gives the desired diagram.

The final case is a little more complicated: the table entry is used as a starting point to carry out a reduction using table 4. That is, a direct or exchange diagram from table 2 or 3 is used to look up a new diagram from table 4. If this diagram has the form  $d(\nu \textcircled{S} V)$  or  $e(\nu \textcircled{S} V)$ , the procedure terminates with  $\nu$  as the parquet diagram whose functional derivative gives the desired diagram. If not, the table entry is used to generate a new table entry. For parquet diagrams, this procedure eventually must terminate.

## DISCUSSION

We are at present at work determining a good form for the three-body integral equations which sum all irreducible diagrams generated by the BK algorithm using parquet as input. The present form of the equations is not particularly enlightening, and will not be presented here.

The main conclusion to be drawn is that two properties of the exact vertex which one would desparately like to maintain, antisymmetry and the conserving

$\lambda$	$d(\lambda) \rightarrow$	$c(\lambda) \rightarrow$
$\alpha \otimes (\beta \otimes \gamma)$	$d((\alpha \otimes \beta) \otimes \gamma)$	$c((\alpha \otimes \beta) \otimes \gamma)$
$\alpha \otimes (\beta \oplus \gamma)$	$d((\alpha \oplus \beta) \otimes \gamma)$	$c((\alpha \oplus \beta) \otimes \gamma)$
$\alpha \otimes (\beta \odot \gamma)$	$d((\alpha \odot \beta) \otimes \gamma)$	$d((\alpha \odot \beta) \otimes \gamma)$
$\alpha \otimes (\beta \oplus \gamma)$	$d((\alpha \oplus \beta) \otimes \gamma)$	$c((\alpha \oplus \beta) \otimes \gamma)$
$\alpha \otimes (\beta \odot \gamma)$	$c((\alpha \odot \beta) \otimes \gamma)$	$c((\alpha \odot \beta) \otimes \gamma)$

Table 4. Iterate using this table until the right-hand term is  $V$ .

property, are incompatible at any level less than parquet. This has been pursued for the purpose of finding out a satisfactory approximation scheme for fermion parquet theory. It appears that to satisfy these properties where they are needed, it will be necessary to use different approximations in different contexts.

#### ACKNOWLEDGEMENTS

The work done here was supported in part by the NSF under grant PHY-8806265. I am grateful to the U. S. Army Research Office for a grant supporting travel to this workshop.

#### REFERENCES

1. G. Baym and L. P. Kadanoff, Phys. Rev. **124**, 287-299 (1961).
2. G. Baym, Phys. Rev. **127**, 1391-1401 (1962).
3. A. D. Jackson, A. Lande and R. A. Smith, Phys. Report **86**, 55-111 (1982).
4. R. A. Smith, Proceedings of the Sixth Pan-American Workshop on Condensed Matter Theories, ed. J. M. C. Chen, J. W. Clark, P. Suntharok-Priesmeyer, (Department of Physics, Washington Univ., St. Louis), 153-154 (1982).
5. A. Lande and R. A. Smith, Phys. Lett. **131B**, 253-256 (1983).
6. A. D. Jackson, A. Lande, R. W. Guitink and R. A. Smith, Phys. Rev. **B31**, 403-415 (1985).
7. A. D. Jackson, A. Lande and R. A. Smith, Phys. Rev. Lett. **54**, 1469-1471 (1985).
8. R. A. Smith, Proceedings of the IX International Workshop on Condensed Matter Theories, San Francisco, Aug. 1985, ed. F. B. Malik, (Plenum Press, New York, 1986), 9-18.
9. E. Krotscheck, R. A. Smith, and A. D. Jackson, Phys. Rev. **A33**, 3535-3536 (1986).
10. R. A. Smith and A. D. Jackson, Nucl. Phys. **A476**, 448-470 (1988).
11. A. D. Jackson and R. A. Smith, Phys. Rev. **A36**, 2517-2518 (1987).
12. R. A. Smith and A. Lande, Proceedings of the XI International Workshop on Condensed Matter Theories, Oulu, July 1987, ed. J. Arponen, R. F. Bishop and M. Manninen (Plenum Press, New York, 1988), 1-9.

13. R. A. Smith and A. D. Jackson, Proceedings of the V International Conference on Recent Progress in Many-Body Theories, Oulu, August 1987, ed. A. Kallio, J. Arponen and R. F. Bishop (Plenum Press, New York, 1987), 327-333.
14. A. Lande and R. A. Smith, Proceedings of the V International Conference on Recent Progress in Many-Body Theories, Oulu, August 1987, ed. A. Kallio, J. Arponen and R. F. Bishop (Plenum Press, New York, 1987), 335-342.
15. R. A. Smith, Proceedings of the XII International Workshop on Condensed Matter Theories, Taxco, August 1988, ed. J. Keller (Plenum Press, New York, 1989).
16. A. Lande and R. A. Smith, Phys. Rev, to be submitted.